FLUX MOTION AND NOISE IN SUPERCONDUCTORS*)

BY

G. J. van GURP

*) Thesis, Technical University Eindhoven, May 1969.
Promotor: Prof. Dr M. J. Steenland.

Philips Res. Repts Suppl. 1969, No. 5.

Abstract

This thesis deals with the d.c. and the noise voltage across a superconductor caused by the motion of regions containing magnetic flux, viz. vortex lines or normal domains. It is shown from measurements of the d.c. voltage that pinning of vortex lines in type-II superconductors is dependent on the structure of the material and may be anisotropic. Anisotropy is caused in vanadium foils by the structure that is introduced by the rolling process and in indium-20% thallium monocrystalline wire by a martensitic transition resulting in parallel twin boundaries. Flux motion gives rise to a noise voltage due to the quantized nature of the moving flux. The power spectra have a cut-off frequency determined by the transit time of the flux. Measured power spectra are in reasonable agreement with theory, if it is assumed that there is a transit-time distribution. In type-II superconductors the flux moves as bundles of vortex lines. The size of the bundles decreases with increasing temperature, current density and magnetic field and after annealing. In type-I superconductors the noise is associated with the voltage component caused by flux motion and not with the voltage component caused by ohmic loss in immobile normal domains. At low fields the dependence of noise on external parameters is similar to type-II superconductors. At higher fields normal domains increase in size with increasing temperature, current density and field. Noise is also caused by temperature fluctuations associated with nucleate boiling in liquid helium I or pressure oscillations above liquid helium II.

CONTENTS

1. INTRODUCTION 1
   1.1. Type-I superconductors; intermediate state 1
   1.2. Type-II superconductors; mixed state 4
   1.3. Noise in the intermediate and mixed states 6
      1.3.1. Introduction 6
      1.3.2. Magnetic measurements 7
      1.3.3. Electric measurements 7
   1.4. Motivation and outline of the present work 8

2. THEORY OF FLUX MOTION IN SUPERCONDUCTORS . . 10
   2.1. The electric field due to flux flow in type-II superconductors . . 10
   2.2. The equation of motion of a vortex line 16
   2.3. Flux flow in the presence of pinning 18
   2.4. Flux creep 21
   2.5. Pinning mechanisms 22
   2.6. Flux flow in type-I superconductors 24

3. MEASUREMENTS OF FLUX-MOTION VOLTAGE IN TYPE-II SUPERCONDUCTORS 28
   3.1. Vanadium 28
      3.1.1. Material properties 28
      3.1.2. Specimens 29
      3.1.3. Flux-flow voltage 30
      3.1.4. Critical current density 34
      3.1.5. Conclusions 37
   3.2. Indium-thallium 37
      3.2.1. Material properties 37
      3.2.2. Specimens 38
      3.2.3. Critical current density 40
      3.2.4. Grain-boundary pinning 42
      3.2.5. Conclusions 44

4. THEORY OF FLUX-MOTION NOISE IN SUPERCONDUCTORS 45
   4.1. Fourier analysis of fluctuations 45
   4.2. Flux-flow noise 47
      4.2.1. Power spectrum of identical pulses 47
      4.2.2. Power spectrum of non-identical pulses 51

4.2.3. Flux-modulation noise 55
4.2.4. Other sources of noise 55
4.2.5. Noise in a Corbino disc 56
4.3. Johnson noise 56
4.4. Flicker noise 57

5. MEASUREMENTS OF FLUX-MOTION NOISE IN TYPE-II SUPERCONDUCTORS 61
5.1. Experimental methods 61
5.1.1. Experimental set-up 61
5.1.2. Measurements 64
5.2. Flux-flow noise in vanadium foils 65
5.2.1. Power spectra 65
5.2.2. Pinned flux fraction 72
5.2.3. Bundle size 74
5.2.4. Low-frequency noise reduction 80
5.2.5. Corbino disc 83
5.3. Flux-flow noise in indium-thallium 83
5.4. Flicker noise 85
5.4.1. Experiments in liquid helium I 85
5.4.2. Experiments in liquid helium II 90
5.5. Concluding remarks 92

6. MEASUREMENTS OF FLUX-MOTION NOISE IN TYPE-I SUPERCONDUCTORS 94
6.1. Experimental 94
6.2. Flux-flow noise-power spectra 95
6.3. Determination of the flux-flow voltage 99
6.4. Domain size 102
6.5. Concluding remarks 103

Acknowledgement 104

References 105

List of symbols 109

Summary 113

1. INTRODUCTION

In this thesis we are concerned with the presence of magnetic flux in superconductors. A magnetic flux through a surface is defined as the surface integral of the magnetic induction B, so we are dealing with the values of B in superconductors.

In a homogeneous superconductor the magnetic induction in zero magnetic field is zero. As regards the response to the application of a magnetic field H, superconductors are divided into two types, which are called type-I and type-II superconductors. In the first two sections of this chapter a brief description of these two types will be given. For a comprehensive treatment reference is made to monographs by Lynton [1]) and De Gennes [2]) and for earlier work (up to the fifties) to those by Shoenberg [3]) and London [4]).

Since in this thesis we are also dealing with the occurrence of a noise voltage due to variations of the local values of B in superconductors, we shall give in the third section a historical review of noise measurements on superconductors.

Finally, a motivation of the investigation and an outline of this thesis will be given in the last section.

1.1. Type-I superconductors; intermediate state

A type-I superconductor which is placed in a magnetic field with a strength below a critical value, has a zero magnetic induction. This phenomenon, the Meissner effect, is caused by a supercurrent flowing in a surface layer which shields the interior of the superconductor from the external field H. This current is often called the Meissner current and the thickness of the surface layer is called the penetration depth λ, which is defined as

$$\lambda = \frac{1}{H} \int_0^\infty H(z)\, \mathrm{d}z, \tag{1.1}$$

where z is the distance from the surface. The value of λ is of the order of 500 to 1000 Å.

The magnetic properties of a superconductor can formally be described in terms of an internal magnetic field H_i and a magnetic moment M per unit volume, which is written *) as $(B - H_i)/4\pi$, so that

$$M = -\frac{H_i}{4\pi}. \tag{1.2}$$

*) Gaussian units are used. Induction, field and flux will in the following denote magnetic quantities, unless otherwise stated.

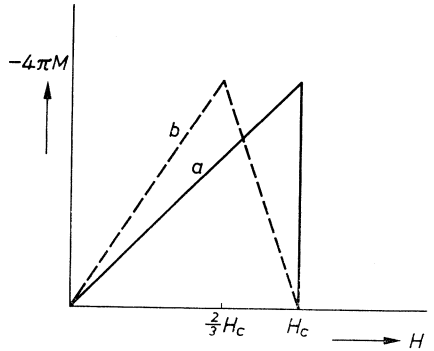

Fig. 1.1. Magnetization curves of a homogeneous type-I superconductor; a: without demagnetization, b: with demagnetization (sphere).

The Meissner effect persists for magnetic-field values up to the critical field H_c where magnetic flux suddenly penetrates and M drops to zero. The material goes over into the normal state by a first-order phase transition. The magnetization curve, which is reversible, is shown in fig. 1.1.

The difference between the Gibbs free energies per unit volume in the normal state and in the superconducting state in zero field is

$$-\int_0^{H_c} M \, \mathrm{d}H = \frac{H_c^2}{8\pi}. \tag{1.3}$$

The value of H_c is dependent on the temperature T and can be written approximately as $H_c = H_0 (1 - T^2/T_c^2)$, where H_0 is the critical field at $T = 0$ and T_c is the critical temperature in zero field.

The foregoing shows that in fields smaller than H_c there is no flux in a long type-I superconductor parallel to the field, so that demagnetization can be neglected.

If a superconductor is inhomogeneous the motion of flux into or out of the material may be hindered so that a situation of non-equilibrium arises. The magnetization curve then exhibits hysteresis and flux may be trapped when the field is returned to zero.

If the shape of the superconductor is such that demagnetizing effects cannot be neglected, the response to a magnetic field is different. A demagnetizing field has to be taken into account and the field at the surface of the superconductor is non-uniform. If the demagnetizing coefficient is N_d (for a sphere $N_d = 4\pi/3$), the field at the equator of a superconducting ellipsoid is written, using eq. (1.2),

$$H_i = \frac{H}{1 - N_d/4\pi}. \tag{1.4}$$

For $H_i = H_c$ the superconductor breaks up into a mixture of superconducting and normal domains. This new state is called the *intermediate state.* The magnetic field in the normal domains equals H_c and is zero in the superconducting domains. The fraction of normal material f_n is equal to B/H_c if B is the induction averaged over the sample. The magnetization curve is shown in fig. 1.1 for a sphere of homogeneous material. For a superconductor which has a non-zero demagnetizing coefficient in the field direction the relation given by eq. (1.3) still holds so that the areas under the curves in the figure are the same.

The structure of the intermediate state has first been studied theoretically by Landau [5]) who assumed that the normal and superconducting domains are layers parallel to the field direction and are arranged in a periodic manner with a periodicity d_i. For a slab with thickness d_0, which is much greater than d_i, minimization of the free energy of the system with respect to d_i yields the relation $d_i \propto {d_0}^{1/2} \Delta^{1/2}$, where Δ is the surface-energy parameter.

This parameter can be written as the difference between two characteristic lengths $\Delta = \xi - \lambda$, as suggested by Pippard [6]), where ξ is the coherence length. The coherence length is the distance from the surface over which the superconducting-electron concentration n_s is decreased relative to the value in the bulk by the application of a magnetic field, and it is of the order of 100 to 5000 Å. The surface energy per unit area of superconducting–normal boundary is

$$\sigma_{ns} = (\xi - \lambda) \frac{{H_c}^2}{8\pi} . \tag{1.5}$$

The structure of the intermediate state has recently been extensively investigated by experimental methods, mainly by Bitter techniques. Haenssler and Rinderer [7]) (who also gave a bibliography of earlier work) have shown for indium and tin discs that a laminar structure only arises when the intermediate state is reached by coming from the normal state. If the field is increased from zero, quite a different structure is observed. Flux is found to penetrate in the form of small cylinders or flux tubes, the size of which depends on the thickness of the specimen, being smaller for thinner specimens, as was shown by Träuble and Essmann [8,9]) on lead discs and foils. These flux tubes contain a number of elementary flux quanta $\varphi_0 = h\,c/2\,e$, ranging from a few tens to a few thousands. When the field is increased further a distribution of small and large normal domains of often meandering shapes could be seen. In general the cross-section of many normal domains becomes elongated when the field is increased. Haenssler and Rinderer, and Baird [10]) showed that flux tubes are nucleated in a surface layer where the flux density is higher than in the bulk. Träuble and Essmann found for a thin foil that at low fields the flux tubes are arranged in a regular manner as a triangular lattice.

1.2. Type-II superconductors; mixed state

We now turn to type-II superconductors and again assume them to be in the form of a long cylinder in a parallel field so that there is no demagnetization.

In low fields type-II superconductors also exhibit the Meissner effect. If the field is increased, flux penetration starts at a lower critical field H_{c1}, so that M is reduced. The flux penetration is complete at the upper critical field H_{c2} where a second-order phase transition to the normal state takes place. The magnetization curve is shown in fig. 1.2 for a homogeneous superconductor without hysteresis. A thermodynamic critical field can be defined as for type-I superconductors by

$$-\int_0^{H_{c2}} M \, \mathrm{d}H = \frac{H_c^2}{8\pi}. \tag{1.6}$$

The value of H_c is also shown in fig. 1.2. For fields $H_{c1} < H < H_{c2}$ the type-II superconductor is said to be in the *mixed state.*

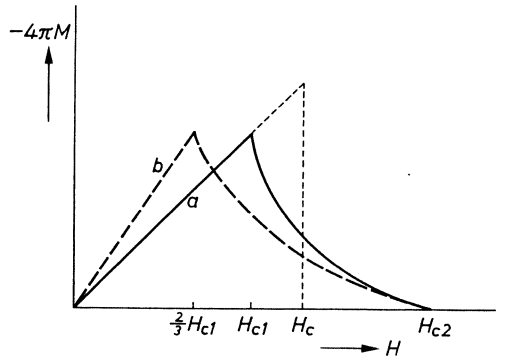

Fig. 1.2. Magnetization curves of a homogeneous type-II superconductor; a: without demagnetization, b: with demagnetization (sphere).

A surface layer parallel to the magnetic field with thickness of the order of ξ remains superconducting up to a critical field $H_{c3} = 1{\cdot}69\, H_{c2}$. In magnetization measurements this is usually not detected because of the small superconducting volume involved.

The criterion which determines whether a superconductor is of type I or of type II is the sign of the surface energy σ_{ns} of a boundary which separates the superconducting from the normal phase.

Type-I superconductors are characterized by a positive value of σ_{ns} which is given by eq. (1.5), because there $\xi > \lambda$ and type-II superconductors by a negative value of σ_{ns}, as $\xi < \lambda$.

It is therefore energetically unfavourable for a type-I superconductor to allow flux penetration, whereas for a type-II superconductor it is not.

Ginzburg and Landau [11]) have shown by a more detailed treatment that the sign of the surface energy depends on the value of a dimensionless parameter $\varkappa$. For $\varkappa < 2^{-1/2}$ the surface energy is positive and for $\varkappa > 2^{-1/2}$ it is negative. The value of $\varkappa$, which is a material constant, is given at temperatures close to T_c by

$$\varkappa = \frac{2^{3/2}\,\pi\, H_c\, \lambda^2}{\varphi_0}. \tag{1.7}$$

Ginzburg and Landau introduced an order parameter Ψ, normalized by taking $|\Psi|^2 = n_s$. The distance over which Ψ is changed by the application of a magnetic field is in their theory $2^{-1/2}\,\lambda\,/\varkappa$ which is to be identified with ξ.

The value of the upper critical field is given by

$$H_{c2} = 2^{1/2}\,\varkappa\, H_c. \tag{1.8}$$

It is customary to denote $\varkappa$, when defined by this relation, by $\varkappa_1$. It is weakly temperature-dependent and has experimentally been found to decrease from $T \approx 0$ to $T = T_c$ by about 30%.

In an impure superconductor, if the electron mean free path l_e is much smaller than the coherence length ξ_0 for the pure material, the values of λ, ξ and $\varkappa$ are dependent on l_e and can be written for $T \approx T_c$, as shown by Gor'kov [12]) and Caroli et al. [13]),

$$\lambda \propto \lambda_L(0)\,(\xi_0/l_e)^{1/2}, \tag{1.9}$$

$$\xi \propto (\xi_0\, l_e)^{1/2}, \tag{1.10}$$

$$\varkappa \propto \lambda_L(0)/l_e, \tag{1.11}$$

where $\lambda_L(0)$ is the penetration depth at zero temperature and zero field, which was earlier introduced by London.

Goodman [14]) has shown that $\varkappa$ can be written, if $l \ll \xi_0$,

$$\varkappa = \varkappa_0 + 7{\cdot}5.10^3\, \gamma_e^{1/2}\, \varrho_n, \tag{1.12}$$

where $\varkappa_0 = \lambda_L(0)/\xi_0$ is the value for pure material, γ_e is the electronic-specific-heat coefficient (in ergs/cm^3 °K^2) and ϱ_n is the residual resistivity (in Ω cm).

The mixed state has been described by Abrikosov [15]) who showed that the magnetic flux is contained in circulating supercurrents or vortices each enclosing one flux quantum φ_0. It was suggested that these vortices are arranged in a regular manner so that they make up a lattice of vortex lines (also called flux lines) that are extended in the field direction. The existence of such a lattice has been verified experimentally from neutron-diffraction experiments by Cribier et al. [16]) and electron microscopy of a refined Bitter technique by Essmann and Träuble [17]). The lattice was found to be triangular as had earlier

been predicted by Kleiner et al. [18]). In this vortex lattice the same types of defects are present as are found in a crystal lattice [19]).

A vortex line can be considered as a normal cylindrical core of radius a, which is of the order of ξ, around which supercurrents flow over a distance λ from the core. Properties of a single vortex line and of a system of vortex lines have been calculated for $\lambda \gg \xi$. A discussion of these properties has been given by Van Vijfeijken [20]).

The energy of a vortex line is composed of kinetic and magnetic energy outside the core and the condensation energy of the core region. This latter contribution can be written as $(H_c^2/8\pi)\,\pi a^2$ per unit length. The energy outside the core per unit length of vortex line (for $\lambda \gg \xi$) is

$$\varepsilon = \left(\frac{\varphi_0}{4\pi\lambda}\right)^2 \ln(\lambda/a). \tag{1.13}$$

The core condensation energy is of the order of $0{\cdot}3/\ln\varkappa$ times the energy outside the core and is therefore negligible for large values of $\varkappa$.

The lower critical field H_{c1} is given by equating the energy increase ε by the creation of a vortex line to the decrease in magnetic energy $\varphi_0 H/4\pi$ by the penetration of a flux φ_0. It follows then with eq. (1.13)

$$H_{c1} = \frac{\varphi_0}{4\pi\lambda^2} \ln(\lambda/a). \tag{1.14}$$

When a type-II superconductor is not in the form of a long thin cylinder in a parallel field, demagnetization affects the magnetization curve in a similar way as for a type-I superconductor, as is drawn in fig. 1.2. This demagnetization, however, does not now give rise to a new state but simply to an extension of the mixed state to lower external-field values. The flux penetrates as vortex lines which contain one flux quantum and which are arranged in a triangular lattice. This lattice was found [21]) to be much more disturbed than in the mixed state without demagnetization.

Thin films of type-I superconductors [22,23]) in a perpendicular field also exhibit properties of the mixed state at induction values below a certain level, depending on $\varkappa$. For higher values of $\varkappa$ this mixed state is found for larger inductions and thicker films. This behaviour is only found with films thinner than about 1 μ.

In this thesis the mixed state denotes the state with single-quantum vortex lines and the intermediate state the state with normal domains with bigger quantum number (flux tubes in low fields).

1.3. Noise in the intermediate and mixed states

1.3.1. *Introduction*

The apparent absence of fluctuations in the Meissner state has been demonstrated by Knol

and Volger [24]) and by Fink and Zacharias [25]), who could not detect any noise component on a persistent current at 5·6 MHz and 5·5 GHz, respectively.

Magnetic and electric measurements on superconductors have revealed the presence of noise in the intermediate and mixed states. For the magnetic measurements the superconductor was usually placed in a varying magnetic field and an induction voltage due to the change of magnetic flux in the superconductor was measured over a pick-up coil around the specimen. For the electric measurements a transport current was supplied to the superconductor and a voltage measured across two potential probes.

These two types of voltage were often reported to be fluctuating. In this section we shall give a brief review of these experiments. We shall ignore some other types of fluctuations that have recently received attention. These include thermodynamic fluctuations of the superconducting-order parameter which causes a broadening of the superconducting transition in quasi-one- and two-dimensional superconductors, the effect of thermodynamic fluctuations on superconducting tunnelling junctions and weak links and fluctuations between quantum states in superconducting loops. For reports on this work the reader is referred to conference proceedings [26,27]).

1.3.2. *Magnetic measurements*

The first attempts to measure noise due to random penetration of flux were reported by Schubnikov and co-workers [28]) in 1936. They had tried to observe the superconducting analogue of Barkhausen noise due to the phase transition in Pb, but as their detection was not sensitive enough they could not measure this phase-transition noise. Six years later Justi [29]) succeeded in detecting this noise close to the critical temperature in NbN and Nb and, by varying the external field, showed that the noise was present in the intermediate state of Sn. The experiments by Van Ooijen and Druyvesteyn [30]) on Pb-In wires showed that phase-transition noise was also present in the mixed state. From the analysis of noise measurements on a search coil around a hollow Sn cylinder in a linearly increasing field, Van Ooijen [31]) concluded that flux penetrated as single flux quanta φ_0, except at low temperatures where many quanta penetrated at the same time. Similar results were obtained by Boata et al. [32]) for a Pb-Tl wire.

In type-II superconductors, where flux penetration is hindered and delayed due to pinning of vortex lines by inhomogeneities, flux gradients arise when the field is varied. These may become so great that when flux starts to penetrate under this influence, heat will be dissipated and more vortex lines will be depinned. This leads to a catastrophic transport of flux accompanied by a considerable rise in temperature. This phenomenon which is called a flux jump, causes large voltage fluctuations in a pick-up coil around the specimen. The problem of flux jumps is very complicated and involves thermal phenomena in the superconductor on which few quantitative analyses [33]) have been carried out as yet. Measurements of voltage fluctuations by Wischmeyer [34]) on Nb-Zr tubes have shown, however, that localized flux motion may be observed in a varying magnetic field without a catastrophic flux jump. This motion involves bundles of about 100 vortex lines.

Recently Heiden and Rochlin [35]) measured flux penetration into Pb-In wires and found that this took place in bundles of vortex lines containing from 10 to 10^4 quanta depending on the value of the magnetic field. By placing two pick-up coils around a specimen at a variable distance Heiden [36]) also measured the correlation between the signals from the two coils and from this the average length of a penetrating flux bundle.

So far we have reviewed experiments with a specimen placed in a varying magnetic field. Kim and co-workers [37]) measured voltage fluctuations in a pick-up coil inside or outside a Nb-Zr tube with the magnetic field kept constant after it had been switched on. In these experiments vortex lines were moving under the influence of a flux gradient. This motion was found to occur in bundles greater than 20 to 50 flux quanta. The number of voltage pulses decreased with time and became inobservably small.

1.3.3. *Electric measurements*

Resistance fluctuations in Sn and Ta wires, when current, field or temperature were varied, were reported by Silsbee et al. [38]).

In an attempt to reproduce these results, Misener [39]) found large spontaneous resistance fluctuations in a Ta wire even when the field was held constant. As these fluctuations were not found in annealed Ta wire they were considered to be a secondary effect. Resistance fluctuations were also found by Andrews et al. [40]) in NbN foil and by Webber [41]) in Ta on cooling the specimens through the superconducting transition. Webber also found that the amplitude of the fluctuations was diminished after annealing the Ta. Irregular resistance

changes of Sn wire were observed by Galkin et al. [42]) in the current-induced transition, which disppeared in a longitudinal magnetic field. The effects were ascribed to the complicated kinetics of growth of superconducting or normal nuclei.

A phenomenon closely related to these fluctuations is the appearance of discrete resistance levels in the superconducting transition. This was observed by Andrews [40]) on NbN, by Love [43]) on very thin wires of Sn, In and Tl and by Kaplan [44]) on an unannealed Ta wire. Kaplan measured the noise spectrum between 250 and 4000 Hz when a transport current was applied. His results show approximately a $1/f$ spectrum. At constant frequency the noise power was roughly proportional to the square of the current. Kaplan showed that the noise could not be due to temperature fluctuations of the specimen as a whole and suggested that it was due to fluctuations of the domain structure of the intermediate state. Resistance levels were also measured in Ta by Baird [45]), who studied low-frequency transitions between the levels. He suggested that the resistance fluctuations and the resistance levels were due to the motion of normal–superconducting domain boundaries between preferred poistions due to imperfections in the superconductor. This explanation is in agreement with the effect of annealing on the fluctuations. The transitions between the resistance levels could be triggered by temperature fluctuations in the helium bath. Step structure of the resistance and related fluctuations were also reported by Lalevic [46]) on inhomogeneous V, Ta and Sn and by Johnson and Chirlian [47]) on Sn films. The last-named found that the noise disappeared when the specimen was cooled through the He λ point and they came to the same conclusion as Baird.

Recently, resistance levels were again reported by Warburton and Webb [48]) on Sn whiskers and by Cape and Silvera [49]) on In-Bi foils. Rochlin [50]) showed that the power spectrum of the fluctuations between levels followed a $(1 + 4\pi^2 f^2 \tau^2)^{-1}$ law in Al films.

The experiments show that in the case of inhomogeneous materials and probably also in specimens with surface irregularities, superconducting–normal domain boundaries may undergo random motion between preferred positions. These transitions are triggered by external causes and cause resistance fluctuations.

1.4. Motivation and outline of the present work

The investigation, the results of which are presented here, was started in 1964 to study the mechanism of voltage generation in a current-carrying type-II superconductor in the mixed state or a type-I superconductor in the intermediate state. This was supposed to be due to motion of vortex lines and normal domains, respectively, as a result of interaction between a transport current and these vortex lines or normal domains, giving rise to a Lorentz force. For this motion we shall use the general term flux motion. It had been reported, as outlined in the previous section, that flux penetration into (or expulsion from) a superconductor is a random process, giving rise to voltage fluctuations. It was therefore thought that, if there is flux motion in a superconductor due to a transport current, voltage fluctuations might then also be present. Such fluctuations superposed on the d.c. voltage, should contain information on the process of this motion. A combination of d.c. measurements and measurements of noise and its power spectrum would be a means of studying the mechanism of flux motion and the hindrance to this motion due to imperfections in the material. The investigation started with experiments on type-II superconductors, because the structure of the mixed state is much more regular than that of the intermediate state and because a fair amount of theoretical work had already been done on the mixed state.

We shall first briefly summarize in chapter 2 some existing theories on flux motion in type-II and type-I superconductors and give the results of these theories where relevant to our experiments.

Chapter 3 deals with measurements of d.c. voltage and critical transport currents for vortex-line motion on a number of type-II superconductors. The results of these experiments throw some light on the phenomenon of pinning of vortex lines by imperfections in the investigated materials. The theory of noise due to flux motion across a superconductor is dealt with in chapter 4, in which various types of noise are described. Noise experiments on type-II superconductors are reported in chapter 5 and compared with the theory. Finally chapter 6 concerns noise due to flux-domain motion in type-I superconductors which is also compared with the theory.

2. THEORY OF FLUX MOTION IN SUPERCONDUCTORS

If a superconductor is in the mixed or intermediate state and the magnetic field or the temperature vary, the distribution of flux-containing vortex lines or normal domains is a function of time. The local values of B are then not constant and there is motion of flux. This motion also takes place when a transport current is applied and is then caused by the interaction of the current with the vortex lines or the normal domains. Shoenberg [51]) was the first to point this out for the laminar intermediate state and Gorter [52]) showed that the vortex lines in the mixed state are subject to a driving force, which is usually denoted as the Lorentz force.

In this chapter we shall briefly summarize some existing theories on the motion of flux in superconductors. They give expressions for the average electric field in the superconductor due to viscous motion of flux, which is called flux flow. We will first treat flux flow in the mixed state of type-II superconductors and discuss the electric field. Next the equation of motion of a vortex line in the presence of a transport current will be given. As regards this equation, the theories give somewhat conflicting results, which is not surprising in view of the different starting points.

The influence of lattice irregularities on the flux transport will be considered. These irregularities (dislocations, grain boundaries, precipitates, etc.) are able to pin vortex lines so that the driving force is counteracted by a pinning force and no flux motion takes place below a certain threshold value of the transport-current density.

At small values of the current density flux motion is described as thermally activated hopping of bundles of vortex lines over pinning barriers (flux creep).

Several mechanisms for the pinning of vortex lines have been proposed. These pinning mechanisms, which may work in parallel, will be reviewed briefly.

In the last section of this chapter the problem of flux flow in the intermediate state of type-I superconductors will be discussed.

2.1. The electric field due to flux flow in type-II superconductors

The motion of vortex lines has been treated in phenomenological theories by Bardeen and Stephen [53]), Van Vijfeijken and Niessen [54]) (later modified by Van Vijfeijken [20])), and by Nozières and Vinen [55]). These theories are local theories, not taking into account coherence effects. They assume that the vortex lines can be considered to have no interaction with each other, which means that the external field is much smaller than the upper critical field H_{c2}. The normal electrons outside the cores are neglected, i.e. the temperature T is assumed to be much smaller than T_c. It is also assumed that there is no pinning, so that the vortex lines can move freely.

In the theories of Van Vijfeijken and Niessen (hereafter called V) and of Nozières and Vinen (hereafter called NV) the superconducting-electron concentration n_s is assumed to jump discontinuously from the zero value inside the core with radius a to the equilibrium value outside it. The theory of Bardeen and Stephen (hereafter called BS) assumes that this transition of n_s occurs over a distance of the order of a in a transition region outside the core. Further differences concern the field dependence of a. In the V theory a field-independent core radius is assumed as given by $\varphi_0 = H_{c2}\,\pi\,a^2$, whereas in the BS and NV theories a has a value between that given by $\varphi_0 = H_{c2}\,\pi\,a^2$ close to H_{c2} and $\varphi_0 = 2\,H_{c2}\,\pi\,a^2$ at very low fields.

The vortex lines are considered to move with a velocity $\mathbf{v}$. This motion may be caused by interaction of a transport-current density $\mathbf{J}$ with the vortex lines [56]), by a temperature gradient in the sample [57]), or by a coupling of the vortex lines to moving vortex lines in another superconductor [58]). In what follows it is assumed that a transport current flows.

We consider a type-II superconductor in the form of a slab in a magnetic field perpendicular to the broad surface.

The theories take their starting point in the hydrodynamic equation of motion for the superfluid per unit volume outside the vortex core

$$n_s\,m\,\frac{\mathrm{d}\mathbf{v}_s}{\mathrm{d}t} = n_s\,e\,\mathbf{e} + \frac{n_s\,e}{c}\,(\mathbf{v}_s \times \mathbf{b}). \tag{2.1}$$

In this equation, where all symbols are used for local quantities, $\mathbf{v}_s$ is the superfluid velocity, $\mathbf{e}$ is the electric field, $\mathbf{b}$ is the induction, m is the electron mass, $e = -1{\cdot}6.10^{-19}$ C is the electronic charge.

By writing

$$\frac{\mathrm{d}\mathbf{v}_s}{\mathrm{d}t} = \frac{\partial \mathbf{v}_s}{\partial t} + (\mathbf{v}_s \cdot \mathrm{grad})\,\mathbf{v}_s = \frac{\partial \mathbf{v}_s}{\partial t} + \tfrac{1}{2}\,\mathrm{grad}\,\mathbf{v}_s^2 - \mathbf{v}_s \times \mathrm{curl}\,\mathbf{v}_s \tag{2.2}$$

and using the Londons' equation

$$\mathrm{curl}\,\mathbf{v}_s = -\frac{e\,\mathbf{b}}{m\,c}, \tag{2.3}$$

it follows that

$$m\,\frac{\partial \mathbf{v}_s}{\partial t} = -\tfrac{1}{2}\,m\,\mathrm{grad}\,\mathbf{v}_s^2 + e\,\mathbf{e}. \tag{2.4}$$

We introduce now the generalized electrochemical potential μ per particle, outside the core, which is written as

$$\mu = \mu_0 + \tfrac{1}{2}\,m\,\mathbf{v}_s^2 + e\,\phi, \tag{2.5}$$

where μ_0 is the chemical potential per particle which is spatially constant at $T = 0$ and ϕ is the electrostatic potential.

The general expression for **e** is

$$\mathbf{e} = -\text{grad}\,\phi - \frac{1}{c}\frac{\partial \mathbf{a}}{\partial t}, \tag{2.6}$$

where **a** is the vector potential.
We obtain from eqs (2.4) to (2.6) for the driving force on the electrons outside the core

$$m\frac{\partial \mathbf{v}_s}{\partial t} = -\text{grad}\,\mu - \frac{e}{c}\frac{\partial \mathbf{a}}{\partial t}. \tag{2.7}$$

The assumption is now made that $\mathbf{v}_s$ can be written as the sum of the circular vortex velocity $\mathbf{v}_v$, which is not changed by the movement, and the imposed velocity $\mathbf{v}_i$, which is assumed to be constant in space and in time, as shown in fig. 2.1. Similarly **a** is written as the sum of corresponding components $\mathbf{a}_v$ and $\mathbf{a}_i$. In the steady state all time-dependent quantities can be written as functions of $(\mathbf{r} - \mathbf{v}\,t)$, where **r** is the space vector and **v** is the vortex velocity.

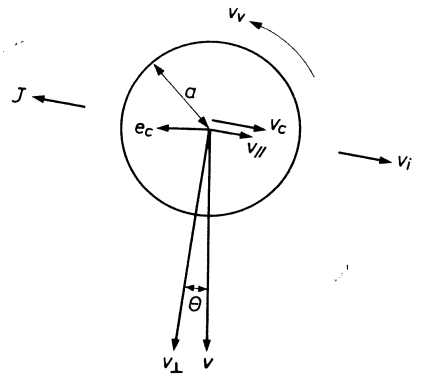

Fig. 2.1. Geometry used in the discussion of vortex motion. The vortex with core radius a has a circular velocity field $\mathbf{v}_v$. The induction in the core is directed into the paper. The imposed transport velocity $\mathbf{v}_i$ (current density **J**) perpendicular to **b**, causes the vortex to flow with velocity **v**, with components $\mathbf{v}_{\parallel}$ and $\mathbf{v}_{\perp}$ parallel and perpendicular to $\mathbf{v}_i$ respectively. This motion gives rise to an electric core field $\mathbf{e}_c$ which in the BS and V theories is perpendicular to **v**. The Hall angle θ is assumed to be small. This means that $\mathbf{v} \gg \mathbf{v}_i$, as discussed in the text.

From the expression of the canonical momentum $\mathbf{p}_v$ of the centre of mass of a superconducting-electron pair,

$$\mathbf{p}_v = 2\,m\,\mathbf{v}_v + \frac{2\,e}{c}\mathbf{a}_v, \tag{2.8}$$

and eq. (2.7) it follows that

$$\text{grad}\,\mu = \tfrac{1}{2}\,(\mathbf{v}.\,\text{grad})\,\mathbf{p}_v = \tfrac{1}{2}\,\text{grad}\,(\mathbf{v}.\,\mathbf{p}_v). \tag{2.9}$$

because curl $\mathbf{p}_v = 0$ outside the core.

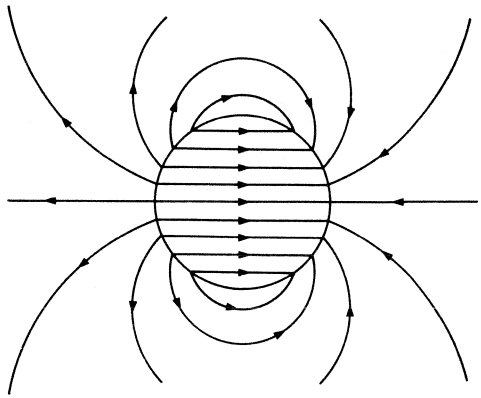

Fig. 2.2. Direction of the driving force on the electrons due to the electrochemical-potential gradient grad μ, in and close to the vortex core caused by vortex motion in a vertical direction corresponding to fig. 2.1 (after Bardeen and Stephen [53]).

Equation (2.9) determines grad μ in the velocity field outside the vortex core. Figure 2.2 shows the grad μ lines, in the neighbourhood of the core. The value of $(\mathbf{v} \cdot \mathbf{p}_v)$ is zero there where the momentum $\mathbf{p}_v$ is perpendicular to the vortex velocity $\mathbf{v}$ so that grad μ is zero in the direction parallel to $\mathbf{v}$. The second term on the right-hand side of eq. (2.7) is much smaller than grad μ close to the core.

In the V and BS theories the assumption is made that the electrochemical potential μ is continuous at the core boundary, so that the electrons there are treated as being in local thermodynamic equilibrium with the lattice. It is then shown that this implies a contact potential at the core boundary which possesses cylindrical symmetry apart from a term $m\,(\mathbf{v}_v \cdot \mathbf{v}_i)/e$. In the BS theory it is shown from a consideration of the dissipation in the core and in the transition region that the electron drift velocity in the core $\mathbf{v}_c$ is equal to the imposed transport velocity $\mathbf{v}_i$ so that the transport current can be treated as a uniform current everywhere. In the V and NV models this is assumed to be also valid and it is made plausible by noting that this distribution corresponds to a minimum kinetic energy. The transport current is driven through the normal core by the electric field in the core which is caused by the motion. For the core region the electrochemical potential is written as

$$\mu_c = \mu_{c0} + \tfrac{1}{2} m \mathbf{v}_i^2 + e \phi_c, \tag{2.10}$$

where the index c denotes quantities in the core.

The uniform current in the core implies a uniform grad ϕ_c, the value of which follows from the continuity of μ at the core boundary.

The direction of grad μ_c, which is perpendicular to the line velocity $\mathbf{v}$, is also indicated in fig. 2.2.

In the NV theory the assumption of continuity of μ at the core boundary is questioned, because vortex motion is a dissipative process so that local thermo-

dynamic equilibrium is doubtful. Nozières and Vinen therefore made a different assumption, namely that the vortex motion does not cause an extra contact potential at the core boundary.

We will now give the expression for the electric field.

Equation (2.6) is written

$$\mathbf{e} = -\text{grad}\ \phi + \frac{1}{c}\,\text{grad}\ (\mathbf{v}\ .\ \mathbf{a}_v) - \frac{1}{c}(\mathbf{v}\times\mathbf{b}), \tag{2.11}$$

where $\mathbf{b} = \text{curl}\ \mathbf{a}_v$. Equation (2.11) is the general expression, valid both inside and outside the core.

For the region outside the core we can write the grad ϕ term, using eq. (2.5),

$$-\text{grad}\ \phi = \frac{1}{2\,e}\,\text{grad}\ (m\,\mathbf{v}_s^2) - \frac{1}{e}\,\text{grad}\ \mu. \tag{2.12}$$

The first term on the right gives rise to a contact potential at the core boundary, as can be shown for the BS and V theories, and does not contribute to a potential difference as measured with a voltmeter. Van Vijfeijken showed that the remaining term in eq. (2.12) gives no contribution when averaged over a unit cell of the vortex lattice.

For the core region we can write

$$\text{grad}\ \phi_c = \frac{1}{e}\,\text{grad}\ \mu_c, \tag{2.13}$$

as follows from eq. (2.10) since the first two terms on the right-hand side are spatially constant.

It was also shown that the contributions of grad ϕ_c in the core and of grad $(\mathbf{v}\ .\ \mathbf{a}_v)$ in and outside the core to $\mathbf{e}$, when averaged over a unit cell, cancel each other, so that we are left with the contribution of $-(\mathbf{v}\times\mathbf{b})/c$. If we write $\mathbf{B}$ as the induction, averaged over a unit cell, we obtain for the average electric field the simple expression

$$\mathbf{E} = -\frac{1}{c}(\mathbf{v}\times\mathbf{B}). \tag{2.14}$$

In fields close to H_{c2} where the unit cell is given by $\pi\,a^2$, the electric field is equal to that in the core $\mathbf{e}_c$. In low fields, if $b_c \ll H_{c2}$, the core and the outside region can be shown to give equal contributions to the measured electric field. As it was assumed that there are no normal electrons outside the core, only the electric-field contribution of the core is dissipative.

In the NV theory the contributions to grad ϕ outside and inside the core are different from the BS and V theories, but eq. (2.14) is also obtained.

The three theories reviewed so far are basically low-field theories valid near $T = 0$. Kulik [59]) and Schmid [60]) have shown that eq. (2.14) is also valid at

fields close to H_{c2} for temperatures close to T_c. This treatment was generalized by Caroli and Maki [61]) to arbitrary temperatures.

The foregoing discussion has shown that there is flux motion in a certain direction if a transport current is flowing through the superconductor. For a finite specimen this would mean that on one side of the superconductor the flux concentration is lowered and on the opposite side it is increased. The vortex density in the superconductor would therefore no longer be in local equilibrium with the external magnetic field on either side. Equilibrium can be maintained, however, by creation of vortices on one side and their annihilation on the other side. The creation of new vortices can take place by introversion of the Meissner current and subsequent splitting off, as illustrated in fig. 2.3. On the opposite

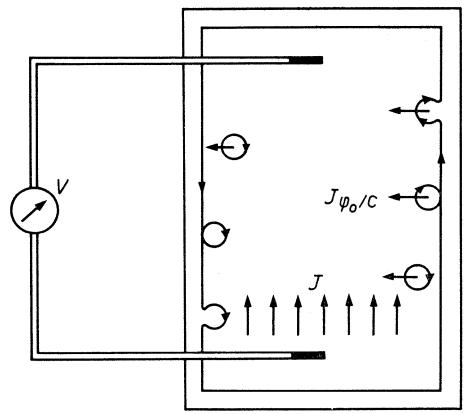

Fig 2.3. Creation and annihilation of vortices on two sides of a superconductor by introversion of the Meissner current. The magnetic field is directed into the paper and the transport-current density J gives rise to a driving force $J\,\varphi_0/c$. Due to the transit of vortices a voltage is measured on the voltmeter.

side of the superconductor the reverse process takes place. Interaction with the Meissner current which, on this side, flows in the other direction, causes the vortex to open on one side so that the circulating current dies out and the flux inside it is annihilated. The flux is contained within supercurrent vortices as long as these circulating currents flow. In this picture the flux in the superconductor remains constant.

The fact that the total flux in the circuit that is formed by the superconductor and the voltmeter should be constant, has in the past caused some confusion. Jones et al. [62]) pointed out that the measured electric field could therefore not be an induction field, as the total magnetic flux in the circuit is constant. Josephson [63]) showed that in this experimental situation $\mathbf{E} = -(\mathbf{v}\times\mathbf{B})/c$ is indeed not an inductive electric field in the usual sense, but is due to the potential difference between two points in the superconductor, caused by the motion of flux across a line connecting the two points.

2.2. The equation of motion of a vortex line

We will now give the equation of motion for the vortex lines. This is derived from the hydrodynamic equation for the electrons in the normal core with concentration n for the stationary state:

$$n\,e\,\mathbf{e}_c + \frac{n\,e}{c}(\mathbf{v}_i \times \mathbf{b}_c) - \frac{n\,m\,\mathbf{v}_i}{\tau_n} = 0. \tag{2.15}$$

The relaxation time τ_n is assumed to be that of the normal metal. Bardeen and Stephen have pointed out that this assumption can also be used when the electron mean free path is larger than the core diameter because the term $m\,\mathbf{v}_i/\tau_n$ should be considered as an average over all electrons going through the core.

The equation of motion is derived from the expressions for the electric core field $\mathbf{e}_c$.
In the BS theory:

$$\frac{e}{c}(\alpha\,\mathbf{v}_i - \mathbf{v}) \times \mathbf{H}_{c2} - \frac{m\,\mathbf{v}_i}{\tau_n} = 0, \tag{2.16}$$

in the V theory:

$$\frac{e}{c}(\alpha\,\mathbf{v}_i - \beta\,\mathbf{v}) \times \mathbf{H}_{c2} - \frac{m\,\mathbf{v}_i}{\tau_n} = 0, \tag{2.17}$$

in the NV theory:

$$\frac{e}{c}(\mathbf{v}_i - \mathbf{v}) \times \mathbf{H}_{c2} - \frac{m\,\mathbf{v}_i}{\tau_n} = 0, \tag{2.18}$$

with $\alpha = b_c/H_{c2}$ and $\beta = (\alpha + 1)/2$.

The difference between (2.16) and (2.17) is caused by the different field dependence of the core radius a in the BS and V theories. Near H_{c2}, where the two models have the same value for a, the two equations are identical. The difference between (2.16) and (2.18) is due to the different assumptions concerning the core boundary. In the BS theory a contact potential, due to the motion, exists at the boundary which gives rise to an electrostatic force on the electrons in the normal core, localized at the interface. This force is absent in the NV model so that the total force on the core electrons is different in the two models [55]).

The equations give the relation between the transport-current density $\mathbf{J} = n_s\,e\,\mathbf{v}_i$ and $\mathbf{v}$. Together with eq. (2.14) they give the resistivity and the Hall effect.

Table I gives the expressions for the components $v_\perp$ and $v_\parallel$ of the vortex velocity perpendicular and parallel to the transport velocity, respectively, the

flow resistivity ϱ_{fl} defined as dE/dJ and the Hall angle θ, for which $\tan\theta = v_{||}/v_{\perp} = E_{\perp}/E_{||}$, where $E_{||}$ and $E_{\perp}$ are the parallel and perpendicular components of the electric field. Further ϱ_n is the normal-state resistivity and $\Gamma = e H_{c2} \tau_n/m c$.

TABLE I

Vortex-line-velocity components, flux-flow resistivity and Hall effect as given by three theories; $\alpha = b_c/H_{c2}$, $\beta = (\alpha + 1)/2$, $\Gamma = e H_{c2} \tau_n/m c$

	BS	V	NV
$v_{\perp}$	v_i/Γ	$v_i/\beta\Gamma$	v_i/Γ
$v_{||}$	αv_i	$\alpha v_i/\beta$	v_i
ϱ_{fl}	$\varrho_n B/H_{c2}$	$\varrho_n B/\beta H_{c2}$	$\varrho_n B/H_{c2}$
$\tan\theta$	$\alpha\Gamma$	$\alpha\Gamma$	Γ

The results for ϱ_{fl} which are essentially the same for the three models are in agreement with experimental results [56]) which show that ϱ_{fl}/ϱ_n at low temperatures is a linear function of B/H_{c2}. The results for the Hall effect for the BS and V models is different from the NV result and are all generally in disagreement with experiment, especially for alloys where $\tan\theta$ increases with decreasing field [64]) or may even change sign [65]). Recently Weijsenfeld [65]) has shown that the results of the BS and V theories can be made to agree very well with the experimental values of θ in alloys, if the normal electron relaxation time τ_n is replaced by a pairing-depairing relaxation time τ_g, when $\tau_g \gg \tau_n$. This is a relaxation time for the electrons entering and leaving the core which was originally proposed by Tinkham [66]). It is determined by the rate at which the energy gap for the superconducting-electron pairs returns to the equilibrium value. In order to get a core conductivity that is the same as in the normal state, one has to assume a decreased carrier concentration in the core. Vinen and Warren [67]) had earlier modified the NV theory and introduced a similar relaxation time in the NV equation of motion.

In this thesis we are only concerned with impure materials for which Γ is of the order of 10^{-3} to 10^{-2}. This implies that the Hall effect can be neglected. Since then $v_{\perp} \gg v_{||}$ the vortex velocity is practically perpendicular to and very much larger than $\mathbf{v}_i$, as illustrated in fig. 2.1. This simplifies the equations of motion which can now be written for the V theory:

$$-\frac{e}{c}\beta\,\mathbf{v}\times\mathbf{H}_{c2} - \frac{m\,\mathbf{v}_i}{\tau_n} = 0, \tag{2.19}$$

and for the BS and NV theories:

$$-\frac{e}{c}(\mathbf{v}\times\mathbf{H}_{c2})-\frac{m\,\mathbf{v}_i}{\tau_n}=0. \tag{2.20}$$

One can write for the balance of forces per unit length of vortex line

$$\frac{1}{c}(\mathbf{J}\times\boldsymbol{\varphi}_0)=\eta\,\mathbf{v}. \tag{2.21}$$

The force on the left is the Lorentz force which is exerted by a uniform transport-current density **J**. The term on the right is a viscous-damping force, which is proportional to the vortex-line velocity. The proportionality constant is the viscosity coefficient η. Using eq. (2.20) one can show that at $T=0$

$$\eta=\frac{\varphi_0\,H_{c2}}{\varrho_n\,c^2}. \tag{2.22}$$

The Joule power, dissipated in the core per unit length of vortex line, can be written as

$$P_J=\frac{n\,m\,v_i^2}{\tau_n}\,\pi\,a^2. \tag{2.23}$$

The total power dissipated to the lattice is given by $P_t=\eta\,v^2$. It can be verified that $P_t=2\,n\,m\,v_i^2\,\pi\,a^2/\tau_n$ at low fields and $P_t=n\,m\,v_i^2\,\pi\,a^2/\tau_n$ close to H_{c2}. Apparently there is another cause of power dissipation at low fields apart from that by Joule heating. In the V and NV models this is due to the momentum which crosses the core boundary and which is assumed to cause power dissipation in the core. This is equal to P_J as was shown by NV. In the BS model the extra power dissipation occurs in the transition region outside the core.

In all these models it is assumed that $T\ll T_c$ so that friction occurs only in the vortex core or in the transition region (BS). At higher temperatures there will be additional dissipation in between the vortices because of the normal electron concentration, as was first pointed out by Volger et al. [68]).

2.3. Flux flow in the presence of pinning

In the previous section the vortices were considered to be moving in a homogeneous viscous medium, which means that there is a vortex velocity for any non-zero value of the driving force. It was assumed that the electron drift velocity in the core $\mathbf{v}_c$ is equal to the imposed transport velocity $\mathbf{v}_i$. If the material is inhomogeneous, the vortex lines may be pinned at inhomogeneities against the driving force.

If they are pinned rigidly, the transport current does not flow through the cores and $\mathbf{v}_c=0$. Consequently there is no dissipation. If there is pinning but

the driving force is greater than the pinning force, there is a non-zero value of $\mathbf{v}_c$, which is smaller than $\mathbf{v}_i$.

Nozières and Vinen have derived the equation of motion, using their model, which is for this case

$$\frac{e}{c}(\mathbf{v}_c - \mathbf{v})\times\mathbf{H}_{c2} - \frac{m\,\mathbf{v}_c}{\tau_n} = 0. \tag{2.24}$$

In the case of no pinning when $\mathbf{v}_c = \mathbf{v}_i$ this equation reduces to eq. (2.18). In the case of complete pinning when $\mathbf{v}_c = 0$ it follows that $\mathbf{v} = 0$. There is then no flux motion.

They derived for the average pinning force per unit length $\mathbf{F}_p$ acting on the core:

$$\mathbf{F}_p = -\frac{n\,e}{c}(\mathbf{v}_i - \mathbf{v}_c)\times\boldsymbol{\varphi}_0. \tag{2.25}$$

If the Hall effect is neglected, eqs (2.24) and (2.25) give

$$\frac{1}{c}(\mathbf{J}\times\boldsymbol{\varphi}_0) + \mathbf{F}_p = \eta\,\mathbf{v}. \tag{2.26}$$

If we define a threshold current density J_t such that $\mathbf{F}_p = -(\mathbf{J}_t\times\boldsymbol{\varphi}_0)/c$, eq. (2.26) can be written

$$\frac{1}{c}\left[(\mathbf{J} - \mathbf{J}_t)\times\boldsymbol{\varphi}_0\right] = \eta\,\mathbf{v}, \tag{2.27}$$

which now takes the place of eq. (2.21).

If we assume that the transport current is perpendicular to the magnetic field, we can drop the vector notation.

If the superconductor is not a plane-parallel slab, but a wire in a perpendicular field, the length of the vortex lines varies over the cross-section, being a maximum in the centre. When a transport current flows through the wire, so that there is flux flow, the length of a vortex line increases initially, goes through a maximum and then decreases. The equation of motion can then be written

$$\frac{1}{c}\left(J - J_t\right)\varphi_0 - \frac{\varepsilon}{L(r)}\frac{\mathrm{d}L(r)}{\mathrm{d}r} = \eta\,v, \tag{2.28}$$

where ε is the vortex-line energy per unit length, $L(r)$ is the length of a vortex line and r is the coordinate in the flow direction, such that $r = 0$ in the centre of the cross-section.

If D is the wire diameter, we can write $L = (D^2 - 4\,r^2)^{1/2}$. It follows then from eq. (2.28)

$$\frac{1}{c}\left(J - J_t\right)\varphi_0 + \frac{4\,\varepsilon\,r}{D^2 - 4\,r^2} = \eta\,v. \tag{2.29}$$

For $r = 0$ the line-energy term vanishes. The equation shows that the vortex-line velocity is not constant but is continuously increasing during its motion across the wire.

Combination of eqs (2.14), (2.22) and (2.27) results in the following expression for the electric field

$$E = \varrho_{f1}(J - J_t) \quad \text{for} \quad J > J_t. \tag{2.30}$$

For a constant value of B there is thus a linear relation between E and $(J - J_t)$. This has recently been found for a Nb-Mo alloy [69]). Usually one finds, however, that the E-J characteristic is curved for small values of J. It has been shown by Jones et al. [70]) that this is due to variations of J_t over the specimen. These authors measured the voltage difference between two potential probes on a Nb-Ta rod, as well as the voltage drop over a number of little segments in between these probes, as a function of the current through the rod. The voltage-current characteristics of the segments were found to have different intercepts with the current axis, i.e. different values of J_t, causing curvature of the characteristic between the two outer probes. At a given value of J only that part of the superconductor is resistive where J is greater than the local value of J_t so that the electric field is only present in part of the specimen.

This problem has also been treated by Baixeras and Fournet [71]). If a distribution function $g(J_t)$ is introduced such that $\int_0^\infty g(J_t)\,\mathrm{d}J_t = 1$, eq. (2.30) is replaced by the following expression:

$$E = \varrho_{fl} \int_0^J (J - J_t)\, g(J_t)\,\mathrm{d}J_t, \tag{2.31}$$

since only in places where $J_t < J$ is there vortex motion giving rise to an electric field.

The average value of J_t is found from the intercept of the linear part of the E-J curve with the J axis. At a given value of J the vortex lines will be pinned in places where $J_t > J$ so that there will be a fraction p not taking part in the motion.

The value of the moving flux fraction $(1 - p)$ for a current density J is given by

$$1 - p = \int_0^J g(J_t)\,\mathrm{d}J_t. \tag{2.32}$$

We write the current-dependent resistivity

$$\varrho(J) = \frac{\mathrm{d}E}{\mathrm{d}J} = \varrho_{fl} \int_0^J g(J_t)\,\mathrm{d}J_t, \tag{2.33}$$

so that

$$1 - p = \varrho(J)/\varrho_{fl}, \tag{2.34}$$

where ϱ_{fl} is the value of $\mathrm{d}E/\mathrm{d}J$ in the linear part of the E-J curve. The moving flux fraction can thus be determined from the slope of this curve.

The distribution function $g(J_t)$ can be obtained from the second derivative of the E-J curve:

$$\frac{\mathrm{d}^2E}{\mathrm{d}J^2} = \varrho_{fl}\, g(J_t). \tag{2.35}$$

We remark here that we have considered the pinning force F_p as a force on a moving vortex line and written it formally in terms of a threshold current density. It was pointed out by Yamafuji and Irie [72]) that such a dynamic pinning force is not the same as the pinning force on a vortex line at rest. The difference is that the moving vortex lattice undergoes a deformation in the vicinity of a pinning centre. This deformation leads to a restoring force due to the elasticity of the lattice. The vortex velocity v is not constant when passing a pinning centre so that this interaction gives rise to a dissipation equal to $\eta\,(\langle v^2\rangle - \langle v\rangle^2)$.

It has recently been shown [73,74]) that the effect of pinning on flux flow can be removed by superimposing an a.c. component on the d.c. magnetic field. This results in a linear E-J characteristic with $J_t = 0$.

In cold-rolled foils the pinning force is usually anisotropic. Certain defects (grain boundaries, surface irregularities) are extended in the rolling direction, thereby causing the flux to flow preferentially in this direction. This effect is most pronounced for low values of the driving force and gives rise to a transverse voltage which, unlike the Hall voltage, does not change sign with magnetic field and may be substantially greater than the Hall voltage. If the vortex lines are moving in one preferred direction which is at an angle ϑ with the current direction, and if there is no pinning force in the direction of motion, the transverse and longitudinal electric field can be written, as was shown by Staas, Niessen and co-workers [75]),

$$E_\perp = \tfrac{1}{2}\,\varrho_{fl}\,J \sin(2\vartheta), \tag{2.36}$$

$$E_\parallel = \varrho_{fl}\,J \sin^2\vartheta. \tag{2.37}$$

2.4. Flux creep

To account for the appearance of a voltage and for a decaying supercurrent in superconductors with pinning, Anderson [76]) put forward a theory on flux creep, i.e. thermally activated motion of vortex lines which are assumed to move in bundles. Individual vortex lines may be pinned to lattice irregularities, but due to interaction with other vortex lines the force acting on these will be transferred to the pinned ones so that they can be depinned.

Anderson considered the driving force on a bundle acting against barriers of a certain height U.

The rate at which the bundles will hop over the barriers is now written

$$R_h = R_0 \exp\left(-\frac{U - J\,B\,\lambda^2\,L\,\xi/c}{k_B T}\right). \tag{2.38}$$

In this expression R_0 is a frequency factor and L is the length over which vortex lines are pinned. The value of U depends on the pinning mechanism. It is probably a function of temperature.

The motion of the flux causes an electric field which is proportional to the jump rate. One can define a critical current density J_c such that the superconductor can carry a current density J without loss for $J < J_c$. When $J = J_c$ the loss due to flux creep becomes measurable. One often takes as a criterion a certain small value of the voltage drop over the superconductor (e.g. 10^{-7} V) as the value which determines J_c. The flux-creep rate then has the critical value R_c. The critical current density can be written

$$J_c = \frac{U - k_B T \ln (R_0/R_c)}{B \lambda^2 L \xi/c} . \tag{2.39}$$

It should be noted that J_c is not identical with J_t, which is usually only found by extrapolation. The difference is, however, small and J_c and J_t can be treated as having the same temperature and magnetic-field dependence.

The theory of flux creep is applicable to low values of J only. At higher current densities the flux creep goes over into flux flow.

2.5. Pinning mechanisms

In this section we shall give a brief qualitative summary of various pinning mechanisms that may be active in the materials used. More detailed treatments can be found in the literature [77–79]).

Pinning is caused by a spatial variation of the Gibbs free energy which gives rise to energy wells and barriers for the vortex lines. It has been pointed out [80,81]) that pinning only arises from changes in free energy over distances of the order of the vortex lattice parameter. More gradual variations over larger distances will cause the vortex density to be adjusted and does not give rise to pinning.

It is often difficult to say what are the dominant pinning mechanisms in a practical material. Different mechanisms may work in parallel in many cases, which makes it hard to reach quantitative conclusions from experimental results regarding the vortex-line pinning.

Dislocations

Pinning is always increased after introduction of dislocations, e.g. by cold work. The following types of dislocation–vortex-line interaction have been proposed.

(a) The interaction of the stress field of a dislocation with the strain associated with the normal vortex core due to the difference in atomic volume between the superconducting and the normal state [80,82,83]). This interaction is linear in the strain (first-order interaction).

(b) The interaction of the stress field of a dislocation with the normal vortex core due to the difference in elastic moduli between the superconducting and normal state [84]). This interaction is quadratic in the strain (second-order interaction).

These two interactions are comparable at atomic distances from a dislocation but at larger distances the first-order interaction dominates. They are interactions with the normal vortex core. The energy of the core is, however, smaller than the magnetic and kinetic energy outside the core as was discussed in sec. 1.1.2. For large values of $\varkappa$ the core energy is negligible, so that interactions based on the properties of the complete vortex are then probably more relevant. This is the case with the following types:

(c) The interaction of a dislocated region with the vortex line due to local depression of the mean free path in this region. This interaction arises by the dependence of the vortex-line energy on $1/\lambda^2$ (eq. (1.13)) which is proportional to l_e as follows from eq. (1.9). The vortex-line energy is therefore a minimum in dislocation tangles [85]).

(d) By analogy with pinning by normal particles, an interaction of a dislocated region with a vortex line was suggested to arise from the local enhancement of $\varkappa$ in this region. If the dislocated region is large enough for the magnetization to be defined (a few times the vortex lattice parameter) there is a difference in magnetization between the dislocated region and an undisturbed region. This difference produces supercurrents at the boundary which repel the vortex lines [86]).

Surfaces

The interaction of a vortex line with a *parallel* surface can be described by the following mechanisms.

(a) The interaction of a vortex with its image [87]) which gives rise to an attraction to the surface, and the interaction of a vortex with the external field which gives rise to a repulsion from the surface. The first interaction causes a barrier for flux entry and the second one for flux exit.

(b) The interaction due to the elastic energy of a vortex line. If a vortex line is nucleated as a half loop [88,89]) its elasticity presents an energy barrier for flux motion away from the surface. The elastic force is greater than the image force by about a factor of $\ln \varkappa$ [20]).

(c) The interaction with a rough surface due to demagnetizing effects. If the roughness is on a scale greater than the vortex-line spacing, there are energy minima for the vortex lines in those places where local surface areas are perpendicular to the vortex lines [90]).

The interaction of a vortex line with a *perpendicular* surface can also arise from surface roughness. This causes spatial variations in the length of the vortex lines and therefore also local line-energy minima and maxima [75]).

Grain boundaries

Pinning of vortex lines by a parallel grain boundary is described qualitatively by the following mechanisms.

(a) The local value of the electron mean free path may be reduced close to a boundary, so that the vortex-line energy has a minimum close to a boundary [79]).
(b) Due to thermal etching of the surface where a grain boundary emerges, vortex lines that are parallel to the boundary are shorter close to the boundary than at some distance and thus have a smaller energy [21]).
(c) If a grain boundary is considered as a layer with high resistivity, pinning of a vortex line may be caused by the attractive interaction with its image on the other side of the boundary. This mechanism will be discussed in chapter 3.

2.6. Flux flow in type-I superconductors

Although the phenomenon of flux flow was originally proposed for the intermediate state in type-I superconductors, relatively little theoretical work has been done on this problem. This may be due to the fact that the structure of the intermediate state is much more complicated than that of the mixed state.

In this section we shall discuss briefly theoretical work concerning the electric field in type-I superconductors in the presence of a transport current and give a qualitative description of the flux-flow state.

In theoretical models of the intermediate state it is usually assumed that the domains are in the form of parallel layers with a width large compared to the penetration depth and extended in the magnetic-field direction.

The response of this structure to an electric field was treated by London [91]). He showed from the continuity of the normal component of the local magnetic induction **b** and of the tangential component of the local electric field **e** at a superconducting–normal boundary, and from the condition that **b** and **e** are zero in the superconducting domains, that $\mathbf{b}_n$ is parallel to the boundary while $\mathbf{e}_n$ is perpendicular to it. The index n denotes the value in the normal domains. This would mean that, when a current is applied, the boundaries set themselves perpendicular to **e** if the Hall effect is disregarded. The value of the average electric field in the superconductor is given by

$$\mathbf{E} = f_n \, \mathbf{e}_n, \tag{2.40}$$

where $f_n = |\mathbf{B}|/H_c$ is the volume fraction of normal layers and the current density is

$$\mathbf{J} = \frac{\mathbf{e}_n}{\varrho_n} = \frac{\mathbf{E}}{f_n \, \varrho_n}. \tag{2.41}$$

The resistivity $\varrho_i = f_n \, \varrho_n$ should thus be independent of current density, if the magnetic field due to the current can be neglected. However, experimentally one finds a strong dependence of the resistance on measuring current: at low

currents the resistance is zero or very small: apparently the current can find a path along the superconducting domains. Shoenberg [51]) suggested that this could be due to the superconducting and normal laminae being parallel to the current. With higher currents, the laminae would be oriented perpendicular to the current direction. He noticed that the low-current situation would be unstable since the field will be greater on one side of a lamina than on the other side. This would cause a movement of the laminae in a direction perpendicular to the current.

The idea of flux motion generating an electric field was first put forward by Gorter [92]). He considered a cylindrical superconducting region, surrounded by a normal medium in which an electric field $\mathbf{e}_n$ exists, perpendicular to the cylinder axis. On the superconducting–normal boundary there is a Maxwell pressure $\mathbf{e}_n^2/8\,\pi$ towards the normal material, parallel and antiparallel to $\mathbf{e}_n$ and a pressure $\mathbf{h}_n^2/8\,\pi$ (due to a magnetic field $\mathbf{h}_n$, generated by the current which accompanies the electric field) towards the superconducting material, perpendicular to $\mathbf{e}_n$, as can be derived from the Maxwell stress tensor [93]). Gorter concluded that these pressures would tend to place the boundaries between the superconducting and the normal region parallel to the electric field.

Assuming this to be generally true, Gorter calculated the voltage due to the motion of the normal and superconducting boundaries, caused by the Lorentz force.

Since in the normal layers $\mathbf{b} = \mathbf{H}_c$, the local electric fields in the normal domains, due to motion with velocity $\mathbf{v}$, is

$$\mathbf{e}_n = -\frac{1}{c}(\mathbf{v}\times\mathbf{H}_c). \tag{2.42}$$

The electric field in the superconducting domains is zero. The average electric field is then

$$E = \frac{f_n\, v\, H_c}{c} \tag{2.43}$$

if the Hall effect is disregarded. The resistivity is given by $\varrho_i = f_n\,\varrho_n$ if there is no power dissipation outside the normal regions, which is the same result as in the London model. By analogy with eq. (2.21) for type-II superconductors we now write for the balance of forces on a normal region with flux Φ, in the absence of pinning, and if J is perpendicular to the applied field,

$$\frac{1}{c} J\,\Phi = \eta'\, v. \tag{2.44}$$

From eqs (2.41) and (2.43) it therefore follows that the viscosity coefficient η' is given by

$$\eta' = \frac{\Phi\, H_c}{\varrho_n\, c^2}, \tag{2.45}$$

a result which is very similar to eq. (2.22) for a type-II superconductor.

Andreev and Sharvin [94]) have given a macroscopic description of the laminar intermediate state in the presence of a small transport current. From Maxwell's equations together with the boundary conditions for **e** and **b**, they find for the average current density in a slab of thickness d_0 in a perpendicular magnetic field H:

$$J = \frac{c\,H_c}{2\,\pi\,d_0} \sin\left(\frac{2\,\pi\,E\,d_0}{c\,H\,\varrho_n}\right) \tag{2.46}$$

if the Hall effect can be neglected. Their theory does not give the orientation of the laminae. If the boundaries are parallel to the current direction, the expression for the flow velocity $v = c\,E/H$ gives

$$v = \frac{c^2\,\varrho_n}{2\,\pi\,d_0} \arcsin\left(\frac{2\,\pi\,J\,d_0}{c\,H_c}\right). \tag{2.47}$$

If the magnetic field due to the current can be neglected, i.e. for $2\,\pi\,J\,d_0 \ll c\,H_c$, this expression is equivalent to eq. (2.44). If the boundaries are perpendicular to the current direction, the flow velocity is zero.

The effect of pinning of superconducting–normal domain boundaries is probably analogous to vortex-line pinning in type-II superconductors. At low current densities the voltage is smaller than corresponds to eq. (2.41) due to forces which counteract the driving force, as was already suggested by Gorter [92]).

The experimental results have long favoured the London model. Powder techniques revealed that in a current-carrying type-I superconductor the domain boundaries are perpendicular to the current and immobile [7,95]).

It was discussed in chapter 1 that at low fields the intermediate state does not have a laminar structure but consists of isolated normal domains in a superconducting matrix. Recently, several different experiments have shown that at low fields flux flow takes place under the influence of a Lorentz force.

By measuring the voltage across a film that was magnetically coupled to a current-carrying film, Solomon [96]) showed that flux flow took place in the current-carrying superconductor. Sharvin [97]) interpreted voltage oscillations between a point contact and a type-I superconductor as proof of a moving normal–superconducting structure (this experiment has been criticized as not being unambiguous proof of a flux-flow process [98,99]). Measurements of the Ettingshausen effect [57]) demonstrated that, under the influence of a transport current, entropy is transported in a direction perpendicular to the current, i.e. in the direction of flux flow. Preliminary results of noise measurements by the author [100]) showed that at low fields the d.c. voltage is caused by flux flow and at higher fields by ohmic loss in immobile normal regions.

A direct proof of the occurrence of flux motion was given in microscopic observations by Severijns [101]) who used Nb powder sprinkled on top of superconducting Pb. The diamagnetic particles were shown to move in a direction perpendicular to current and field. Similar experiments were reported by Solomon [102]). Evidence for flux motion was also given by Träuble and Essmann [9]) who evaporated small ferromagnetic particles on a superconductor in a small magnetic field during flux motion. Since these particles stick to the surface in places where domain boundaries emerge, flux motion was made visible by parallel lines of particles. These lines showed that the velocity of the flux was variable both as regards the

magnitude and the direction. The flux was shown to start off from the edge of the superconductor at certain nucleation sites, in agreement with earlier work by Baird [10]). It was further found that not all the flux was moving: a fraction of the flux remained where it was, presumably held by some pinning force. Grain boundaries were found to be the main pinning centres in lead. This pinning by grain boundaries was also found by Severijns.

These experiments show that the current-carrying intermediate state can be described as a flux-flow state at low fields and as a laminar structure without flux flow at higher fields.

The measured d.c. voltage across a type-I superconductor is believed to be due to flux flow at low fields only and is a combination of a flux-flow voltage and voltage due to ohmic loss in immobile normal regions at higher fields.

In the flux-flow state there is an electric field in the normal domains which is parallel to the current direction. This is accompanied by a Maxwell pressure $\mathbf{e}_n^2/8\,\pi$ towards the normal material in the direction of $\mathbf{e}_n$ and $\mathbf{h}_n^2/8\,\pi$ towards the superconducting material perpendicular to $\mathbf{e}_n$. This tends to place the boundaries perpendicular to the current. When the field is increased the normal domains get bigger and their cross-section becomes elongated and eventually get a length equal to the width of the specimen. There is then no longer a driving force on these domains which have become immobile.

The effect of pinning of domain boundaries is that domains, which may have arbitrary shapes, get stuck in the superconductor. These domains act as pinning centres for small domains that can still move.

The effect of increasing the current is an increase of the electric field so that then the domain boundaries are more aligned perpendicular to the current.

The magnetic field at the surface of the superconductor, generated by the transport current, can usually be neglected. In small fields, if the current is large, this may be not justified. The current then produces a vortex ring [103]) along the circumference of the specimen which, due to a Lorentz force, will shrink and thereby also generate a flux-flow voltage.

3. MEASUREMENTS OF FLUX-MOTION VOLTAGE IN TYPE-II SUPERCONDUCTORS

It was discussed in chapter 2 that in the mixed state of a type-II superconductor transport-current densities greater than a certain critical value give rise to flux motion. This motion causes a voltage drop over the superconductor. In this chapter we shall describe measurements of this flux-motion voltage and of the critical current density and their dependence on the material structure and external parameters, in order to study the effect of pinning on flux motion.

The materials used in the experiments were the type-II superconductors vanadium [104]) and indium-20 at.% thallium [105]).

Vanadium was chosen because its critical temperature is convenient and its critical current density and upper critical field have easily attainable values. It can be cold-rolled to small thicknesses and can be annealed in vacuum.

Indium-20 at.% thallium lends itself to a study of the pinning effect of twin boundaries, which are present in indium-thallium alloys, due to a martensitic phase transformation.

The magnetic field was generated with an electromagnet or a pair of Helmholtz coils outside the helium cryostat. The currents for the magnet and the superconductor were taken from stabilized power supplies. The voltage across the specimens was measured with a Keithly microvoltmeter and a Moseley X-Y recorder. The temperature was controlled by the vapour pressure above the liquid helium.

3.1. Vanadium

3.1.1. *Material properties*

The material used was obtained from A.C. Mackay Ltd. in the form of sheet of 99·9% purity (irrespective of gaseous impurities). It was zone-melted and subsequently cold-rolled to foil of 30 μ thickness. Specimens were cut and current and potential leads were spot-welded. The foils could be annealed by resistance heating in an ultra-high vacuum at pressures down to 10^{-10} Torr. The annealing removes lattice defects and also most metallic impurities but does not lead to expulsion of all non-metallic impurities such as nitrogen and oxygen [106]). The annealing temperature was about 1600 °C.

Cold-rolled vanadium has a fibre structure in the form of ribbons parallel to the rolling plane [107]). The fibres are elongated in the rolling direction and have a thickness of the order of a few microns and a width of a few hundred microns. Within the fibres the rolling has introduced a three-dimensional cellular dislocation structure with low dislocation density within the cells and high dislocation density in the cell walls [85,108]). The cells are flat and have dimensions of the order of 0·5 μ in the rolling plane and 0·1 μ perpendicular

to the rolling plane [109]). On annealing, the dislocation network and the fibre structure disappear and recrystallization takes place, resulting in crystals with diameter of up to about 150 μ and thickness equal to the foil thickness.

The surface of the cold-rolled material exhibits ridges that are extended along the specimens in the rolling direction. These surface irregularities were found to be most pronounced in some annealed foils, where they were presumably accentuated by thermal etching during the annealing.

3.1.2. *Specimens*

Specimens were cut with various widths up to several millimetres and lengths between the potential probes of 5 to 10 mm. The long direction was cut at an angle ϑ to the rolling direction. The transport current was applied in the long direction, so that ϑ was also the angle between current and rolling direction. The plane of the foils was oriented perpendicular to the magnetic field.

One annealed specimen was cut as a Corbino disc. This is a circular disc with one contact in the centre and one around the circumference of the disc [110]). The electric field in such a disc is directed radially and in the flux-flow state the vortex lines flow in concentric circles, if the specimen is isotropic. The central current and potential contact was a spot-welded V-shaped platinum wire. The outer current and potential contacts were connected to a copper ring, soldered to a platinum foil that was spot-welded to the circumference of the vanadium foil. The surface of the Corbino disc did not show appreciable ridges in the rolling direction.

Figure 3.1 shows the specimen configurations and table II gives some material properties of the specimens. In this table the resistance ratio RR = $R_{300\ °K}/R_{4{\cdot}2\ °K}$; H_{c2} is determined either from magnetization measurements

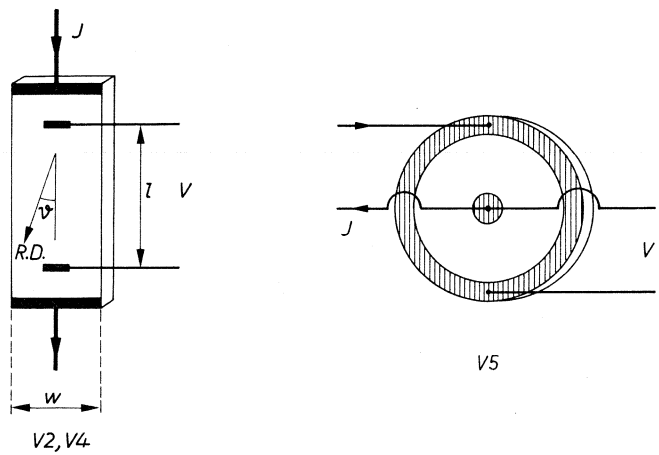

Fig. 3.1. Specimen configurations of vanadium foils for the specimens V2 and V4 and the Corbino disc V5. R.D. means rolling direction.

TABLE II
Material properties of cold-rolled vanadium specimens

specimen	annealed	ϑ (degrees)	RR	T_c (°K)	$\varkappa_1$ at 4·2 °K	H_{c2} at 4·2 °K (kOe)
V2a	yes	15	15	5·15	2·0	1·2
V2b, d, e, f	no	0	10	5·07	2·6	1·5
V2c	no	15				
V4a, b	no	90				
V5	yes	Corbino disc	7·4	4·95	3·3	1·2

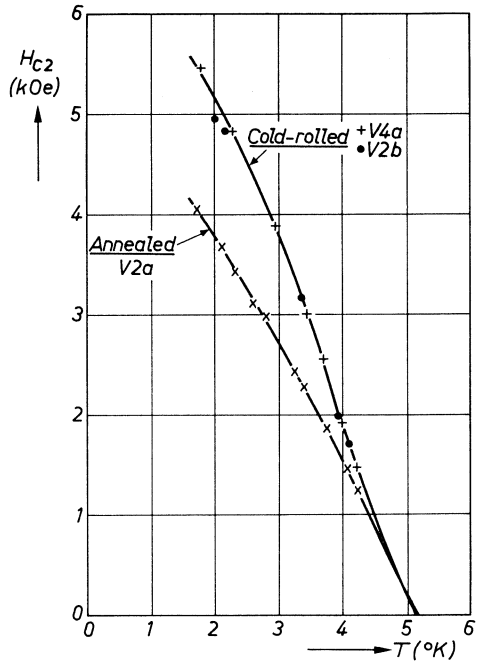

Fig. 3.2. Temperature dependence of H_{c2} for cold-rolled and annealed vanadium foils with resistance ratios 10 and 15 respectively.

or from a linear extrapolation of J_c to zero. The value of $\varkappa_1 = H_{c2}/2^{1/2}H_c$ at 4·2 °K is calculated from measured values of H_{c2} and values of H_c obtained from magnetization measurements on a single crystal of comparable purity [111]). The temperature dependence of H_{c2} is shown in fig. 3.2.

3.1.3. *Flux-flow voltage*

The flux-flow voltage V was found to be a linear function of the current I except at low values of I, in agreement with eq. (2.31). This is shown in fig. 3.3

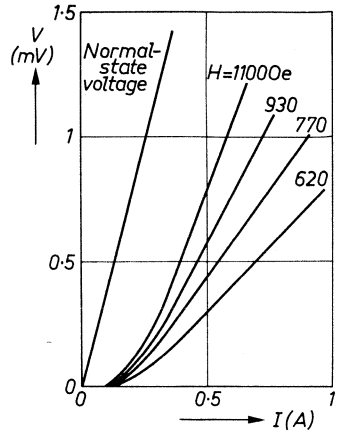

Fig. 3.3. Flux-flow voltage V as a function of current I for various values of magnetic field at $T = 4{\cdot}2$ °K for specimen V2c, for which $l = 4{\cdot}7$ mm, $w = 1{\cdot}1$ mm.

for specimen V2c at $T = 4{\cdot}2$ °K for various values of the magnetic field.

In the Corbino disc the V-I characteristic exhibits a curvature caused by the radial variation of the current density J, apart from that due to a distribution of J_t values, as discussed in sec. 2.3. As the current density is inversely proportional to the distance r from the centre, it is lowest at the edge of the disc. The V-I characteristic is linear when the current density at the edge is greater than J_t. For lower current densities there is only flux flow in the central part of the disc. Furthermore, due to the dependence of J on r, the vortex-line velocity is lower for greater distance from the centre. This implies a continuous shear of the vortex lattice, which means that the vortex lattice cannot be rigid. It is also remarked that the flux-flow voltage in a Corbino disc does not involve generation and annihilation of vortex lines at the edges, as in foils where the

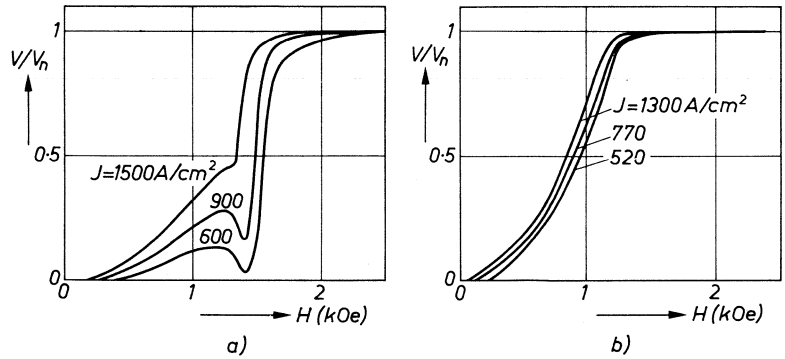

Fig. 3.4. Flux-flow voltage V relative to normal-state voltage V_n in vanadium foils as a function of magnetic field for various values of the current density at $T = 4{\cdot}2$ °K; a: cold-rolled, specimen V2c; b: annealed, specimen V2a.

current flows in one direction. Similar conclusions were also reached by Shaw and Solomon [112]) and by McKinnon and Rose-Innes [113]).

The effect of magnetic field on flux flow is shown in fig. 3.4, where the flux-flow voltage at constant current values for specimens V2c and V2a is plotted as a function of field. The main difference between the two sets of curves is the shape of the curves which exhibit a maximum and a minimum in specimen V2c, whereas the voltage increases smoothly in specimen V2a. The origin of the voltage maximum and minimum is still obscure. Apparently in cold-worked materials an additional pinning effect sets in at higher fields. The voltage minimum has been shown to be accompanied by a redistribution of current in the specimen such that the current density in the edges is increased [114]) and consequently the driving force on the vortex lines in the bulk is decreased. The transverse voltage, which is due to a flux-flow velocity component $v_{\parallel}$ parallel to the transport current, was measured on specimens V2a and V2b. This voltage is caused partly by vortex lines flowing in a preferred direction and partly by the Hall effect as was shown by Staas, Niessen and co-workers [75]). The vortex lines flow preferentially in the rolling direction because fibre boundaries and

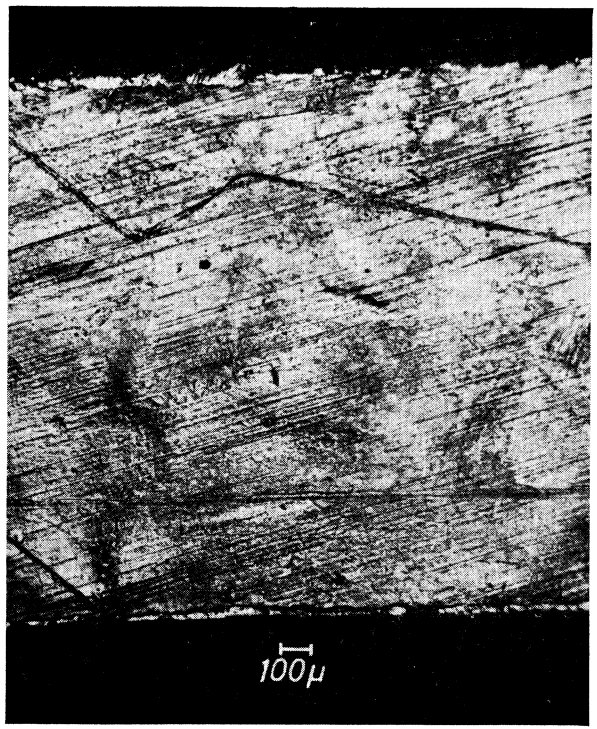

Fig. 3.5. Micrograph of the surface of annealed vanadium, specimen V2a. The edges are parallel to the current direction.

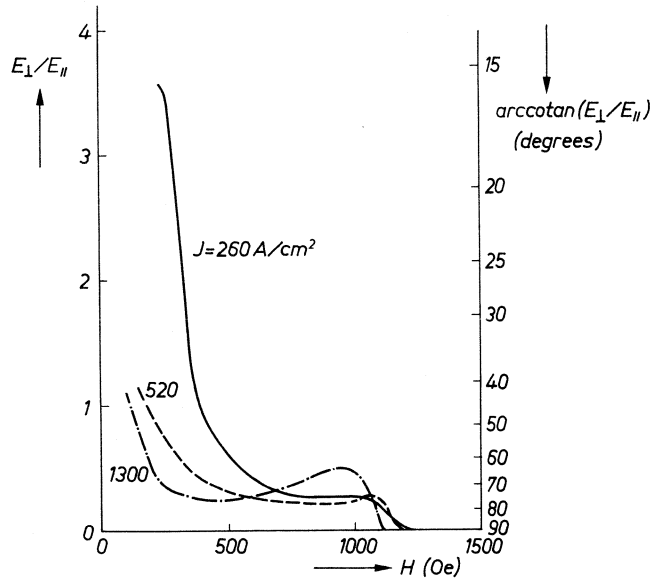

Fig. 3.6. Transverse electric field $E_\perp$ divided by the longitudinal electric field $E_{||}$ as a function of magnetic field for various values of the current density at $T = 4{\cdot}21$ °K for specimen V2a ($\vartheta = 15°$). Also indicated is arccotan $(E_\perp/E_{||})$ which is the angle between the flux-flow and the current directions.

surface ridges are extended in this direction. These surface ridges are shown for specimen V2a in fig. 3.5. There are then parallel channels where the vortex-line energy is smaller, which gives rise to a preferred direction for flux flow.

Figure 3.6 shows the value of the transverse electric field $E_\perp$ divided by the longitudinal electric field $E_{||}$ as a function of field for specimen V2a at $T = 4{\cdot}2$ °K for various values of the current density. It can be seen that $E_\perp/E_{||}$, which is equal to $v_{||}/v_\perp$, where $v_\perp$ is the flux-flow velocity component perpendicular to the transport current, may have a large value at low fields. It follows from eqs (2.36) and (2.37) for flux flowing in the rolling direction that $E_\perp/E_{||} = \text{cotan}\ \vartheta$, which is a large number at small values of ϑ. Figure 3.6 also shows the values of arccotan $(E_\perp/E_{||})$ which is the angle between the transport current and the flux-flow direction. The results show that at low currents and fields the flux flow is in the rolling direction. Increase of current density or magnetic field causes the flux to jump over the barriers so that $E_\perp/E_{||}$ decreases. For specimen V2b, where the surface valleys were much less pronounced than for specimen V2a, $E_\perp$ was less than 1 % of $E_{||}$ for current densities down to 500 A/cm².

The Hall voltage was determined for specimen V2b as the difference between the transverse voltages for the magnetic field and current in reversed directions. In the normal state the Hall tangent tan θ was proportional to the magnetic

field with a slope of 4.10^{-7}/Oe. It was found to increase below H_{c2} with decreasing field and to go through a maximum as in alloys. At low temperatures ($T < 2$ °K) tan θ changed sign at about $0{\cdot}6\, H_{c2}$. This sign reversal has also been found in Pb-In alloys [65]), V [115]) and Nb [116]).

For specimen V2a the Hall voltage could not be determined with sufficient accuracy, due to the large transverse voltage caused by the anisotropic pinning.

The low values of tan θ and $E_\perp$ in unannealed foils show that it is justified to treat the vortex lines as moving perpendicularly to the transport current and to neglect the Hall effect. This applies also to annealed foils for sufficiently high currents and fields.

3.1.4. *Critical current density*

Flux pinning was also studied by measuring the critical current density J_c. It is defined as the current density (assuming a homogeneous current distribution) which gives rise to a voltage drop of 10^{-7} V between the potential probes. J_c was measured as a function of field at various temperatures. The influence of structure is shown in fig. 3.7 where J_c-H curves for $T = 4{\cdot}2$ °K are drawn for cold-rolled vanadium with the current parallel and perpendicular to the rolling direction, respectively, and annealed vanadium. J_c drops to low values at $H \approx H_{c2}$ as the bulk of the superconductor then goes normal. At fields above H_{c2} the critical current density is related to the surface layer which is superconducting up to H_{c3}. The difference between curves a and b is presumably caused by the structure of the foil. Since in cold-rolled foils the fibres are elongated in the rolling direction, flux flowing perpendicular to this direction has to cross many more fibre boundaries than flux flowing in the rolling direction. There is thus more pinning when the current flows in this direction than perpendicular to it, so that J_c is higher in the former case.

An alternative explanation of the anisotropy is pinning by the valleys on the surface which are extended in the rolling direction. Apart from these mechanisms, isotropic pinning is caused by the dislocation cells. Evidence of this pinning was given by Sarma and Moon [117]) who found Bitter patterns essentially similar to the dislocation cell structure.

After annealing, the dislocations have disappeared and the pinning is reduced considerably (curve c). There is still a finite value of J_c, which shows that there is still flux pinning. This may be caused partly by the presence of grain boundaries which now lie parallel to the vortex lines. Pinning is further caused by the elongated structures in the surface and by the edges that are parallel to the field, as was discussed in chapter 2.

The pinning in the foils is thus generally a combination of different mechanisms, such as those caused by fibre boundaries, dislocation networks, grain boundaries and surfaces.

The field dependence is different for the unannealed and the annealed foils.

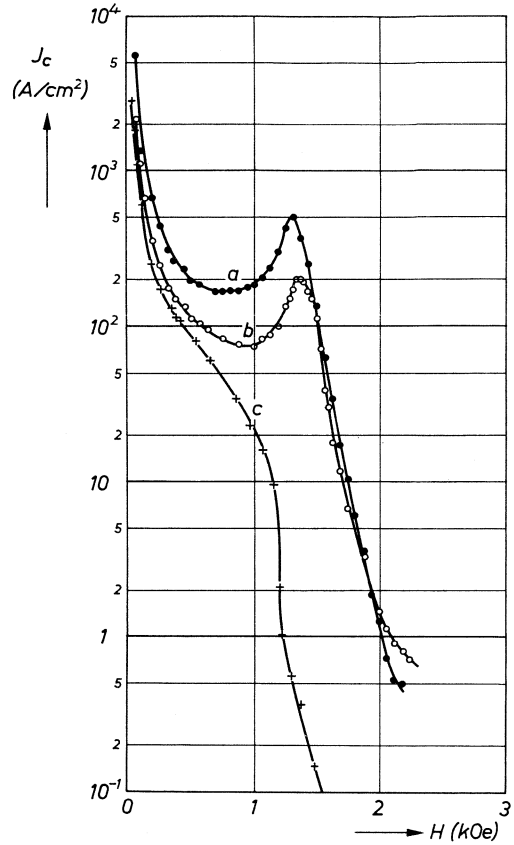

Fig. 3.7. Critical current density J_c as a function of magnetic field for vanadium foils at $T = 4{\cdot}2$ °K; a: cold-rolled, $\vartheta = 0$ (specimen V2d, $w = 3$ mm); b: cold-rolled, $\vartheta = 90°$ (specimen V4b, $w = 3$ mm); c: cold-rolled and annealed, $\vartheta = 15°$ (specimen V2a, $w = 1{\cdot}3$ mm).

For the annealed material J_c decreases with increasing field. If the total pinning force per unit volume is constant or only weakly dependent on B, the pinning force per vortex line and therefore also J_c, decreases with increasing field. In the unannealed material J_c is found to go through a rather broad minimum and a maximum before it drops to low values at H_{c2}. This maximum in the J_c-H curve, which is usually called the peak effect, is related to the minimum in the V-H curve as was shown in fig. 3.4, and is obviously caused by a pinning effect which dominates at high fields.

The role played by the edges is illustrated by the dependence of J_c on foil width. The value of J_c in the minimum of the J_c-H curve decreases almost by a factor of 2 when the width is increased from 1·2 to 5·8 mm. This corresponds to a decrease of the surface (parallel to the field)-to-volume ratio by a factor of 5.

The temperature dependence of J_c is illustrated in fig. 3.8 where J_c at

$H/H_{c2} = 0{\cdot}6$ is shown as a function of temperature for cold-rolled and annealed vanadium. For cold-rolled material this value of H/H_{c2} corresponds to J_c in the minimum of the J_c-H curve. For comparison J_c in the maximum of the J_c-H curve is also drawn. The full curves in fig. 3.8 are proportional to $(1 - T^2/T_c^2)^2$, which is the temperature dependence of H_c^2.

It was shown in sec. 2.4 that in the flux-creep model J_c can be written

$$J_c = \frac{U - k_B T \ln (R_0/R_c)}{B \lambda^2 \xi L/c}, \tag{3.1}$$

where U is the average height of the pinning barriers, R_c is the critical jump rate and R_0 is a constant. The value of U can be determined from the critical current density at $T = 0$. By substituting values for the various quantities in eq. (3.1), U is found to be of the order of 10^{-2} eV in the cold-rolled foils.

If B is a constant fraction of H_{c2}, the denominator in eq. (3.1) is little temperature-dependent except close to T_c. Anderson suggested that U is proportional to the condensation energy $H_c^2/8\pi$. This seems to be in agreement with the temperature dependence of J_c and would imply that the thermal-diffusion term in eq. (3.1) is less significant than U.

Whether U should be proportional to $H_c^2/8\pi$, however, is not certain. As was discussed in sec. 2.5, pinning is caused by various effects such as the image force, vortex-line-energy variations, interaction with dislocations and also by the mechanism causing the peak effect. These effects may have different temperature dependences. No attempt has therefore been made to treat the temperature dependence of J_c quantitatively.

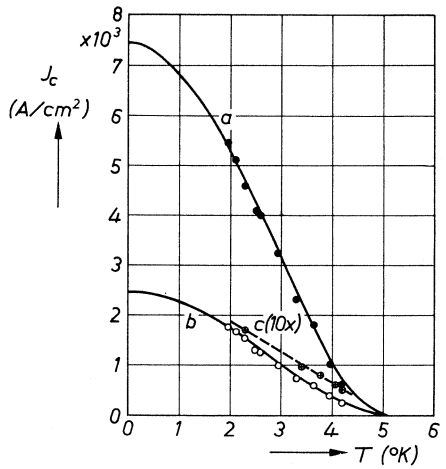

Fig. 3.8. Critical current density J_c as a function of temperature for vanadium foils; a: cold-rolled (specimen V2f, $w = 2$ mm) as measured in the maximum of the J_c-H curve; b: idem in the minimum of the J_c-H curve; c: annealed (specimen V2a, $w = 1{\cdot}3$ mm) for $H = 0{\cdot}6$ H_{c2}. The full curves are a $(1 - T^2/T_c^2)^2$ fit to the experimental points.

3.1.5. *Conclusions*

The experimental results show that the voltage across a current-carrying vanadium foil can be described as a flux-flow voltage. This flux flow is hindered by pinning of vortex lines by several types of defects so that at low currents there is a fraction of flux that does not take part in the motion. The pinning defects include fibre boundaries, dislocations, surface irregularities and the edges of the specimen. The anisotropic defect structures of fibre boundaries and surface irregularities give rise to anisotropic critical current density J_c for flux flow.

In an annealed specimen at low current densities and fields the anisotropic structure causes the vortex lines to move preferentially in the current direction, if this is parallel to the rolling direction. At higher values of J and H the vortex lines move at 70 to 90 degrees to the current direction. In unannealed foils the component of the vortex-line velocity in the current direction can be neglected.

The value of J_c decreases with increasing temperature and in annealed vanadium also with increasing field. In unannealed vanadium the J_c-H curve exhibits a peak effect.

In a Corbino disc, where there is no generation and annihilation of vortex lines at the edges, there cannot be a rigid vortex lattice during flux flow.

3.2. Indium-thallium

3.2.1. *Material properties*

Grain boundaries are known to act as pinning centres. For parallel grain boundaries the pinning is a maximum when the vortex lines lie in the parallel direction. This was found from measurements of critical current and magnetization in electro-deposited Nb foils [107]). Fibre boundaries in cold-rolled vanadium may also act as pinning barriers, as was discussed in the previous section. Since the boundary energy of twins is much less than the grain-boundary energy [118]), the question arose whether twin boundaries would also act as pinning centres for flux lines. The influence of twin boundaries on pinning was studied on an indium-thallium alloy *).

Part of the phase diagram [119–120]) is shown in fig. 3.9. The transformation from the face-centred cubic to the face-centred tetragonal structure is martensitic and can be observed even at liquid-helium temperatures [120,121]). The c/a ratio of the f.c.t. structure depends on composition and temperature and is 1·03 for In-20 at.% Tl at room temperature [122]). The transformation can be formally described as two subsequent shears in $\langle 110 \rangle$ directions on two $\{110\}$ planes that are at 60 degrees to each other. For example, a first shear of magni-

*) The author is indebted to Prof. Dr A. Wegener Sleeswijk for his suggestion to study In-Tl alloys.

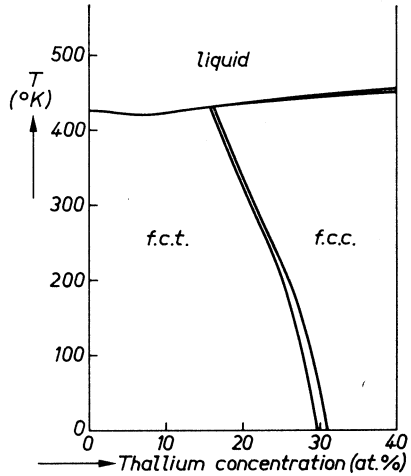

Fig. 3.9. Tentative phase diagram of indium-thallium system for thallium contents up to 40 at. %

tude 2 γ on the (101) plane in the [10$\bar{1}$] direction, followed by a second shear of the same magnitude on the (110) plane in the [1$\bar{1}$0] direction, transforms a cubic into a tetragonal crystal.

By this transformation, an originally cubic crystal exhibits sets of parallel tetragonal twins. The alternating twin structure occurs because on either side of a twin boundary the material has the same first shear but a second shear that is in opposite $\langle 110 \rangle$ directions to each other, as for example a first shear (101) [10$\bar{1}$], 2 γ, followed by a second (110) [1$\bar{1}$0], 2 γ and a first shear (101) [10$\bar{1}$], 2 γ, followed by a second (110) [$\bar{1}$10], 4 γ. The value of γ is 0·01 for a c/a ratio of 1·03.

Starting from a single crystal of In-18·5% Tl the transformation was found [123]) to take place on cooling by the migration of one single interface between the cubic and tetragonal phase, lying along a {110} plane.

The tetragonal structure then consists of a set of fine twins with boundaries on {110} planes.

If twin boundaries are able to pin vortex lines one would expect such a structure to give rise to pinning when the vortex lines are parallel to the boundaries.

3.2.2. *Specimens*

The attempt was made to grow single crystals of the compositions In-17% Tl and In-20% Tl from high-purity materials obtained from Johnson, Matthey & Co and A.S.R.C. respectively *). This was done by the Bridgman method in which the alloy was kept in a ceramic tube of 2 mm inner diameter and the liquid-solid interface travelled through the alloy. After cooling down, the

*) The crystal growing was kindly carried out by P. Hokkeling and A. I. Luteijn.

ceramic tube was removed. Cross-sections of the wires so obtained were electrolytically polished and etched in a HNO_3-HCl solution in carbitol [120]). It was found that the surface layer of In-17% Tl wires was polycrystalline.

The In-20% Tl wires were monocrystalline; isolated small crystals on

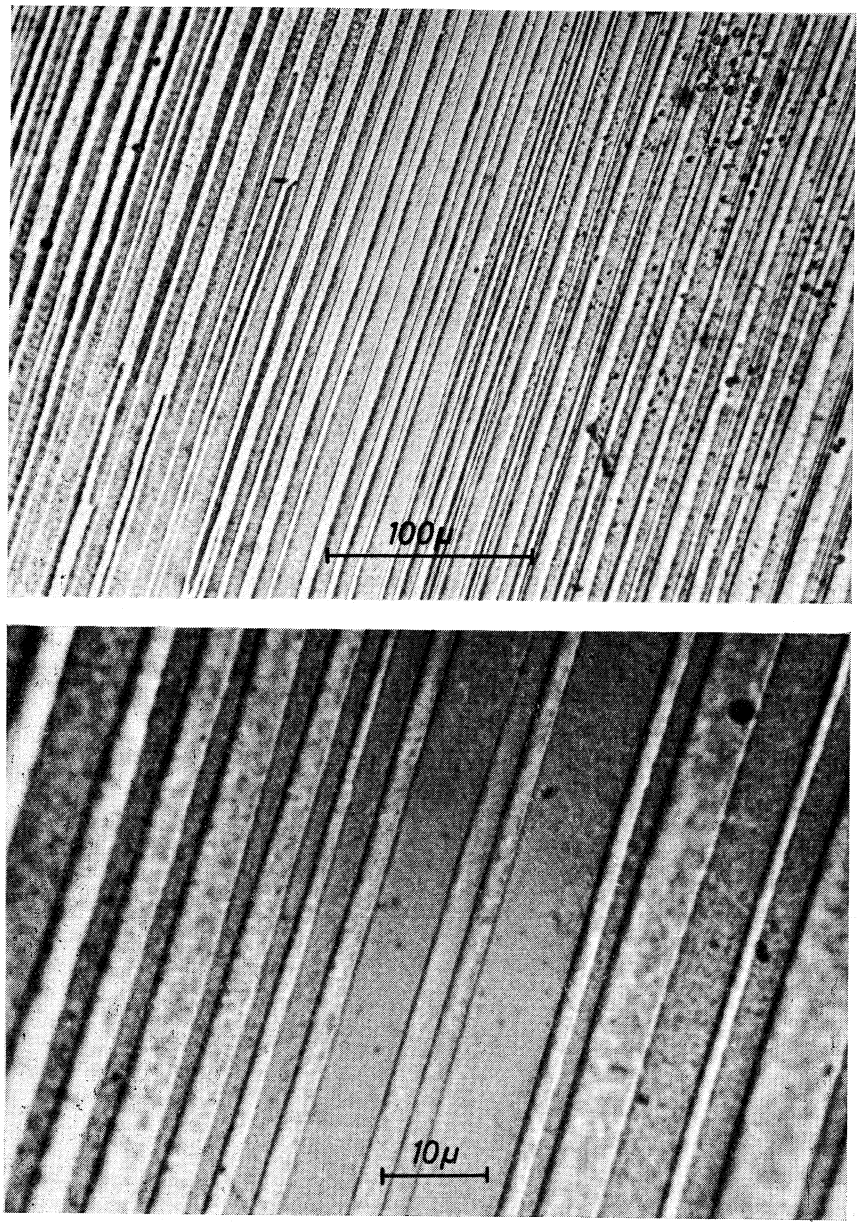

Fig. 3.10. Micrographs of an electro-polished and etched cross-section of In-20 at.% Tl ⟨111⟩ crystal after transformation to the f.c.t. phase.

the outside were removed by electrolytic polishing. From the directions of the twin boundaries and from a Laue pattern the orientation of the crystals was found to be approximately ⟨111⟩ along the wire axis. Microscopic observations of a cross-section showed that in the greater part the transformation was on one set of {110} planes and parallel twin boundaries could be seen as is shown in fig. 3.10. The micrographs show twin boundaries in a ⟨110⟩ direction. The twin width varied between about 1 and 10 μ. In isolated parts of the cross-section some other twin boundaries were found at 60 degrees to the main set of boundaries.

For the measurements, current contacts were pressed on the end of a crystal and potential contacts were mounted with a silver paste at several 5-mm intervals as shown in the inset of fig. 3.12. The crystal could be rotated about its axis in a perpendicular field.

The resistivity at 4·2 °K was 1·2 μΩ cm. Spectrochemical analysis showed that the thallium content was 19·7 at.%.

The value of H_{c2} was determined from a linear extrapolation of critical current to zero. The temperature dependence of H_{c2} is shown in fig. 3.11. The value of $\varkappa_1$ was found to lie in between 0·8 at $T = T_c = 3{\cdot}23$ °K and about 1·2 near $T = 0$. For the determination of $\varkappa_1$, values of H_c obtained from magnetization measurements were used.

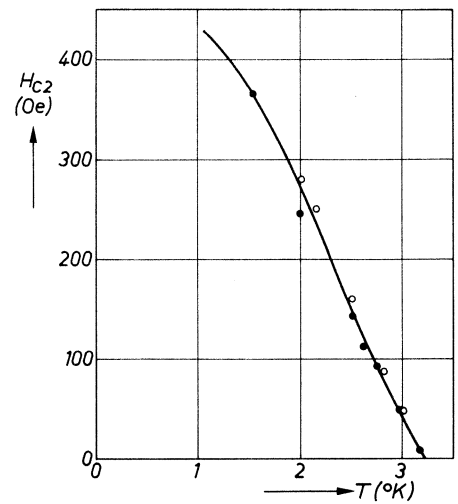

Fig. 3.11. Temperature dependence of H_{c2} for two In-20 at.% Tl crystals.

3.2.3. *Critical current density*

The critical current density J_c was measured as a function of the angle of rotation δ in a constant perpendicular field at various temperatures. In fig.3.12 J_c is plotted as a function of δ for two neighbouring parts of the wire at

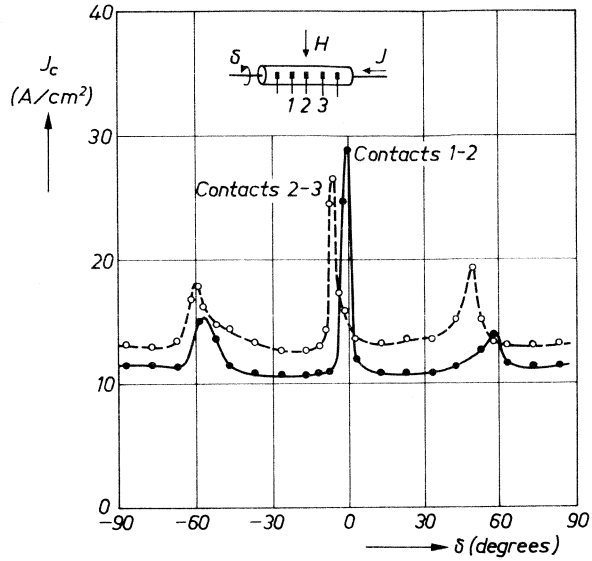

Fig. 3.12. Angular dependence of critical current density J_c for two neighbouring parts of In-20 at.% Tl crystal (contacts 1-2 and 2-3) in a perpendicular field, as illustrated in the inset; $T = 2{\cdot}51$ °K, $H = 106$ Oe. The peaks correspond to ⟨110⟩ directions.

$T = 2{\cdot}51$ °K and $H = 106$ Oe ($0{\cdot}8\ H_{c2}$). The measurements show maxima of J_c for field orientations at about 60 degrees to each other, of which one maximum is very sharp. This maximum was found to occur when the field was parallel to the main set of twin boundaries. The anisotropy for one set of contacts was greater and the submaxima lower than for the other set of contacts. Apparently there was somewhat more transformation on other {110} planes in the latter piece of the wire.

The maxima for the two parts of the crystal were found at somewhat different field orientations. This was also measured in other parts of the wire. The crystal was apparently twisted over the length of the wire by about 6 degrees per cm, as was found from measurements not shown here.

The anisotropy is also shown in fig. 3.13 where J_c-H curves are drawn for $\delta = 0°$ and $\delta = 10°$ at $T = 1{\cdot}53$ °K. The orientation $\delta = 0°$ corresponds to the field being parallel to the twin boundaries. The anisotropy disappears at fields above H_{c2} where only a surface layer is superconducting. The critical-current anisotropy became more pronounced by decreasing the temperature. This was manifested by a narrower peak at $\delta = 0$ and a somewhat greater ratio between maximum and minimum values of J_c.

The critical current density was found to decrease with increasing temperature.

The voltage as a function of field is drawn in fig. 3.14 for $T = 1{\cdot}50$ °K and $J = 106$ A/cm² for two orientations of the magnetic field: δ=0° and

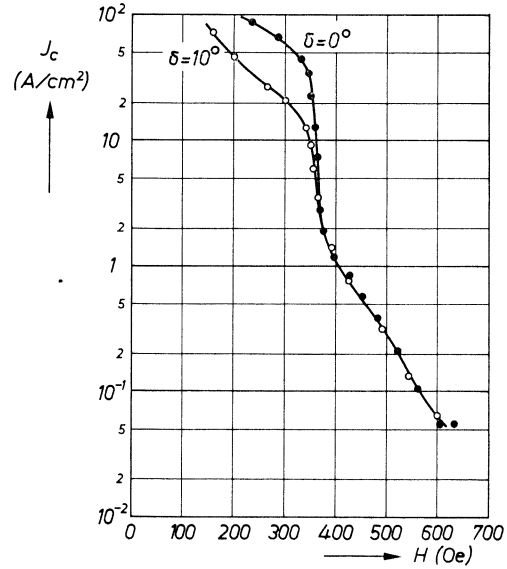

Fig. 3.13. Critical current density J_c for In-20 at.% Tl crystal as a function of magnetic field at $T = 1{\cdot}53\ ^\circ\mathrm{K}$, measured between potential contacts 1-2 for orientations $\delta = 0^\circ$ and $\delta = 10^\circ$ (see fig. 3.12).

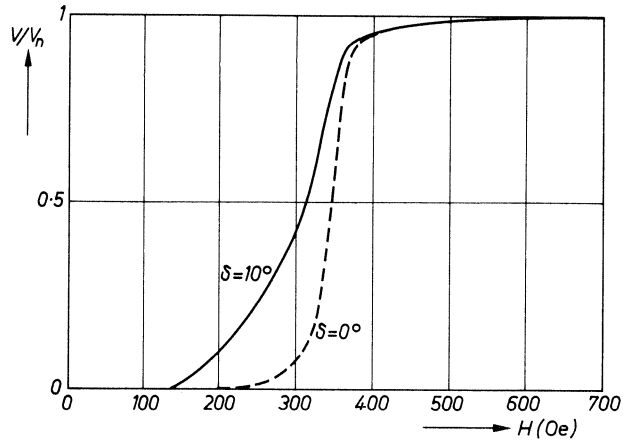

Fig. 3.14. Flux-flow voltage V relative to normal-state voltage V_n for In-20 at.% Tl crystal as a function of magnetic field for $J = 106\ \mathrm{A/cm^2}$ at $T = 1{\cdot}50\ ^\circ\mathrm{K}$, measured between potential contacts 1-2 for orientations $\delta = 0^\circ$ and $\delta = 10^\circ$ (see fig. 3.12).

$\delta = 10^\circ$. The flux-flow voltage is greater for $\delta = 10^\circ$ which, in agreement with the results for J_c, means that there is less pinning.

3.2.4. *Grain-boundary pinning*

The pinning by twin boundaries and more generally grain boundaries will be explained in terms of an image force at the boundary. We assume the boundary

to be a plane barrier with small thickness, which has a resistivity higher than the material on either side of the barrier. Following Boyd [124]) we treat the boundary as a tunnelling barrier with a transmissivity for electrons t_r. For zero barrier thickness $t_r = 1$. For $0 < t_r < 1$ supercurrents tunnel through the barrier. For $t_r = 0$ the barrier can be treated as a free surface and the interaction of a vortex with the barrier can be written as the interaction of a vortex with its image. A vortex will therefore be trapped at the barrier at a distance of the order ξ. Figure 3.15 shows for $t_r = 0$ the vortex energy $\varepsilon(z)$ as a function of distance to the surface z which can be described by the equation [87])

$$\varepsilon(z) = \varepsilon - \left(\frac{\varphi_0}{4\pi\lambda}\right)^2 K_0(2z/\lambda), \tag{3.2}$$

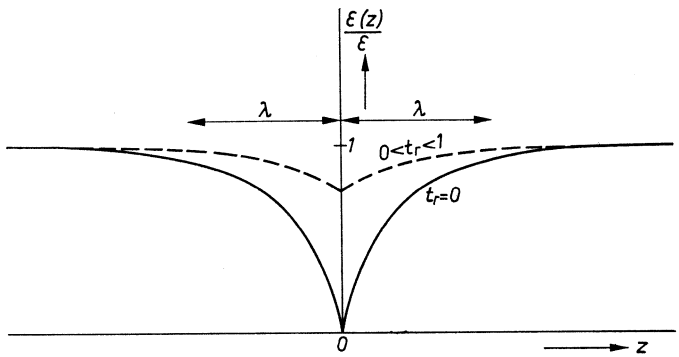

Fig. 3.15. Reduced vortex-line energy near a boundary with transmission t_r as a function of the distance z to the boundary for $t_r = 0$ and $0 < t_r < 1$. The boundary is located at $z = 0$.

where ε is the single-vortex-line energy and K_0 is the zero-order Hankel function of the second kind. For $0 < t_r < 1$ the barrier has zero resistance for small currents. Supercurrents greater than the critical tunnelling current cannot cross the barrier. The vortex can therefore not come too close to the barrier, as the circulating supercurrents would become greater than the critical current of the barrier. Since smaller currents can cross the barrier, the image vortex is at a greater distance from the barrier than the vortex itself. Linear interpolation would give an energy minimum at the barrier of the order $(1 - t_r)\,\varepsilon$. This is also drawn in fig. 3.15. Since ε is large, a large pinning effect is the result even if $(1 - t_r)$ is small.

The concept of the image vortex applies to vortices that are parallel to a wall. This pinning mechanism can be very pronounced for twin boundaries, as these are very plane boundaries. This is in agreement with the experiments, as shown in fig. 3.12.

Additional pinning effects at the twin boundaries may be the stress field of the boundaries and the presence of surface tilts along the boundaries [123]). These effects are presumably too small to account for the observed anisotropy. This is probably also true for the effect of locally reduced mean free path close to the boundary on the vortex-line energy [79]) which is proportional to the mean free path.

3.2.5. *Conclusions*

The anisotropy of the critical current density and the flux-flow voltage in In-20 at. % Tl show clearly that vortex lines can be pinned by twin boundaries and that this pinning is a maximum when vortex lines and boundaries are oriented parallel to each other. The mechanism of this pinning is presumably the attraction of a vortex line by its image.

4. THEORY OF FLUX-MOTION NOISE IN SUPERCONDUCTORS

When there is flux motion, a d.c. voltage is generated across the superconductor, as was discussed in chapters 2 and 3. We shall now discuss the voltage fluctuations that are inherent in this mechanism of voltage generation and derive expressions for the power spectrum of the noise voltage. After a brief survey of the theory of Fourier analysis of fluctuations, the noise voltage due to flux flow will be discussed in detail. This noise arises due to the randomness and quantized nature of the flux flow. Next an expression for Johnson noise will be derived, which is closely analogous to the Nyquist formula. Finally the phenomenon of flicker noise will be dealt with. This noise is due to temperature fluctuations in the specimen surface and originates from fluctuations in the heat transfer from the specimen to the helium bath.

4.1. Fourier analysis of fluctuations

In this section Fourier analysis will be used to derive expressions for the noise-power spectrum.

Let us consider a statistically stationary fluctuating signal $y(t)$, i.e. a signal, the statistical properties of which are independent of time t. It is assumed that the ergodic theorem holds, which states that time average and ensemble average are identical. The signal $y(t)$ is the response of a measuring instrument to a random process. We suppose that this can be thought of as caused by a great number of elementary events, which are identical and independent of each other. If $u(t)$ is the response of the instrument to an elementary event, we can write

$$y(t) = \sum_{t_i = -\infty}^{t} u(t - t_i), \tag{4.1}$$

where the event $u(t - t_i)$ starts at $t = t_i$.

If the elementary events are random and occur at an average rate N, the average value of $y(t)$ is

$$\langle y(t) \rangle = N \int_0^\infty u(t)\, \mathrm{d}t, \tag{4.2}$$

where the event $u(t)$ starts at $t = 0$.

It can further be shown that the mean-squared fluctuation of $y(t)$ is

$$\langle \delta y^2 \rangle = \langle [y(t) - \langle y(t) \rangle]^2 \rangle = N \int_0^\infty u^2(t)\, \mathrm{d}t. \tag{4.3}$$

Equations (4.2) and (4.3) are known as *Campbell's theorems*. They can be proved by dividing the time scale into infinitesimal elements δt and attaching

to each event a probability of occurrence in this time interval equal to $N\,\delta t$.

We write the function $u(t)$ as a Fourier integral

$$u(t) = \int_{-\infty}^{\infty} F(f) \exp(2\pi i f t)\,\mathrm{d}f, \tag{4.4}$$

where $F(f)$ is the Fourier transform of $u(t)$ and f is the frequency:

$$F(f) = \int_{-\infty}^{\infty} u(t) \exp(-2\pi i f t)\,\mathrm{d}t. \tag{4.5}$$

By taking the product of two functions $u_1(t)$ and $u_2(t)$ one can write

$$\int_{-\infty}^{\infty} u_1(t)\,u_2(t)\,\mathrm{d}t = \int_{-\infty}^{\infty} F_1(f)\,F_2{}^*(f)\,\mathrm{d}f = \int_{-\infty}^{\infty} F_1{}^*(f)\,F_2(f)\,\mathrm{d}f, \tag{4.6}$$

where $F_1{}^*(f)$ and $F_2{}^*(f)$ are the complex conjugates of $F_1(f)$ and $F_2(f)$.

For $u_1(t) = u_2(t)$ one obtains *Parseval's theorem*

$$\int_{0}^{\infty} u^2(t)\,\mathrm{d}t = \int_{-\infty}^{\infty} |F(f)|^2\,\mathrm{d}f. \tag{4.7}$$

where the integration of $u^2(t)$ is from $t = 0$ to infinity, as we chose $u(t) = 0$ for $t < 0$. Combination of eqs (4.3) and (4.7) leads to

$$\langle \delta y^2 \rangle = N \int_{-\infty}^{\infty} |F(f)|^2\,\mathrm{d}f = 2N \int_{0}^{\infty} |F(f)|^2\,\mathrm{d}f. \tag{4.8}$$

If $\langle y(t) \rangle$ is assumed to be zero, the power in the signal is proportional to $\langle \delta y^2 \rangle$, which is written

$$\langle \delta y^2 \rangle = \int_{0}^{\infty} W(f)\,\mathrm{d}f. \tag{4.9}$$

This expression defines the power spectrum $W(f)$. It follows from eqs (4.8) and (4.9) that we can write

$$W(f) = 2N\,|F(f)|^2, \tag{4.10}$$

which is known as *Carson's theorem*. It shows that the power spectrum of a noise signal is directly related to the Fourier transform of the elementary event. This event will in the next section be shown to be a voltage pulse.

We will now give an expression for the autocorrelation function $\psi(s)$. This is defined by

$$\psi(s) = \langle \delta y(t)\,\delta y(t+s) \rangle. \tag{4.11}$$

It is independent of time and expresses the amount of correlation in the noise signal.

If $F'(f)$ is the Fourier transform of $u(t+s)$, one can write

$$F'(f) = \exp(2\pi i f s)\, F(f). \tag{4.12}$$

Using eq. (4.6) it follows that

$$\int_{-\infty}^{\infty} u(t)\, u(t+s)\, \mathrm{d}t = \int_{-\infty}^{\infty} |F(f)|^2 \exp(2\pi i f s)\, \mathrm{d}f. \tag{4.13}$$

From eqs (4.1) and (4.11) one can derive that

$$\psi(s) = N \int_{0}^{\infty} u(t)\, u(t+s)\, \mathrm{d}t. \tag{4.14}$$

Since $\psi(s)$ is real, combination of eqs (4.13) and (4.14) gives

$$\psi(s) = N \int_{-\infty}^{\infty} |F(f)|^2 \cos(2\pi f s)\, \mathrm{d}f. \tag{4.15}$$

With eq. (4.10) it follows that

$$\psi(s) = \int_{0}^{\infty} W(f) \cos(2\pi f s)\, \mathrm{d}f \tag{4.16}$$

and the inverse

$$W(f) = 4 \int_{0}^{\infty} \psi(s) \cos(2\pi f s)\, \mathrm{d}s. \tag{4.17}$$

This last expression is known as the *Wiener-Kintchine theorem*. It relates the power spectrum to the autocorrelation function of the fluctuating signal.

For a more complete treatment of this subject the reader is referred to the literature [125–129]. 127 A. van der Ziel } 128 " " " " }

4.2. Flux-flow noise

4.2.1. *Power spectrum of identical pulses*

We shall now describe the noise voltage, generated by the viscous flow of flux and derive expressions for the power spectrum of the noise. The treatment of this problem is analogous to that of shot noise in a vacuum diode, where the noise is due to the random emission and transport of discrete charge entities from the cathode to the anode, so that current pulses are generated. In the case of flux flow there is transport of discrete magnetic-flux entities from one edge of the superconductor to the other which causes the generation of voltage pulses.

We consider a superconducting slab of width w and length l between the potential probes in a perpendicular magnetic field. A transport current flows in a direction perpendicular to the field and along the length of the sample, as shown in fig. 3.1.

The following assumptions are made:

Discrete flux entities of magnitude Φ, which is an a priori unknown multiple of the flux quantum φ_0, are generated at the edge of the superconductor at random times. They subsequently flow, independently of each other, across the superconductor and it takes a time τ for them to cross the specimen. The flux entities, which in type-II superconductors are bundles of vortex lines (flux bundles) and in type-I superconductors normal domains, are assumed to follow the same velocity–time function, so that identical voltage pulses are generated.

The flux is moving in a direction perpendicular to current and field, which means that guided motion and the Hall effect are neglected.

The total flux in the specimen is constant.

We will treat the noise due to flux flow in type-II superconductors, but the results are also applicable to type-I superconductors.

As follows from eq. (2.14), the flow of one flux bundle gives rise to a potential difference between the probes, for $0 < t < \tau$:

$$V(t) = \frac{\Phi}{c\,w} v(t), \tag{4.18}$$

where $v(t)$ is the velocity, which may be time-dependent. The area under the voltage pulse is determined by the amount of flux that is transported and is equal to Φ/c.

If N is the average flux-bundle-generation rate, the average voltage across the sample can be written, according to eq. (4.2),

$$V \equiv \langle V \rangle = N \int_0^\tau V(t)\,\mathrm{d}t = N\frac{\Phi}{c}. \tag{4.19}$$

The mean-squared noise voltage in a frequency band between f and $f + \mathrm{d}f$ is

$$\langle \delta V_f^2 \rangle = W(f)\,\mathrm{d}f. \tag{4.20}$$

The power spectrum $W(f)$ can be calculated using eqs (4.10) or (4.14) and (4.17) from the Fourier transform or the autocorrelation function of the elementary pulse, if the pulse form is known. This is not known a priori but the results of the calculations of $W(f)$ will be given for a number of different pulse forms.

(1) If the generation and annihilation of the bundles is instantaneous and the velocity is constant, the resulting voltage pulse is a rectangular one:

$$V(t) = \Phi/c\,\tau \qquad \text{for} \qquad 0 \leqslant t \leqslant \tau,$$
$$V(t) = 0 \qquad \text{otherwise},$$

$$W(f) = \frac{2\,\Phi\,V}{c}\left[\frac{\sin(\pi f \tau)}{\pi f \tau}\right]^2. \tag{4.21}$$

This spectrum is zero at integer values of $f\tau$, and is shown in fig. 4.1.

(2) If the generation and annihilation of the bundles is not instantaneous, the pulse will have a trapeziumlike appearance. As an extreme example we consider a triangular pulse

$$V(t) = 4\,\Phi\, t/c\,\tau^2 \qquad \text{for} \quad 0 \leqslant t \leqslant \tau/2,$$
$$V(t) = 4\,\Phi\,(t-\tau)/c\,\tau^2 \qquad \text{for} \quad \tau/2 \leqslant t \leqslant \tau,$$
$$V(t) = 0 \qquad \text{otherwise},$$

$$W(f) = \frac{2\,\Phi\, V}{c}\left[\frac{\sin(\pi f\tau/2)}{\pi f\tau/2}\right]^4. \tag{4.22}$$

This spectrum has the same value for $f = 0$ as eq. (4.21) but has a higher cut-off frequency. The spectrum goes to zero, when $f\tau/2$ is an integer, and is also shown in fig. 4.1.

(3) As an intermediate case a sinusoidal voltage pulse is considered:

$$V(t) = (\pi\,\Phi/2\,c\,\tau)\sin(\pi\, t/\tau) \qquad \text{for} \quad 0 \leqslant t \leqslant \tau,$$
$$V(t) = 0 \qquad \text{otherwise},$$

$$W(f) = \frac{2\,\Phi\, V}{c}\left[\frac{\cos(\pi f\tau)}{1-4f^2\tau^2}\right]^2. \tag{4.23}$$

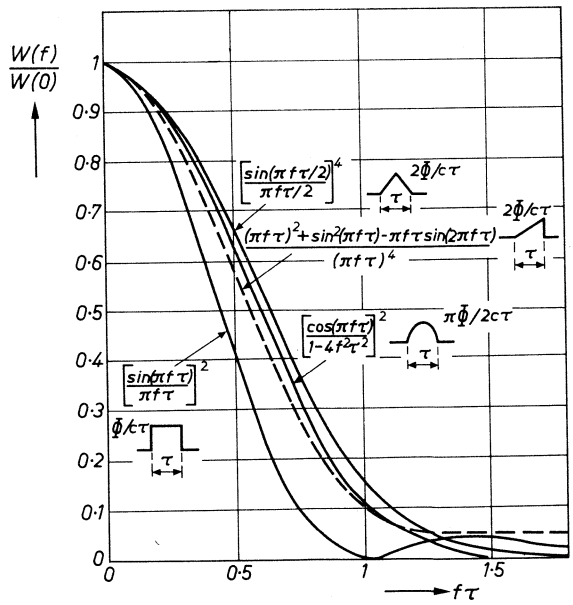

Fig. 4.1. Theoretical flux-flow noise-power spectra for various voltage pulses.

This spectrum is close to eq. (4.22), but it has a lower value for the cut-off frequency. $W(f)$ goes to zero for $f\tau = 3/2, 5/2$, etc. The spectrum is drawn in fig. 4.1.

(4) If the length of the vortex lines goes through a maximum when they move, as is the case when they cross a wire, the velocity increases as a function of time, as was discussed in sec. 2.3. In order to simplify this case the following triangular voltage pulse is assumed:

$$V(t) = 2\,\Phi\, t/c\,\tau^2 \qquad \text{for} \qquad 0 \leqslant t \leqslant \tau,$$
$$V(t) = 0 \qquad \text{otherwise},$$

$$W(f) = \frac{2\,\Phi\, V}{c} \frac{(\pi f \tau)^2 + \sin^2(\pi f \tau) - \pi f \tau \sin(2\pi f \tau)}{(\pi f \tau)^4}. \tag{4.24}$$

The spectrum is also shown in fig. 4.1. It has minima at integer values of

The power spectra for these four cases are very similar. Apparently the power spectrum is not very sensitive to the actual pulse shape. The extrapolated value at zero frequency is given by

$$W(0) = \frac{2\,\Phi\, V}{c}. \tag{4.25}$$

The voltage-time function for an elementary event as given by eq. (4.18) is only valid for $l > w$. Voltage pulses for various l/w ratios have been calculated by Clem [130]) under the assumptions that Φ and v are constant and the potential probes are point contacts, situated in the centre of the slab. For a flux bundle, moving in a plane between the probes, the voltage pulse was found to have a maximum when the flux bundle is in between the probes. This maximum is higher for smaller l/w ratios. For $l/w > 1$, the pulse is almost rectangular.

Flux bundles, passing close to a potential probe, give rise to high voltage peaks.

Clem also calculated the noise spectrum from the autocorrelation function of a pulse for the cases $l \ll w$ and $l \gg w$. In both cases the spectrum exhibits a $1/f$ tail at high frequencies, which arises from flux bundles passing near the probes. There is a noise cut-off at high frequencies due to the finite size of the potential probes and of the flux bundles.

When the potential probes are spot-welded, they are not point contacts, but are elongated as indicated in fig. 3.1. The generated voltage pulses then do not have a sharp maximum but are broadened, and more nearly rectangular for constant Φ and v. The effect of flux bundles passing close to the probes is then diminished.

If the experimental spectra agree with the theory, the measurements will permit the determination of two quantities: the values of the bundle size Φ and the transit time τ.

The value of Φ can be determined from the value of $W(0)$, and the d.c. voltage V by using eq. (4.25).

The second quantity to be found from the experimental spectra, is the transit time τ. This determination is only possible if the theoretical spectrum is known. As shown in fig. 4.1 this is dependent on the shape of the elementary voltage pulse. Since this is not known with certainty, the value of τ can therefore not be determined very accurately.

It was shown in sec. 2.3 that at low current densities only a fraction $(1 - p)$ of the number of vortex lines is moving. Equation (2.14) is then modified and reads $E = v\,B\,(1 - p)/c$. It follows then for the potential difference:

$$V = \frac{l\,w\,B\,(1-p)}{c\,\tau}. \tag{4.26}$$

Determination of τ from the noise measurements will therefore yield the value of the moving flux fraction $(1 - p)$.

4.2.2. *Power spectrum of non-identical pulses*

It was assumed so far that the elementary voltage pulses are identical, because bundle size Φ and velocity v are the same for each bundle. This condition of identity may not be fulfilled. If there is a distribution of bundle sizes, the value of Φ in the expressions for $W(f)$ will simply be the mean value.

If the velocity v follows a distribution function, the transit time τ will also be determined by this distribution function.

(a). A physical reason for a distribution of v is the distribution of threshold current densities J_t over the sample, as was pointed out by Fournet and Baixeras [131]).

If N_i is the generation rate of flux bundles with transit time τ_i, one can write

$$N_i = \frac{l\,w\,B\,(1-p)}{\Phi\,\tau_i}. \tag{4.27}$$

The values of τ_i are given by a distribution function $g(\tau_i)$ such that

$$\int_{\tau''}^{\tau'} g(\tau_i)\,\mathrm{d}\tau_i = 1,$$

where τ' and τ'' are the maximum and minimum values of τ_i respectively. It is not difficult to show that the power spectrum is now

$$W(f) = 2\,\frac{l\,w\,B(1-p)}{\Phi}\int_{\tau''}^{\tau'} |F(f,\tau_i)|^2\,g(\tau_i)\,\frac{\mathrm{d}\tau_i}{\tau_i}. \tag{4.28}$$

It depends on $g(\tau_i)$ how the spectrum is modified. In general the minima in the previously calculated spectra disappear and a tail will be found at the high-frequency side.

If a rectangular distribution function is assumed, i.e.

$$g(\tau_i) = 1/(\tau' - \tau''),$$

and with

$$|F(f,\tau_i)|^2 = (\Phi^2/c^2)\,[\sin(\pi f \tau_i)/\pi f \tau_i]^2,$$

as for rectangular pulses, the power spectrum is

$$W(f) = \frac{2\,\Phi\,V}{c \ln(\tau'/\tau'')}\left\{\tfrac{1}{2}\left[\frac{\sin(\pi f \tau'')}{\pi f \tau''}\right]^2 - \tfrac{1}{2}\left[\frac{\sin(\pi f \tau')}{\pi f \tau'}\right]^2 + \right.$$
$$\left. + \frac{\sin(2\pi f \tau'')}{2\pi f \tau''} - \frac{\sin(2\pi f \tau')}{2\pi f \tau'} - \mathrm{Ci}(2\pi f \tau'') + \mathrm{Ci}(2\pi f \tau')\right\}, \tag{4.29}$$

where

$$\mathrm{Ci}(\zeta) \equiv \int_{\infty}^{\zeta} \frac{\cos x}{x}\,\mathrm{d}x.$$

This spectrum is shown in fig. 4.2*a* and *b* as a function of $f\tau'$ for $\tau' = 5\,\tau''$.

A distribution of transit times is accompanied by a distribution of pulse heights, since the area under the pulse is constant.

(b). A different mechanism for a distribution of τ values is one, in which the motion of a flux bundle is interrupted due to interaction with pinning centres. Two times are now involved: the time, during which a flux bundle is free and is moving, and the time, during which it is pinned. This is similar to the case of generation-recombination noise in semiconductors, as was treated by Machlup [132]). Assuming an exponential distribution function for the two characteristic times, the noise power was found to have a $[1 + (2\pi f \tau_m)^2]^{-1}$ frequency dependence, where τ_m^{-1} is the sum of the two inverse time constants.

As a special case of this interaction, we assume that the flux bundles are halted for such short times that the total transit time τ is not affected to a first approximation, as is illustrated in the inset of fig. 4.3. The generation rate N is thus not affected by this mechanism. The transit of a flux bundle gives rise to a series of pulses with duration times τ_i.

The power spectrum can be written

$$W(f) = 2\,N \int_{\tau''}^{\tau} |F(f,\tau_i)|^2\, g(\tau_i)\,\mathrm{d}\tau_i. \tag{4.30}$$

This spectrum has been calculated for a number of distribution functions and for rectangular pulses:

(1) A rectangular distribution function, $g(\tau_i) = 1/(\tau - \tau'')$. The power spectrum is

$$W(f) = \frac{2\,\Phi\,V}{c}\left\{\frac{\tau''}{\tau}\left[\frac{\sin(\pi f \tau'')}{\pi f \tau''}\right]^2 - \left[\frac{\sin(\pi f \tau)}{\pi f \tau}\right]^2 + \right.$$

$$\left. + \frac{1}{\pi f \tau}\left[\mathrm{Si}(2\pi f \tau) - \mathrm{Si}(2\pi f \tau'')\right]\right\}, \quad (4.31)$$

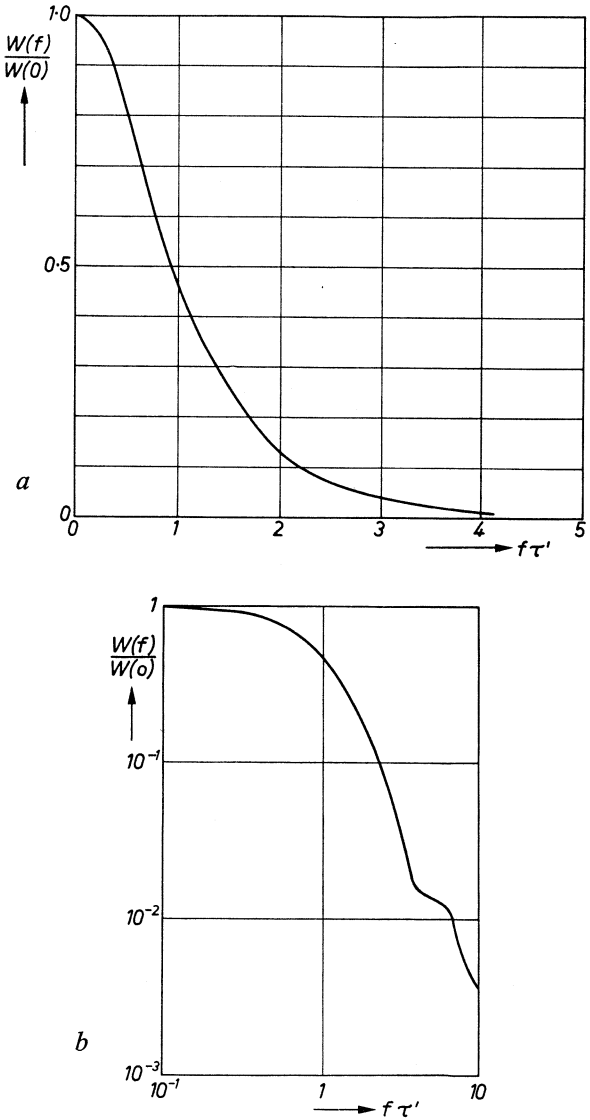

Fig. 4.2. Theoretical flux-flow noise-power spectrum of eq. (4.29) for rectangular voltage pulses with a distribution of transit times $g(\tau_i) = 1/(\tau' - \tau'')$ with $\tau' = 5\,\tau''$. (*a*) Linear scale; (*b*) log-log scale.

where

$$\mathrm{Si}(\zeta) \equiv \int_0^{\zeta} \frac{\sin x}{x}\,\mathrm{d}x.$$

For $\tau \gg \tau''$ we may write for frequencies less than $1/\tau''$:

$$W(f) = \frac{2\,\Phi\,V}{c}\left\{\frac{\mathrm{Si}\,(2\,\pi f\,\tau)}{\pi f\,\tau} - \left[\frac{\sin(\pi f\,\tau)}{\pi f\,\tau}\right]^2\right\}. \tag{4.32}$$

This power spectrum is calculated numerically with the help of tables published in the literature and is shown in fig. 4.3, curve c. At high frequencies the spectrum varies as $1/f$.

(2) Exponential distribution function with predominantly short pulses

$$g(\tau_i) = C_1 \exp(-\tau_i/\tau_1), \tag{4.33}$$

with

$$C_1 = \{\tau_1\,[1 - \exp(-\tau/\tau_1)]\}^{-1},$$

where τ_1 is a constant.

The calculation of $W(f)$ was done on a computer for $\tau_1 = \tau/3$ and for $\tau_1 = \tau$ and assuming $\tau \gg \tau''$. The results are shown in fig. 4.3, curves a and b.

At high frequencies the spectra follow also a $1/f$ frequency dependence. The spectra are shifted to higher frequencies with respect to the spectrum of eq. (4.31) because by this distribution function more short pulses are assumed.

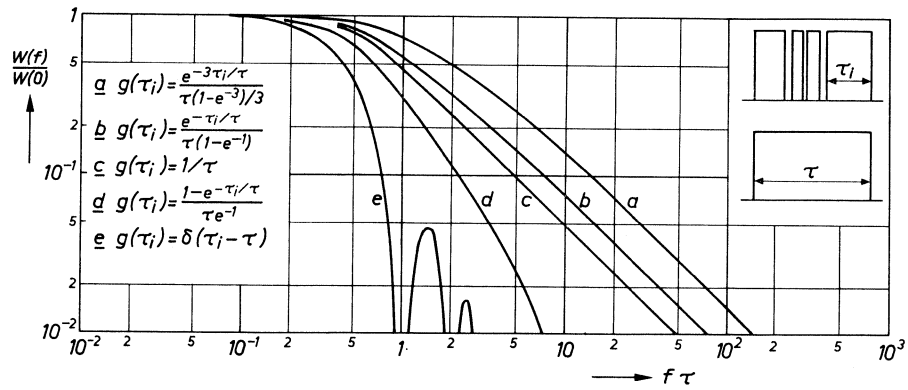

Fig. 4.3. Theoretical flux-flow noise-power spectra $W(f)/W(0) = \int_0^{\tau} g(\tau_i)[\sin(\pi f\tau_i)/\pi f\,\tau_i]^2\,\mathrm{d}\tau_i$ for various distributions of duration times $g(\tau_i)$ of rectangular pulses. In the inset: voltage pulses with and without halting, transit time τ.

(3) Exponential distribution function with predominantly long pulses

$$g(\tau_i) = C_2\,[1 - \exp(-\tau_i/\tau_1)], \tag{4.36}$$

with

$$C_2 = \{\tau + \tau_1\,[\exp(-\tau/\tau_1) - 1]\}^{-1}.$$

The power spectrum has been derived from the previous two cases for $\tau_1 = \tau$ and is drawn in fig. 4.3, curve d. It exhibits an $1/f$ behaviour for $f\tau > 10$ (not drawn).

(4) If for the distribution function a delta function is taken, the spectrum is simply given by eq. (4.21). This is also shown in fig. 4.3, curve e, for $g(\tau_i) = \delta(\tau_i - \tau)$.

It has been remarked by Heiden [133]) that the $1/f$ dependence occurs for a wide class of distributions $g(\tau_i)$, regardless of the pulse shape.

4.2.3. *Flux-modulation noise*

The value of Φ was so far assumed to be constant for a given bundle. In fact it is likely that due to interaction with pinning centres the bundle size will undergo random fluctuations during the transit across the superconductor by picking up and losing vortex lines. If the duration times of these fluctuations follow an exponential distribution with average value τ_2, the autocorrelation function of the bundle-size fluctuations $\delta\Phi(t)$ can be written as [134])

$$\langle \delta\Phi(t)\,\delta\Phi(t+s)\rangle = \langle \delta\Phi^2\rangle \exp(-s/\tau_2). \tag{4.35}$$

The power spectrum of this modulation noise voltage can be calculated with eq. (4.17):

$$W(f) = 4\,V^2\,\frac{\langle \delta\Phi^2\rangle}{\Phi^2}\,\frac{\tau_2}{1 + (2\pi f\tau_2)^2}. \tag{4.36}$$

By analogy velocity fluctuations δv give rise to a flux-modulation noise-power spectrum:

$$W(f) = 4\,V^2\,\frac{\langle \delta v^2\rangle}{v^2}\,\frac{\tau_2}{1 + (2\pi f\tau_2)^2}. \tag{4.37}$$

Fluctuations of N are related to the bundle-size fluctuations and the velocity fluctuations.

4.2.4. *Other sources of noise*

It was assumed that the generation and annihilation of a vortex line does not give rise to voltage pulses. This agrees with the evidence that in a type-II super-

conductor with a reversible magnetization curve, where the heat-absorption process in isothermal magnetization and demagnetization is also reversible [135]), the generation and annihilation of a vortex is not dissipative [136]) and does thus not give rise to noise. It is not known whether this also applies to irreversible superconductors. The effect may be an extra source of noise.

The number of vortex lines in the superconductor was so far taken to be constant, because the average generation and annihilation rates are equal. In fact, the flux content of the superconductor may undergo fluctuations. If d is the distance between the vortex lines, the characteristic time for these fluctuations is of the order of d/v. The resulting noise therefore has a cut-off frequency of the order of v/d.

If the flux motion in a type-II superconductor is not in the form of independent flux bundles, but as a rigid vortex lattice, there is no noise, as the generation at the edge is then not random. It was pointed out by Kulik [59]) and by Caroli and Maki [61]) that the current then contains an a.c. term with frequencies $f = k\,v/d$, where k is an integer. This is due to the uniform motion of the periodic vortex structure, which thus gives rise to a line spectrum probably in the MHz range.

4.2.5. *Noise in a Corbino disc*

In a Corbino disc, where one potential contact is in the centre and the other along the entire circumference, no flux-flow noise is generated. The electric field is directed radially and the flux bundles flow in concentric circles. There is then no transit of flux from one edge to another, but there is a continuous motion, and no generation and annihilation of vortex lines occur. Consequently the motion of a flux bundle does not generate a voltage pulse, but a constant voltage, if the velocity and bundle size are constant. There is thus no flux-flow noise. If there are fluctuations of v and Φ there will be flux-modulation noise.

4.3. Johnson noise

We shall now derive an expression for the Johnson-noise voltage across a type-II superconducting slab analogous to the Nyquist formula for a resistor.

Consider a vortex line with effective mass M_v per unit length, which determines the inertia when a force is applied. We assume Langevin's equation to apply

$$M_v \frac{\mathrm{d}v}{\mathrm{d}t} + \eta\, v = \frac{F(t)}{L}, \tag{4.38}$$

where $F(t)$ is the fluctuating force on a vortex line, and L is the length of the vortex lines, which is assumed to be constant. It is further assumed that $\langle F(t) \rangle = 0$.

The autocorrelation function for the velocity can be written

$$\langle v(t)\, v(t+s)\rangle = \langle v^2(t)\rangle \exp(-s/\tau_3), \tag{4.39}$$

with $\tau_3 = M_v/\eta$.

In the case of thermal equilibrium $\langle v^2\rangle = k_B\, T/M_v\, L$. It then follows for the mean squared velocity fluctuations

$$\langle v_f{}^2\rangle = \frac{4\, k_B\, T/\eta\, L}{1 + (2\,\pi f\,\tau_3)^2}\, \mathrm{d}f. \tag{4.40}$$

The voltage between the potential probes, due to motion of one vortex line, is $V = v\, \varphi_0/c\, w$. With the help of eqs (2.22) and (2.30) the m.s. voltage fluctuations due to all the vortex lines in the superconductor can be shown to be

$$\langle \delta V_f{}^2\rangle = \frac{4\, k_B\, T\, R_{fl}}{1 + (2\,\pi f\,\tau_3)^2}\, \mathrm{d}f, \tag{4.41}$$

where $R_{fl} = \varrho_{fl}\, l/L\, w = V/(I - I_t)$ and I_t is the threshold current. It is assumed that the individual fluctuations of the vortex lines are random.

The equation is analogous to Nyquist's formula for Johnson noise in a resistor with resistance R_{fl}. The value of τ_3, as given by Bardeen and Stephen [53]) for a superconductor with negligible Hall angle, is $\tau_3 = 2\,\tau_n$ close to H_{c_2} and $\tau_3 = \tau_n$ at low fields.

In the derivation of eq. (4.41) thermal equilibrium was assumed. It is not certain that this is the case when a transport current is present. According to Clem [137]) temperature gradients exist near a vortex line, which may cause thermal non-equilibrium for high vortex velocities.

4.4. Flicker noise

In this section we will deal with the noise that is due to local temperature fluctuations in the superconductor. This type of noise follows roughly a $1/f^2$ frequency dependence. Since it is due to temperature fluctuations, it will be called flicker noise. We use a model that is based on the hypothesis that the temperature fluctuations are caused by fluctuations in the transfer of Joule heat from the superconductor to the helium bath.

When heat is transferred from a heater to a liquid, three principal heat-transfer mechanisms can be distinguished in the stationary state. This is shown for liquid helium I [138]), in fig. 4.4, where the heat flux q is drawn as a function of the difference between the heater temperature T_h and the temperature T_l of the liquid. At low values of $(T_h - T_l)$, the mechanism of heat transfer is convection of the liquid, giving rise to a heat flux q proportional to $(T_h - T_l)$. If there is turbulence in the liquid, this may cause temperature fluctuations in the heater. At higher power levels a second mechanism is superposed on the

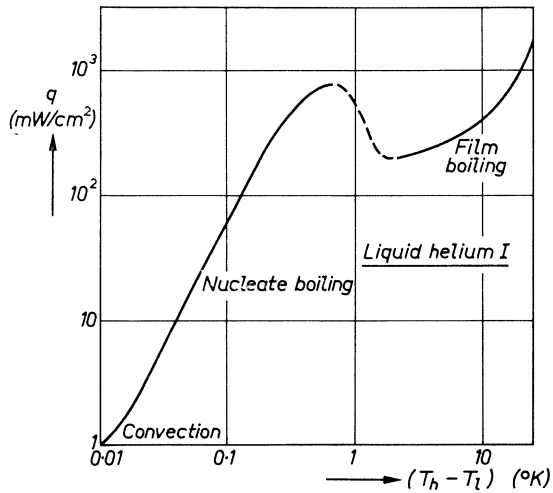

Fig. 4.4. Experimental heat-transfer curve for liquid helium I [139]). The heat flux q is plotted as a function of the difference between the heater temperature T_h and the bath temperature T_l.

convective heat transfer, namely nucleate boiling. Due to formation of vapour bubbles on the surface, the heat transfer is improved considerably. In liquid helium the heat flux varies with the temperature difference in this regime as $q \propto (T_h - T_l)^2$ for a smooth surface [139]).

When the dissipated power is greater than a critical value, called the peak heat flux, the bubble formation is so vigorous, that the bubbles coalesce and a vapour film is formed with a much lower heat-transfer rate. This phenomenon is called film boiling.

In the nucleate-boiling regime the heat transfer at a particular site increases during formation and growth of a bubble, so that there the surface temperature drops. After departure of the bubble [140]) the heat transfer is decreased and the surface temperature increases slowly until a new bubble is formed. These local temperature fluctuations have been studied in boiling water and organic liquids or mixtures by using small thermocouples or thin-film thermometers [141–144]).

The fluctuations could be identified with bubble formation. This formation takes place at certain nucleation sites, the number of which increases with increasing power dissipation. At low values of the heat flux the bubbles at a particular site are formed at irregular time intervals, but at higher heat flux this occurs more or less periodically.

No data on these temperature fluctuations are available for liquid helium, but the heat-transfer mechanism appears to be the same as in other liquids, and the temperature–time function of the fluctuations is therefore assumed to be roughly the same.

In order to deal with the problem analytically the time function of the local-surface-temperature pulse is assumed to be given by

$$\begin{aligned} \Delta T(t) &= -\Delta T_m \, t/\tau_b && \text{for} \quad 0 \leqslant t \leqslant \tau_b, \\ \Delta T(t) &= -\Delta T_m \exp\left[(\tau_b - t)/\tau_0\right] && \text{for} \quad t > \tau_b, \end{aligned} \tag{4.42}$$

where at $t = \tau_b$ the bubble leaves the surface and τ_0 is the surface-heating time constant. The function is shown in the inset of fig. 4.5. The pulse form is close to what was found experimentally in other liquids.

For the calculation of the voltage fluctuations across the superconductor due to these temperature pulses it is necessary to know the temperature dependence of the flux-flow voltage, which is a function of the threshold current density J_t, the pinned fraction p and the viscosity coefficient η. This function is not known in analytical form. In order to be able to calculate the m.s. voltage fluctuations it is therefore assumed (which was verified by the experiments) that the resistance changes linearly with temperature, i.e. $\Delta R = k_1 \, \Delta T$.

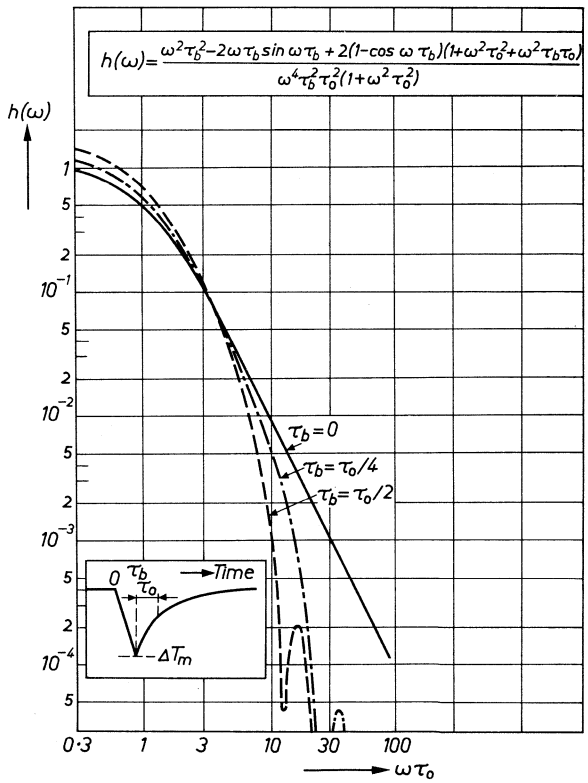

Fig. 4.5. Theoretical flicker-noise-power spectra of eq. (4.44) for three pulse forms. The inest shows the temperature–time pulse.

It is further assumed that the resistance changes in an area equal to the cross-section of a bubble. If the current distribution is not affected by the local resistance change, and the foil width is w, the voltage change across the specimen due to one bubble with diameter D_b for a current I is

$$\Delta V = I \frac{D_b}{w} k_1 \Delta T. \tag{4.43}$$

If the bubbles are distributed across the surface independently of each other and if they are generated at random at a rate N, thereby generating temperature pulses as given by (4.42), the noise-power spectrum can be written

$$W(f) = 2N \left[I \frac{D_b}{w} k_1 \Delta T_m \tau_0 \right]^2 h(\omega), \tag{4.44}$$

with

$$h(\omega) = \frac{\omega^2 \tau_b^2 - 2\omega \tau_b \sin(\omega \tau_b) + 2[1 - \cos(\omega \tau_b)][1 + \omega^2 \tau_0^2 + \omega^2 \tau_b \tau_0]}{\omega^4 \tau_b^2 \tau_0^2 (1 + \omega^2 \tau_0^2)}$$

and $\omega = 2\pi f$.

This spectrum is shown in fig. 4.5 as a function of $\omega \tau_0$ for various values of τ_b/τ_0. The oscillatory behaviour at high frequencies will only be found if the lifetime of a bubble τ_b is constant everywhere on the surface. It is to be expected that due to a distribution of lifetimes these minima and maxima will be smeared out.

For $\tau_b = 0$ the noise spectrum reduces to

$$W(f) = \frac{2N(I D_b k_1 \Delta T_m \tau_0/w)^2}{1 + \omega^2 \tau_0^2}. \tag{4.45}$$

For frequencies higher than $1/\tau_0$ this noise has a $1/f^2$ frequency dependence.

5. MEASUREMENTS OF FLUX-MOTION NOISE IN TYPE-II SUPERCONDUCTORS

In this chapter the results of noise measurements on type-II superconductors are presented and compared with the theory, as given in chapter 4 and with the results of the d.c. measurements, as given in chapter 3. After a description of the experimental conditions, we shall first show a number of power spectra, measured on vanadium foils for various combinations of field, transport current and temperature. The measurements allow the determination of the fraction of flux that is pinned and the flux-bundle size. These quantities are given as a function of field, current and temperature. Next the noise reduction at low frequencies will be treated. Results of noise measurements are also given for In-20 at. % Tl wire. Measurements of flicker noise due to temperature fluctuations are shown and discussed. Finally the interpretation of the noise measurements and the implications for the mechanism of flux flow are discussed in the last section.

5.1. Experimental methods

5.1.1. *Experimental set-up*

The power spectra of the mean-squared noise voltages were measured by using a network as shown in fig. 5.1 in a block diagram. The a.c. signal across the potential probes of the superconductor is transformed up using a transformer with mu-metal core. The signal is then amplified about 100 times by a low-noise broad-band amplifier. The amplified signal is fed into a wave analyzer. This is an instrument operating on the heterodyne principle which can be tuned to any frequency f_0 between about 10 Hz and 16000 Hz.

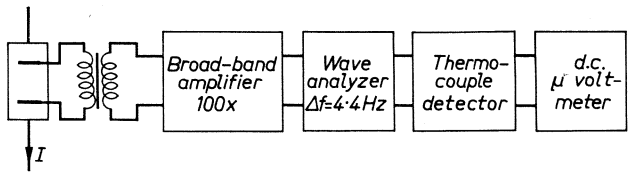

Fig. 5.1. Block diagram of measuring set-up for noise-power spectra.

The input signal is mixed with a signal of frequency 50 kHz $-f_0$. If the frequency f_0 is present in the incoming signal, the sum frequency is passed through a 50-kHz band-pass filter on to the second stage where it is mixed with a signal of frequency 51·5 kHz. The difference frequency is filtered out with adjustable bandwidth Δf and amplified.

The output signal is rectified by a quadratic detector. This is a detector which directly measures the noise power. Two thermocouple valves Philips TH1 are

used in series, which are protected against overloading. The output signal of the detector is measured with an electronic microvoltmeter (Philips GM 6020).

The time constant of the detecting circuit is almost entirely determined by the thermocouples and is equal to 2·5 s. Either of two input transformers was used. One had a flat frequency characteristic above 30 Hz and a transformation ratio of about 100. The other had a more or less flat frequency characteristic between 10 Hz and 1000 Hz and a transformation ratio of about 190. The latter was only used for measurements at low frequencies. The broad-band amplifier used in the early stages of the work was a valve amplifier. Later a transistor amplifier (Philips PM 6045) was used because of the higher amplification at low frequencies.

The wave analyzer used was a Radiometer (Copenhagen) type FRA 1. For measurements below 20 Hz use was sometimes made of type FRA 2, because of its better stability at low frequencies. The measuring circuit has a power-transfer function $G(f)$. If the noise power at the input is $W(f_0)$, the power at the output is proportional to $W(f_0)\,G(f_0)$, if the circuit is a linear system. The power-transfer function was determined from measurements of the thermal e.m.f., with a known signal on the input transformer. The calibration was carried out by means of a Philips RC generator (20-16000 Hz) or a Peekel RC generator (5-11000 Hz). By using a voltage divider a voltage of 1 μV was fed into the input transformer, the wave analyzer was tuned to the signal frequency and the voltage on the μV meter (GM 6020) was measured for different frequencies. The resistance that was put across the input transformer was 0·01 Ω, being of the same order of magnitude as the specimen resistance.

Figure 5.2 gives the reading on the μV meter for an input signal of 1 μV on the wave analyzer with 1000× amplification and for the two transformers. The

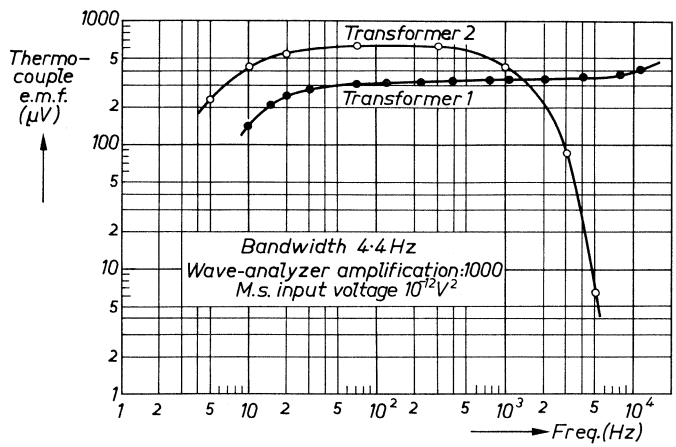

Fig. 5.2. Calibration of the noise-measuring circuit for two different input transformers. The thermal e.m.f. is shown as a function of wave-analyzer frequency for 10^{-12} V^2 on the input.

thermocouple voltage was found to be linearly dependent on m.s. input voltage for a thermal e.m.f. of up to 3 mV. Due to the linearity of the system, the power-transfer function is the same for other wave-analyzer amplifications.

The limit of detection of the set-up was about 5.10^{-19} V^2 across a specimen resistance of about 5 mΩ. This is the difference between readings with the noise source switched on and off. This limit was mainly determined by the sensitivity of the wave analyzer.

The bandwidth Δf of the measuring circuit if defined as the integrated passband divided by the power-transfer function $G(f)$ at the tuned frequency f_0,

$$\int_0^\infty G(f)\,\mathrm{d}f = \Delta f\, G(f_0), \tag{5.1}$$

was found by graphical integration to be 4·4 Hz. If defined as

$$G(f_0 \pm \Delta f/2) = \tfrac{1}{2}\, G(f_0), \tag{5.2}$$

Δf was 4·0 Hz. The ratio $G(f)/G(f_0)$ is shown in fig. 5.3 for $f_0 = 220$ Hz.

The output signal $A(t)$ of the thermocouple detector is composed of a d.c. and a noise component. The relative error of a single measurement is now defined as

$$\alpha_r = \frac{\langle\{A(t) - \langle A(t)\rangle\}^2\rangle^{1/2}}{\langle A(t)\rangle}. \tag{5.3}$$

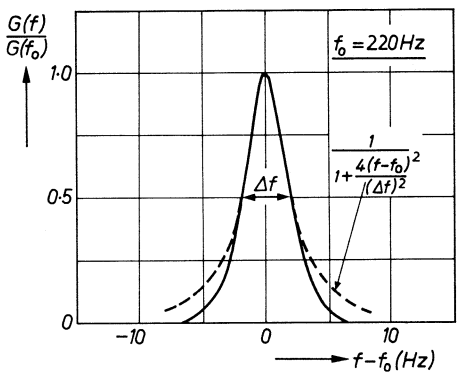

Fig. 5.3. Power-transfer function of the measuring circuit in normalized units for $f_0 = 220$ Hz. The bandwidth Δf as defined by the width at $G(f)/(G f_0) = 0{\cdot}5$ is indicated.

For a detector circuit of time constant τ_d and a frequency passband with spectrum,

$$G(f) = \frac{G(f_0)}{1 + 4\,(f - f_0)^2/(\Delta f)^2}, \tag{5.4}$$

as indicated in fig. 5.3 and where Δf is defined by eq. (5.2), it can be shown [145]) that the value of α_r is given by

$$\alpha_r = (4\,\Delta f\,\tau_d)^{-1/2}. \tag{5.5}$$

Since $\Delta f = 4$ Hz and $\tau_d = 2{\cdot}5$ s, the r.m.s. fluctuation about the average reading amounts to about 16%. Individual fluctuations can of course be much higher.

5.1.2. *Measurements*

The noise was measured as the difference between microvoltmeter reading with transport current switched on and off. It was always verified that the measured noise was due to the mixed state by also carrying out the same measurement in zero field as well as in a field above H_{c2}. This rules out possible noise caused by current fluctuations in the specimen or in the electromagnet.

Frequency spectra were measured by setting the wave analyzer at different frequencies, whereby the 50-Hz mains frequency and its harmonics were avoided. Sufficient time was taken at each frequency to get an averaged reading. The reading was averaged by visual observation. In some experiments the output of the GM 6020 microvoltmeter was connected to a recorder to find the average. There was no difference in the results from both methods.

The spectra were measured for different values of magnetic field, transport current and temperature. This was done on the vanadium foils and the indium-20% thallium wire, the dimensions of which are given in table III. The material properties are given in table II (sec. 3.1.2). The magnetic field was always first decreased to zero from above H_{c2} and then increased to a chosen value.

TABLE III

Length between potential probes and width of specimens for noise measurements

specimen	length (mm)	width (mm)
V2a	5·8	1·3
V2b	10·8	2·8
V2c	4·7	1·1
V2e	5·4	1·2
V4a	9·9	0·85
V5	2·5	
In-20% Tl	5	2

The potential and current leads to the specimens were properly shielded. This shielding was done in the helium cryostat by a German-silver tube.

It was found that the measurements were sometimes not reproducible from run to run, if the specimen was allowed to warm up in between different helium runs. This may be caused by different conditions of stress in the sample. The irreproducibility could be avoided if the specimens were glued rigidly to the holder and kept cold (in liquid nitrogen) in between successive helium runs.

5.2. Flux-flow noise in vanadium foils

5.2.1. *Power spectra*

Typical flux-flow noise-power spectra are drawn in fig. 5.4 for two values of the magnetic field. The corresponding oscillograms of the noise measured with a band pass between 1 and 2000 Hz are shown in fig. 5.5.

In some cases the noise spectra at low frequencies exhibited either a very sharp rise due to the flicker effect or a decrease. These effects will be discussed later. In the discussion of the flux-flow noise they will be neglected for the time being and they are disregarded for the determination of $W(0)$. The flux-flow noise can be distinguished from the flicker noise by the different power spectrum. Figure 5.6 shows measurements where both flicker noise and flux-flow noise are found. The value of $\langle \delta V_0{}^2 \rangle$ due to flux flow is determined by extrapolation. This introduces an uncertainty in $W(0)$, which in some cases may be appreciable.

Some of the measured spectra are shown in figs 5.7 and 5.8 for specimens V2c and V2a for various combinations of field, current and temperature. The power spectra $W(f)$ are given in normalized units, relative to the extrapolated value at zero frequency $W(0)$. Also shown in the figures is the theoretical spectrum for sinusoidal pulses with transit time τ, as given in chapter 4:

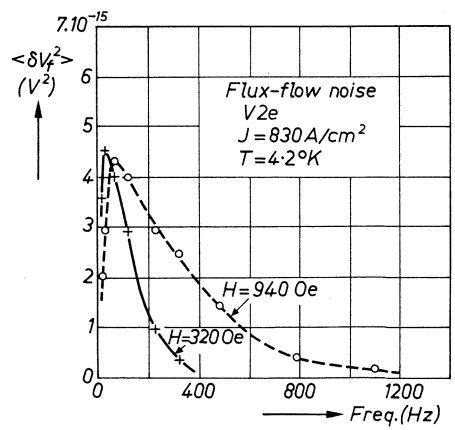

Fig. 5.4. Experimental flux-flow noise-power spectra for two values of the magnetic field, specimen V2e, $J = 830$ A/cm^2.

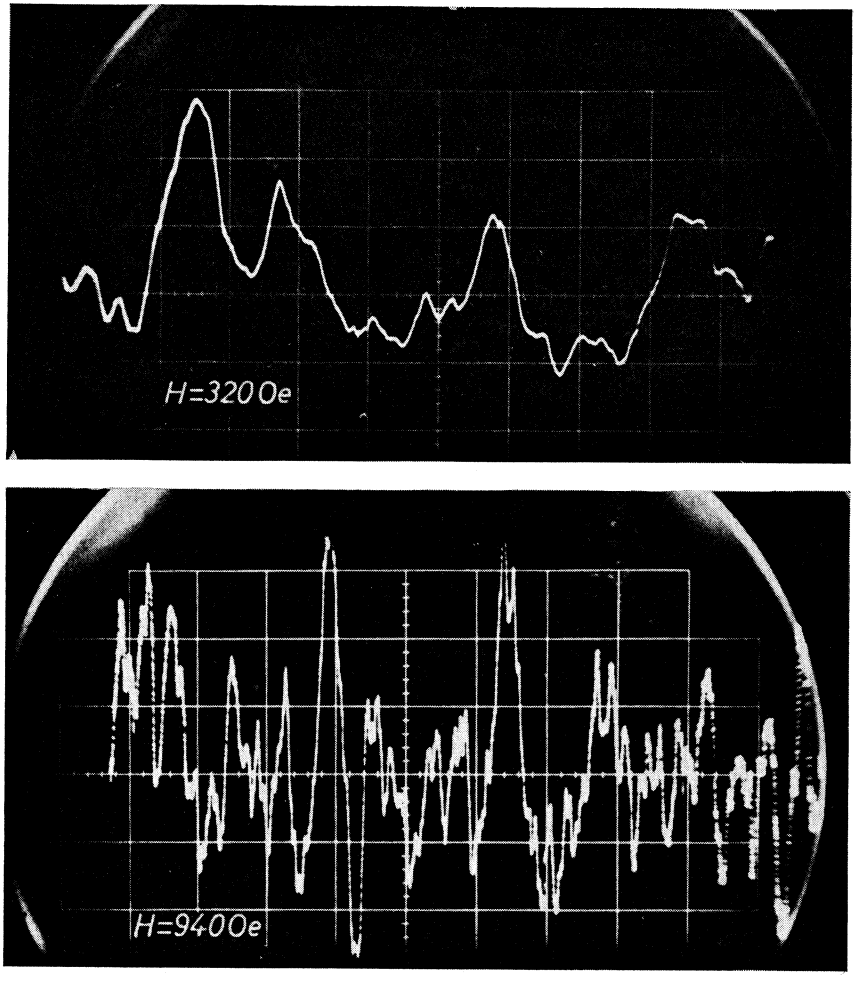

Fig. 5.5. Oscillograms of noise voltage, corresponding to the spectra of fig. 5.4. Vertical deflection 0·5 μV/div; horizontal deflection 5 ms/div.

$$W(f) = \frac{2\,\Phi\,V}{c}\left[\frac{\cos(\pi f \tau)}{1-4f^2\tau^2}\right]^2. \tag{5.6}$$

This was fitted to the experiments by drawing the theoretical curve systematically through or below the experimental points, because of the possibility that there is extra noise by some other causes. The flicker-noise and the low-frequency-noise reduction were disregarded in this procedure. The cut-off frequency of the noise $f_c = 1/\tau$ gives the value of the transit time. If it is assumed that flux motion is in a direction perpendicular to transport current and field, τ is also given by

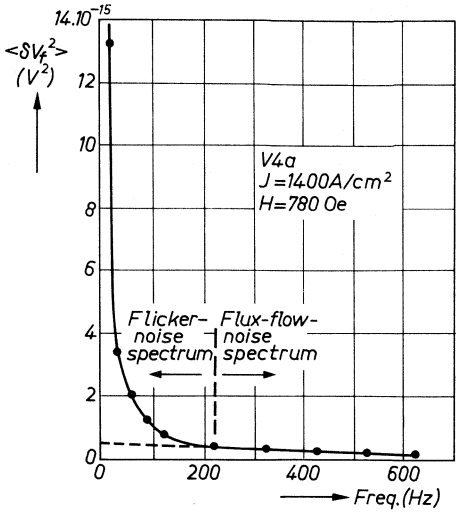

Fig. 5.6. Experimental power spectrum when both flux-flow noise and flicker noise are present, specimen V4a.

$$\tau = \frac{l\, w\, B\,(1-p)}{c\, V}\,; \tag{5.7}$$

as follows from eq. (4.28). The experimental results thus allow the determination of p as B and V are known.

The values of magnetic field H, current density J and temperature T are given for each spectrum, as well as the values of d.c. voltage V, $\langle \delta V_0{}^2 \rangle$, bundle size Φ and pinned fraction p.

Figure 5.9 shows experimental spectra for specimen V2b at $T = 4{\cdot}21$ °K. For some spectra eq. (5.6) could not be fitted to the experimental points, as this would mean a negative value of p. The spectra of fig. 5.9 are therefore compared with the theoretical spectrum of eq. (4.21) for rectangular voltage pulses. That this spectrum fits the experimental results better might be due to the fact that specimen V2b is much wider than the others, so that the edge effects are less important and the elementary voltage–time function resembles a rectangular pulse.

In specimen V2a at low currents and fields the assumption of flux motion perpendicular to current and field is not justified, as was discussed in sec. 3.1.3. For the lowest currents and fields, where noise measurements were carried out, the angle between the directions of motion and transport current is about 50°, as follows from fig. 3.6. The distance over which a flux bundle travels is then not equal to w, but about 30% greater and the transit time is greater than w/v by the same amount. At higher values of current and field the flux motion is at about 70° to the current direction and the transit time is then about 6% greater than w/v.

The measured power spectra, as shown in figs 5.7 to 5.9, agree reasonably well with the theoretical spectra for pulses with one transit time, except at low temperatures. This agreement is found especially for the unannealed samples

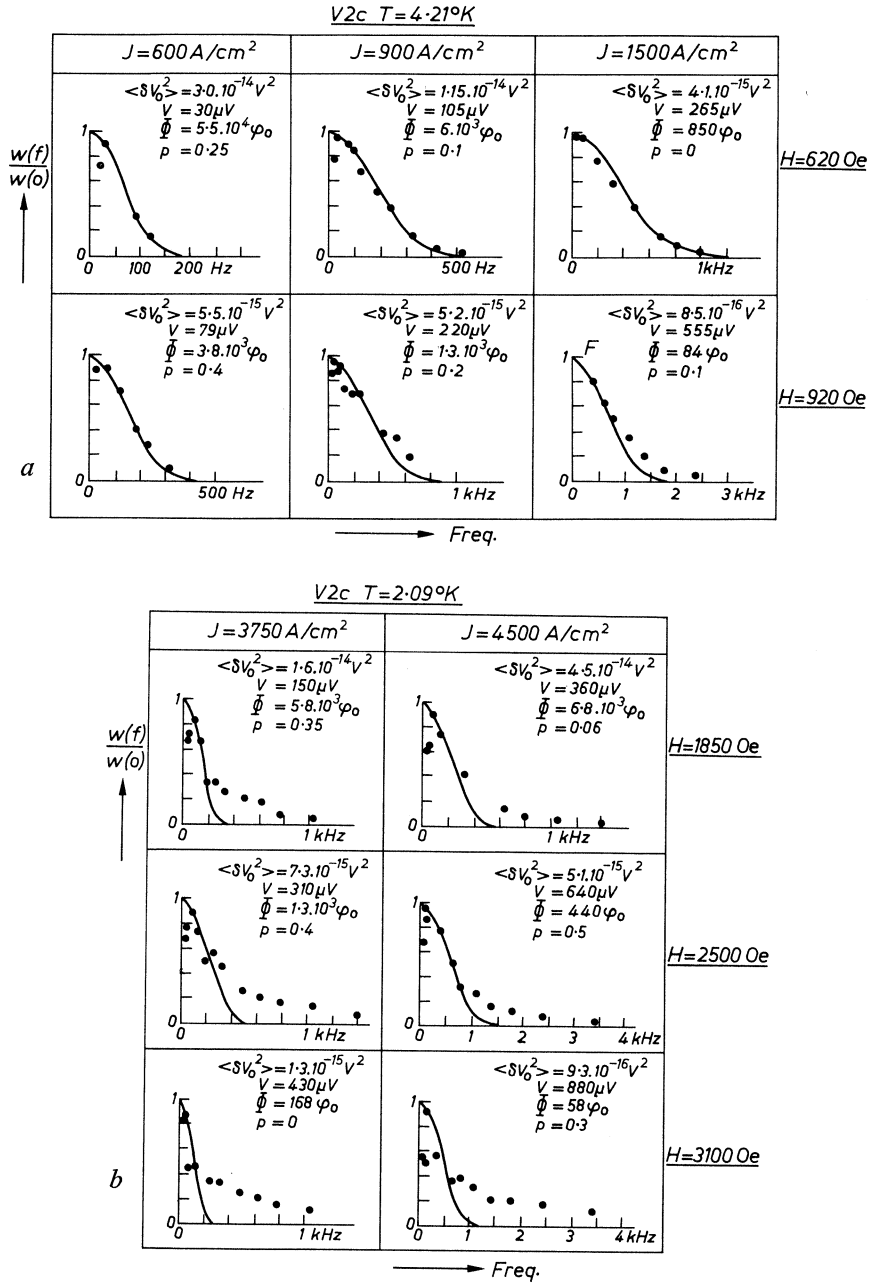

Fig. 5.7. Experimental flux-flow-noise spectra normalized at $W(0)$ for specimen V2c at different values of transport-current density J and magnetic field H. The drawn curves are the spectra given by eq. (5.6) which is fitted to the experimental points by choosing the value of p. The symbol F indicates the presence of flicker noise. The figures give the value of the extrapolated m.s. noise voltage $\langle \delta V_0^2 \rangle$, d.c. voltage V, bundle size Φ and pinned fraction p; (*a*) $T = 4{\cdot}21$ °K, (*b*) $T = 2{\cdot}09$ °K.

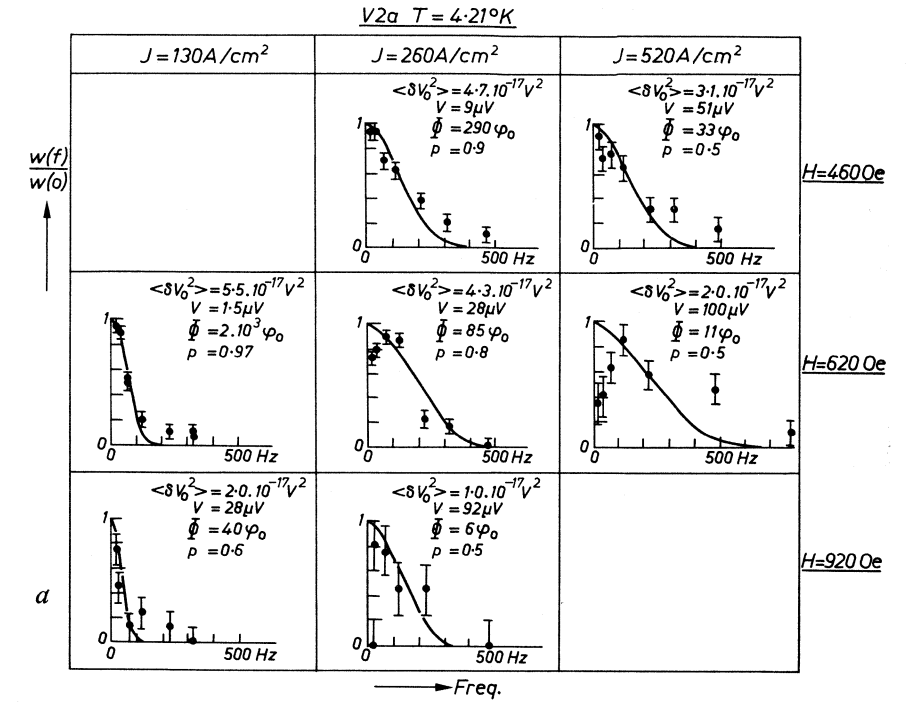

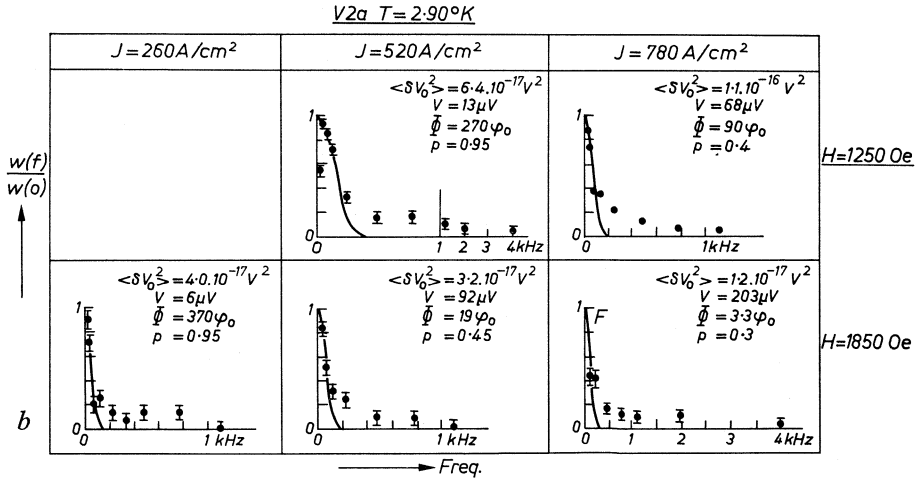

Fig. 5.8. The same as for fig. 5.7, for specimen V2a; vertical bars denote the uncertainty in $W(f)$. (*a*) $T = 4{\cdot}21$ °K, (*b*) $T = 2{\cdot}90$ °K.

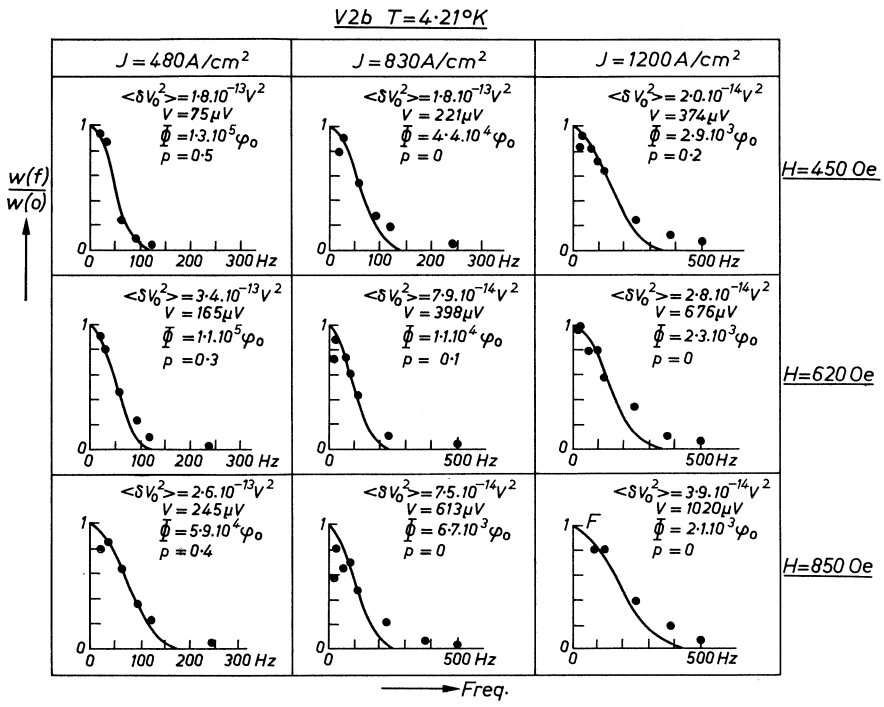

Fig. 5.9. The same as for fig. 5.7 for specimen V2b; $T = 4{\cdot}21$ °K. The drawn curves are the spectra, given by eq. (4.21).

V2b and V2c. The transit times, as determined from these spectra, varied in the experiments between 0·5 and 10 ms, which corresponded to a velocity range between 10 and 150 cm/s.

At low temperatures the theoretical spectra for pulses with one transit time do not fit the experimental points very well. In most cases a high-frequency tail on the spectra is found which is absent on the theoretical spectra, as can be seen in fig. 5.7*b* for specimen V2c and in fig. 5.8*b* for specimen V2a. The high-frequency behaviour is also illustrated in fig. 5.10 where some spectra for these two specimens are drawn on a log-log plot. The figure shows that the noise spectra for specimen V2c fall off with frequency more rapidly than the spectra for specimen V2a. In the latter case there is a large error at high frequencies due to the low noise level. These spectra are likely to be caused by a distribution of pulse durations, as was discussed in sec. 4.2.2. It was shown there that the theoretical spectra are dependent on the actual distribution function $g(\tau_i)$ and on the mechanism that causes the distribution of pulse durations. If this mechanism is a distribution of values of the threshold current density J_t over the specimen, a possible spectrum is that which was shown in fig. 4.2*a* and *b* for a rectangular distribution function of rectangular pulses. A jerky motion

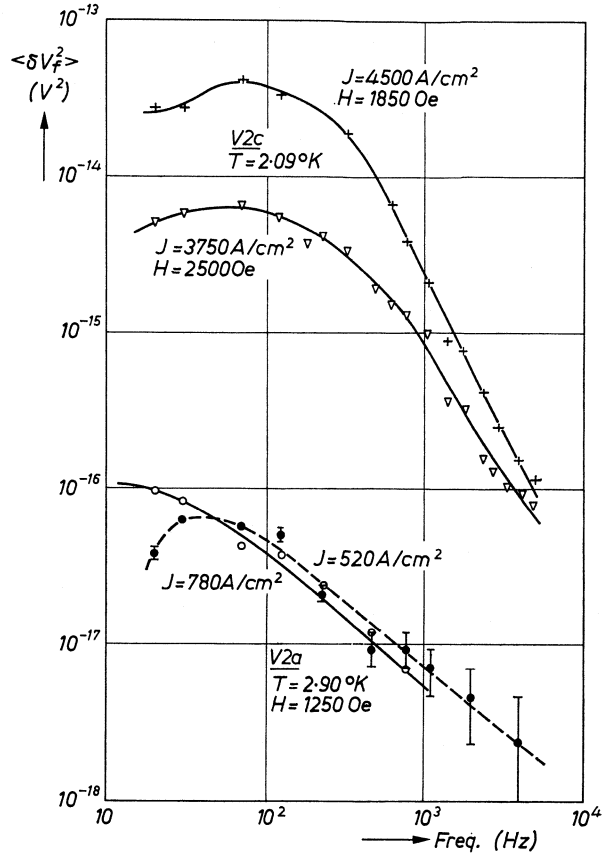

Fig. 5.10. Experimental flux-flow-noise spectra on a log-log scale for specimens V2c (T = 2·09 °K) and V2a (T = 2·90 °K). For clarity the error bars have been omitted from one of the curves for specimen V2a.

of flux bundles with constant total transit time gives $1/f$ noise for various types of distribution functions, as shown in fig. 4.3. A jerky motion with random pulse durations gives $1/f^2$ behaviour at high frequencies. This is also the case for flux-modulation noise due to random fluctuations of bundle size or velocity, as was discussed in sec. 4.2.3.

A quantitative comparison of the experimental curves with theory is difficult because of the variety of possible spectra. We will therefore only give some qualitative conclusions about these spectra. The spectra for specimen V2a, which were found to fall off with frequency roughly as $1/f$, are probably caused by a jerky motion of flux bundles with negligible pinning times. The spectra for specimen V2c, which fall off with frequency more rapidly, are probably caused by a distribution of J_t values and not by a jerky motion. In the latter case the cut-off frequency does not give the correct value for the moving flux fraction $(1-p)$ with eq. (5.7), as will be discussed in the next section.

There may be also flux-modulation noise present in the experimental spectra, also giving rise to a high-frequency tail, but a quantitative evaluation is not possible. The same applies to a high-frequency tail from flux bundles passing very close to the potential probes [130]), as discussed in sec. 4.2.1.

The different behaviour between specimens V2a and V2c may be caused by the difference in structure. In specimen V2a the pinning is partly due to grain boundaries, which lie parallel to the vortex lines. The number of these grain boundaries, encountered by a moving flux bundle is relatively small and in between there is probably very little pinning. The motion of a flux bundle is thus likely to be interrupted a number of times, as was also observed with a Bitter technique [146]). The interaction with surface valleys probably also causes the flux bundles to move in an irregular manner.

Specimen V2c contains very many dislocations, arranged in cells of about 0·5 μ diameter. In this specimen the pinning centres are much more homogeneously distributed and there is less chance for a flux bundle to be stopped once it is moving. There will probably be only small fluctuations in the flow velocity.

The pinning effects, which cause the high-frequency tail on the spectrum, are much more severe at low temperatures, as was discussed in chapter 2. This explains why the discrepancy between the experimental spectra and the simple theory is mainly found at the lower temperatures.

5.2.2. *Pinned flux fraction*

The value of the pinned flux fraction p that was found by matching the theoretical power spectrum to the experiments was determined for various values of magnetic field, current and temperature. In some cases this determination was not unambiguous, due to the scatter of the experimental points, so that then the value of p was uncertain. Uncertainty also arose if there was flicker noise present.

According to eq. (2.34) the moving fraction of vortex lines should be proportional to the slope of the E-J characteristic $\varrho(J)/\varrho_{fl}$.

The value of $(1-p)$ as found from the noise measurements should therefore agree with the value obtained from the derivatives of the E-J curve. This is demonstrated in figs 5.11 and 5.12 where $\varrho(J)/\varrho_{fl}$ is drawn as a function of transport-current density for two values of magnetic field and temperature for specimens V2c and V2a. Also shown are the values of $(1-p)$ as determined from the noise spectra. The figures show that for specimen V2c the values of $(1-p)$ from the noise spectra are of the same order of magnitude as those derived from the d.c. experiments.

There is, however, discrepancy between the results of the two methods for the annealed vanadium V2a. The value of $(1-p)$ from the noise spectra is systematically below the value of $\varrho(J)/\varrho_{fl}$. In the previous section it was suggested that in specimen V2a the flux motion is interrupted for very short times,

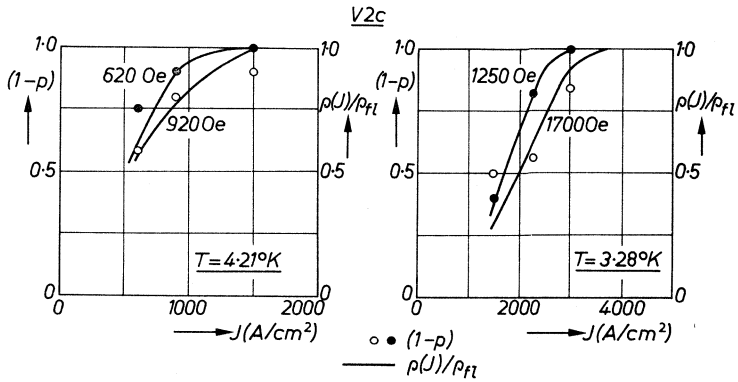

Fig. 5.11. Moving flux fraction $(1-p)$ as determined from noise measurements (open and filled circles) and normalized flux-flow resistivity as determined from d.c. measurements (drawn curves) as a function of transport-current density J for different values of magnetic field and temperature. Specimen V2c.

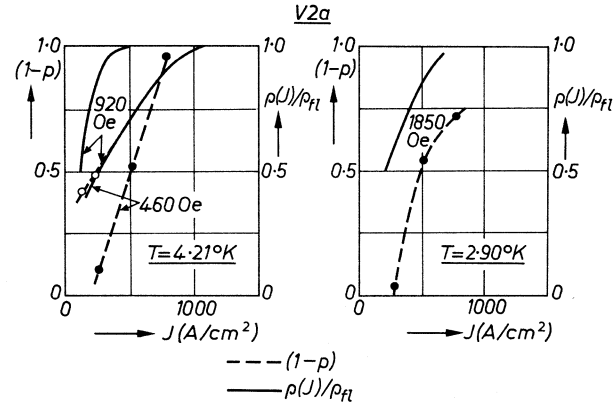

Fig. 5.12. The same as for fig. 5.11. Specimen V2a. Drawn curves: $\varrho(J)/\varrho_{fl}$; dashed curves: $(1-p)$.

so that a distribution of pulse durations is found. Theoretical power spectra for this case, as shown in fig. 4.3, have a cut-off frequency that is much larger than $1/\tau$. Consequently the value of $(1-p)$, as determined from eq. (5.7) by equating the cut-off frequency to $1/\tau$, is then much smaller than the real value.

The power spectrum of eq. (4.29) (fig. 4.2*a* and *b*), which is believed to be applicable to the measurements on specimen V2c, gives about the same value for $(1-p)$ as the spectrum of eq. (5.6). This can be derived from the expression for the d.c. voltage, which can be shown to be for $g(\tau_i) = 1/(\tau'-\tau'')$

$$V = \frac{l\, w\, B\,(1-p) \ln(\tau'/\tau'')}{c\,(\tau'-\tau'')}. \tag{5.8}$$

For $\tau'/\tau'' = 5$ this expression becomes

$$V \approx \frac{l\, w\, B\, (1-p)}{c\, \tau'/2}. \tag{5.9}$$

Figure 4.2*a* shows that the cut-off frequency for this case is about $2/\tau'$, so that the resulting values of $(1-p)$ from eqs (5.7) and (5.9) are about the same.

The magnetic-field dependence of $(1-p)$ with constant current density is also different for specimens V2a and V2c. In the annealed specimen V2a the value of $(1-p)$ increases with field, whereas in specimen V2c the value of $(1-p)$ decreases with increasing field for values above 0·4 H_{c2}. This is in agreement with the field dependence of the critical current density J_c, which decreases with increasing field in specimen V2a and increases with field in specimen V2c, as was shown in fig. 3.7. For a constant value of the transport-current density the number of vortex lines that are moving should increase when J_c decreases and the reverse.

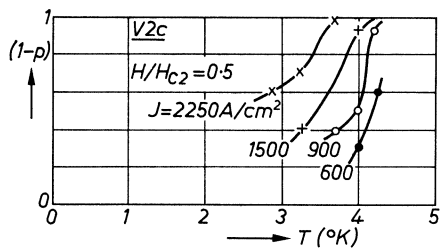

Fig. 5.13. Moving flux fraction $(1-p)$ (interpolated values) as a function of temperature for $H/H_{c2} = 0{\cdot}5$ and various current densities. Specimen V2c.

The temperature dependence of $(1-p)$ at constant current is shown for specimen V2c in fig. 5.13 for $H = 0{\cdot}5\ H_{c2}$. The value of $(1-p)$ increases with temperature, which is in agreement with the temperature dependence of J_c, as was shown in fig. 3.8. For specimen V2a the value of $(1-p)$ also increases with temperature, but this is not shown in a figure, as the absolute value of $(1-p)$ is uncertain as was shown in fig. 5.12.

5.2.3. *Bundle size*

The expressions for the power spectrum of the flux-flow noise at $f = 0$ all give a value

$$W(0) = 2\, \Phi\, V/c. \tag{5.10}$$

This provides a possibility of determining the value of the flux-bundle size Φ, since V is known from d.c. measurements.

The value of Φ was determined for some of the specimens shown in table III

for different values of transport current, magnetic field and temperature. The value of Φ is expressed as the number of single flux quanta φ_0. As was remarked earlier, the presence of flicker noise may cause some uncertainty in this determination. The results are shown in figs 5.14 to 5.16. The presence of flicker noise is denoted in figs 5.14 and 5.15 by the symbol *F*.

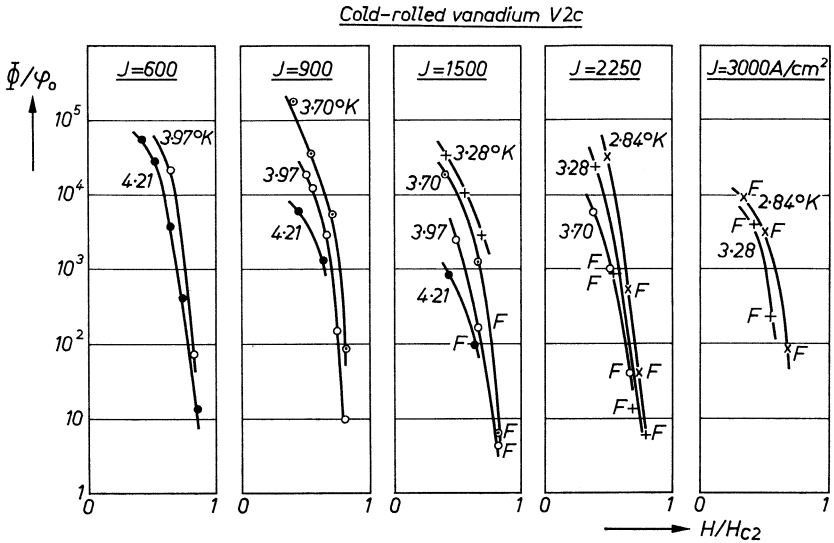

Fig. 5.14. Flux-bundle size versus reduced field for different values of transport-current density and temperature. The symbol *F* means presence of flicker noise. Specimen V2c.

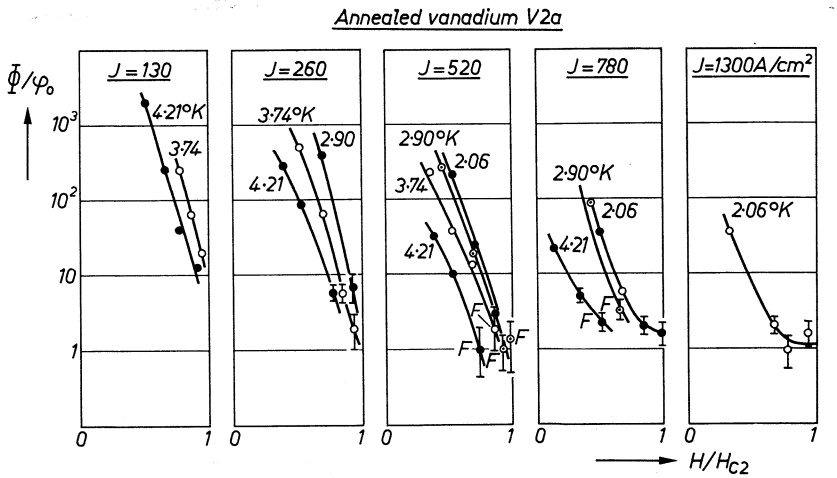

Fig. 5.15. The same as for fig. 5.14. Specimen V2a. For small bundles the uncertainty is indicated by vertical bars.

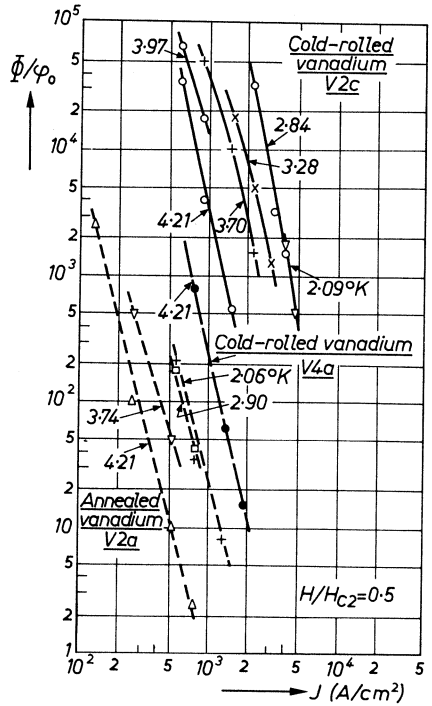

Fig. 5.16. Flux-bundle size (interpolated values) versus transport-current density for $H/H_{c2} = 0{\cdot}5$ at various temperatures for three vanadium foils.

Figures 5.14 and 5.15 give the dependence of Φ/φ_0 on H/H_{c2} for various values of transport-current density and temperature of specimens V2c and V2a. Figure 5.16 gives Φ/φ_0 as a function of current density at $H/H_{c2} = 0{\cdot}5$ for specimens V2c, V2a and V4a at various temperatures, as found from the dependence of Φ/φ_0 on H/H_{c2}. The figures show that Φ may be considerably greater than φ_0 and that values differing by five orders of magnitude are found.

Figure 5.16 shows that the bundle size decreases rapidly with increasing current density when the temperature is held constant and varies roughly as J^{-4}. From a comparison of the results at constant values of J and T for the three specimens it follows that Φ/φ_0 is smaller in the material with less flux pinning. It was discussed in sec. 3.1.4 (fig. 3.7) that there is less pinning if the flux flows in the rolling direction, as in specimens V4a and V4b, than when the flux flows perpendicularly to the rolling direction as in specimens V2c and V2d. The pinning effects are smaller still in the annealed specimen V2a.

The bundle size for a constant value of J also decreases with increasing temperature. It was earlier discussed, in sec. 3.1.4, that a temperature increase causes a reduction of the pinning.

These effects are qualitatively in agreement with the dependence of Φ/φ_0

on J, for a greater value of J causes a greater value of the driving force on the vortex lines, so that the influence of pinning is diminished.

The bundle size also decreases drastically with increasing field and drops to low values near H_{c2}, where the bundles are of the order of 10 φ_0 in the unannealed specimen V2c and φ_0 in the annealed specimen V2a.

As the value of Φ is found from extrapolation of the flux-flow-noise spectrum to $f = 0$, the determination of Φ is inaccurate when flicker noise is present. Moreover, since the flicker noise is caused by temperature fluctuations, the value of H_{c2} will also fluctuate so that in a constant field close to H_{c2} the specimen undergoes fluctuations into the normal state where Φ is no longer defined. Extrapolation of the flux-flow-noise spectrum to $f = 0$ therefore gives then only an order of magnitude for Φ.

It is, however, possible to remove the flicker noise for not too large current densities by cooling the helium bath through the λ transition. By doing this, it was found in specimen V2a that when Φ has reached the value φ_0, it does not decrease any further with increasing field. Figure 5.15 shows that there $\Phi = \varphi_0$ within the accuracy of measurement.

The decrease of Φ/φ_0 with increasing field in specimens V2c and V2a cannot be interpreted as due to diminished pinning effects, since in specimen V2c the pinning increases with field, whereas in specimen V2a the pinning decreases with increasing field, as was shown in secs 3.1.4 and 5.2.2.

Summarizing, we conclude that the flux bundles become smaller when the magnetic field is increased and when the effects of pinning are diminished. The experiments further present evidence for a limiting value of the bundle size, equal to φ_0.

A model for the bundling of the vortex lines should take account of these results.

This bundling of vortex lines was originally proposed by Anderson [76]) in his theory of flux creep. He suggested that vortex lines would not jump over pinning barriers alone, but would move in bundles. If the driving force on a single vortex line is not large enough to push it over a barrier, clustering may occur. If only some of the vortex lines are pinned, the mutual repulsion between the vortex lines causes the unpinned ones not to move individually, but to push the pinned ones over the barriers. The size of the bundles may be governed by the amount of pinning. For high barriers, or a small driving force, a large cooperative pressure is needed for flux motion and large flux bundles will be found. If there is little pinning or a large driving force on the vortex lines, only a small bundle size is needed for flux motion.

This model is in qualitative agreement with the observed dependence of Φ/φ_0 on pinning conditions.

An explanation of the field dependence may be given in terms of overlapping vortices. To give an indication of these overlapping effects we calculate the

interaction energy between one vortex line and its neighbours and compare this energy with the vortex-line self energy ε, as given in eq. (1.13).

The interaction energy per unit length can be written [2]) as

$$\sum_i U_i = 6\left(\frac{\varphi_0}{4\pi\lambda}\right)^2 \left(\frac{\pi\lambda}{2d}\right)^{1/2} \exp(-d/\lambda) \tag{5.11}$$

for $d \gg \lambda \gg \xi$, where d is the distance of a vortex line to its 6 nearest neighbours.

The value of λ is found from eq. (1.14) and the theoretical dependence of H_{c1} on $\varkappa$ [147]).

The results of the calculation is shown in fig. 5.17 where $(\sum U_i)/\varepsilon$ is shown as a function of H/H_{c2}. The interaction energy becomes a significant fraction of the line energy for distances less than about 3 λ, that is at reduced fields of the order of 0·2 to 0·3, depending on pinning conditions and temperature. The measurements all fall in the region $H > 0{\cdot}2\ H_{c2}$.

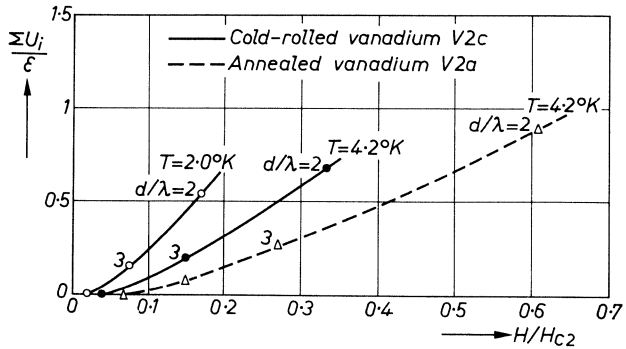

Fig. 5.17. Calculated vortex-line-interaction energy $\Sigma\ U_i$ relative to the line energy ε versus reduced field for specimens V2c and V2a. The numbers at the points denote values of d/λ, where d is the vortex-line separation.

We suggested earlier that flux movement in the form of bundles takes place by a joint pressure of the vortex lines on each other. The value of this pressure is determined by pinning conditions, transport current and temperature. When the magnetic field is increased, the vortex lines get closer together so that they exert a greater repulsive force on each other. For a given combination of pinning conditions, current and temperature a smaller bundle is now sufficient for flux movement since the mutual pressure of the vortex lines is now greater. In consequence the average bundle size necessary for flux movement is decreased.

Another effect of the field may be the lowering of the surface barrier for flux entry [87]), so that the surface may also play a role.

Direct experimental evidence for the model of flux-bundle flow is not available. It may be possible to test it by a recently developed high-resolution (1 μ) magneto-optical technique [148]). In a stationary situation flux bundling does occur as has been observed by electron microscopy of Bitter patterns [117,149]). The experiments on the Corbino disc have also shown that the flux does not move as a rigid lattice (sec. 3.1.3). Träuble and Essmann [19]) have demonstrated that the vortex lattice is far from perfect and contains many types of defects, such as dislocations, stacking faults (rectangular lattice), orientation boundaries, depleted zones and even liquid-like structures. It would therefore not be surprising if the vortex lattice breaks up into smaller parts when flux motion sets in, like the breaking up of a two-dimensional soap-bubble crystal after stirring [150]). Apparently the flux motion is then presumably due to motion of vortex crystallites or grains that slide past each other. These grains may have somewhat different velocities in different parts of the specimen due to a distribution of threshold current densities. If the field is increased, the grains get smaller and close to H_{c2} the flux motion appears to be in the form of single vortex lines. The limiting value φ_0 for the bundle size at high fields suggests that the decrease of the noise with increasing field is indeed due to a reduction of the bundle size and not to some correlation effect. This would mean that the vortex crystal has a liquid-like structure at high fields.

The motion of flux as bundles does not necessarily mean that a flux bundle, once it is generated, retains its identity all the way across the superconductor. A moving flux bundle may pick up vortex lines and leave others behind. This would give rise to fluctuations of Φ.

Chilton [151]) has suggested that the flux moves as elongated bundles, one vortex wide and many vortices after one another. These vortex-lattice planes would be uncorrelated to neighbouring lattice planes. Such a type of flux flow would give pulses longer than τ and thus a noise cut-off frequency lower than $1/\tau$. This is contrary to what is found experimentally so that this suggestion is probably not justified.

As an alternative mechanism for flux-bundle formation, Druyvesteyn [152]) suggested that the bundle size may be determined by the irregularities in the specimen edge. If the edge of the superconductor, where vortex lines are created, is not smooth, but irregular, the vortex lattice is disturbed in a surface layer with depth of the order of the irregularities. The size of a flux bundle may now be governed by the scale of the irregularities. The decrease of Φ with decreasing pinning effects and increasing field may then be caused by the increased flow velocity. A higher flow velocity would only permit a smaller nucleation time for the flux bundles, which means that the bundle size would also be smaller.

This hypothesis could be tested by carrying out noise measurements on a specimen with perfectly smooth edges. The noise would then be much reduced.

One could carry out the experiment with only one edge smoothed and measure the noise with the transport current in either direction. Reversing the current should then give different results.

We want to close this section with the following remarks concerning the possibility of flux motion by motion of vortex-lattice dislocations. This was neglected so far, but the vortex lattice is known to contain many dislocations whose motion has been demonstrated [19]). However, although the dislocation density increases when the field is increased, the number of vortex lines in between two vortex dislocations remains constant, since the dislocation density is proportional to the vortex density [153]). The large variation of Φ/φ_0 with field is therefore difficult to explain in terms of increased dislocation density. Especially for Φ to be equal to φ_0 an extremely high dislocation density would be required. Therefore, we believe that the size of the flux bundles is not determined by the vortex dislocations. The motion of the flux may, however, take place by vortex-dislocation motion, as well as by vortex–grain-boundary glide.

5.2.4. *Low-frequency noise reduction*

In many of the noise spectra the noise is partly suppressed at frequencies below 30 Hz. This effect is mainly present at low transport currents and fields and at low temperatures. It was found that the maximum in the noise spectrum was shifted to a somewhat higher frequency if the specimen was not glued on the holder, but was only mounted on the current contacts.

The occurrence of a maximum in the noise-power spectrum has been dealt with in the literature. It is usually found if there is correlation between two successive events. The power spectrum can then be written as

$$W(f) = W_0(f)\, I(f), \tag{5.12}$$

where $W_0(f)$ is the spectrum if no correlation is present and $I(f)$ is an interference term, which modifies the spectrum.

In order to explain space-charge reduction of shot noise in vacuum tubes MacDonald [154]) introduced a model by which he considered the compensating effect of the space charge on fluctuations of the electron current. If an excess of electrons over the average value of the current is emitted, then the increased space-charge density will have an inhibiting effect on the general current flow and vice versa.

The power spectrum is calculated for a simplified model where fluctuations from the average value of the current, positive or negative at random, are accompanied by a compensating pulse. For the flux-flow case this is shown in fig. 5.18 for rectangular pulses. A pulse with duration time τ and height $\Phi/c\,\tau$, is followed after a time $k_2\,\tau$ by a negative pulse with the same duration and with height $-k_3\,\Phi/c\,\tau$, where k_2 and k_3 are constants. The power spectrum

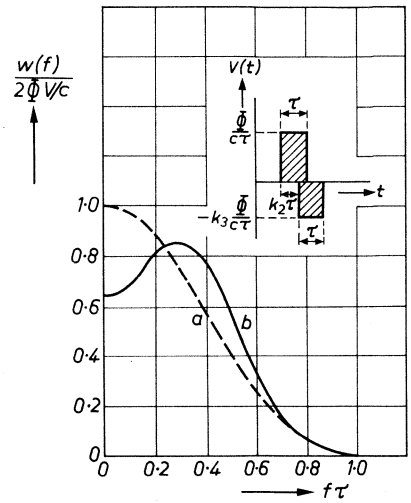

Fig. 5.18. Theoretical noise-power spectra for rectangular voltage pulses; a: without noise reduction; b: with noise reduction calculated with MacDonald's model of compensating pulses (shown in the inset), for $k_2 = 1$ and $k_3 = 0{\cdot}2$.

can be calculated from the autocorrelation function of such a pulse combination and it is then found that

$$I(f) = 1 - 2\,k_3 \cos(2\,\pi\,k_2\,f\,\tau) + {k_3}^2. \tag{5.13}$$

The value of the noise voltage for $f = 0$ is reduced by a factor $(1 - k_3)^2$. The spectrum exhibits a maximum as is shown in fig. 5.18 for $k_2 = 1$ and $k_3 = 0{\cdot}2$.

The time $k_2\,\tau$ is the waiting time for the mechanism to set in after a primary fluctuation has started. The frequency at which the maximum is found, is governed by the value of k_2: if this value is increased, the place of the maximum is shifted to lower frequencies.

The low-frequency reduction of noise due to flux jumps into or out of a type-II superconductor was discussed by Heiden [133]), who calculated the noise spectrum of a series of pulses with coupling between the area under a pulse and the time preceding or following it to the next pulse. This coupling occurs when the inhibiting effect of an event on the following one is proportional to the size of the primary event. The physical mechanism for the coupling in this case is the change of the local value of the external magnetic field following a flux jump. This change increases with the size of the jump. The power spectrum was calculated for a series of rectangular pulses with duration time τ. The time τ_j between the beginning of two successive pulses is assumed to follow an exponential distribution function $(1/\tau_4)\exp(-\tau_j/\tau_4)$. The pulse height $\Phi_j/c\,\tau$ is proportional to τ_j, as is shown in fig. 5.19. The interference term is then

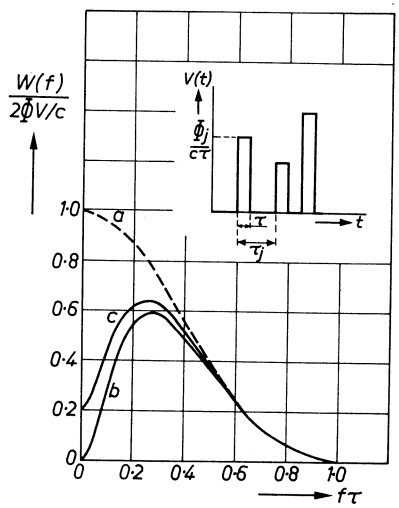

Fig. 5.19. Theoretical noise-power spectra for rectangular voltage pulses; a: without noise reduction; b: with noise reduction calculated with Heiden's model of coupling $\Phi_j \propto \tau_j$ (shown in the inset); c: idem with coupling $\Phi_j \propto (\tau_j + \tau)$.

$$I(f) = \frac{1}{1 + (2\pi f \tau_4)^{-2}}. \tag{5.14}$$

The resulting power spectrum is shown in fig. 5.19 for $\tau_4 = \tau$ and also for the case of partial coupling $\Phi_j \propto (\tau_j + \tau)$, as was also calculated by Heiden.

Another explanation for a maximum in the noise spectrum is the occurrence of resonance at the frequency of the maximum. In order to investigate this possibility, the low-frequency behaviour of a specimen with noise reduction was studied by measuring the a.c. voltage across the specimen in the flux-flow state when a small a.c. current was superposed on the d.c. current, as a function of frequency between 3 Hz and 100 Hz. The a.c. voltage on the specimen was not dependent on frequency, so that it is unlikely that the noise maximum is caused by some resonance phenomenon.

A mechanism leading to noise reduction may be the following. A positive fluctuation in the average generation rate of flux bundles may correspond to a positive fluctuation in the vortex-line density. This would mean that the vortex lines get closer to each other. This increased vortex-line density would mean increased interaction between the vortex lines, and, according to the reasoning in the preceding section (5.2.3), the average bundle size of the moving flux would go down, so that the noise would decrease. By the same argument the effect of a negative fluctuation of the vortex-line density is an increase in the noise voltage. An alternative mechanism, following Heiden's model, is that the (nucleation) time preceding the departure from the edge of a big flux bundle is longer than for a small flux bundle.

Consideration of the experimental noise spectra shows that the noise reduction takes place at frequencies much lower than $1/\tau$. To achieve this with MacDonald's or Heiden's models, it is required that the waiting time be longer than τ, which is not very likely for the mechanisms just described.

Although the theroretical spectra of these models agree qualitatively with the experiment, there is thus no quantitative agreement.

5.2.5. *Corbino disc*

Measurements were taken on the Corbino disc (specimen V5) at $T = 4{\cdot}2$ °K for various values of the field and with transport currents of 0·3 and 0·1 A (corresponding to current densities at the edge of 60 and 20 A/cm^2 respectively). No flux-flow noise was found in these experiments within the measuring accuracy (10^{-18} V^2). At a current of 1 A flicker noise appeared with approximately f^{-2} behaviour. In order to get rid of this noise, measurements were also taken at $T = 2{\cdot}15$ °K. Some noise was found there, corresponding to average bundle sizes of 10 to 100 φ_0, but it was at least an order of magnitude less than for specimen V2a, at comparable values of field and current density. This noise may be caused by the fact that the central current contact is not exactly in the middle, so that some flux may cross from one side of the specimen to the other. Since the current density is very low at the edge, this flux moves in the form of large bundles and may then give rise to a measurable noise voltage. Furthermore fluctuations of velocity or size of the moving flux bundles may cause flux-modulation noise.

The results agree with the assumption that the flux moves in circles and should therefore not give flux-flow noise. We wish to point out that noise would also be absent if the noise cut-off frequency were lower than the lowest measuring frequency, which in these experiments was 20 Hz. It would be desirable to make noise measurements on a Corbino disc down to lower frequencies and with greater sensitivity.

5.3. Flux-flow noise in indium-thallium

For the noise measurements on the indium-20 % thallium single-crystal wire thin copper potential leads were soldered on to the specimen with the same alloy.

It was found that flicker noise was present at very low frequencies ($f < 30$ Hz) and it was usually very much greater than the flux-flow noise, which could hardly be detected. The measurements of the flux-flow noise were therefore made at temperatures below the helium λ point, in order to avoid interference with the flicker noise which is then not present. The measurements were taken as the difference between the microvoltmeter reading with the magnetic field switched on and off. This was done because switching on and off the transport current

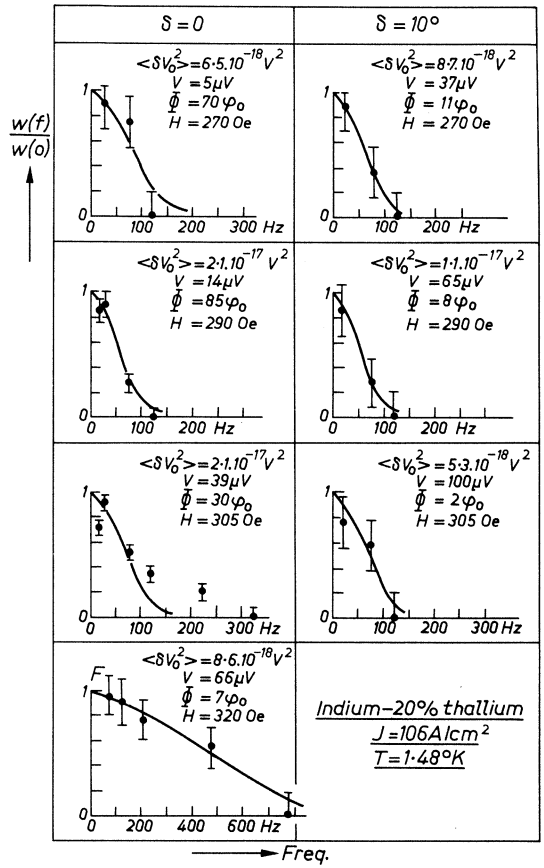

Fig. 5.20. Experimental flux-flow noise-power spectra for the In-20 % Tl crystal for two orientations with respect to the field direction, at $T = 1{\cdot}48$ °K, compared with theoretical spectrum of eq. (4.24). Values of m.s. noise voltage, d.c. voltage, bundle size and magnetic field are indicated.

made the temperature rise and fall, due to the Joule-heat dissipation caused by the current in the current leads.

Measurements were taken with $J = 106$ A/cm² at $T = 1{\cdot}48$ °K for various fields. Higher current values caused a large temperature rise and at lower current values the noise was too slight to be detected accurately. The specimen was oriented either with the field parallel to the twin boundaries ($\delta = 0$) or at an angle of 10°. Some noise spectra are shown in fig. 5.20. The noise spectrum of eq. (4.24) is drawn in the figures for comparison, fitted to the experimental points. The cut-off frequencies are generally higher than those calculated for a triangular voltage pulse with $p = 0$. We do not attempt to explain this discrepancy by a pinned fraction because of the inaccuracy of the results and the

doubt about the validity of the assumption that the elementary voltage pulses are triangular.

The bundle size was again determined from the extrapolated value of $W(f)$ at $f = 0$. Figure 5.21 shows the values of Φ/φ_0 as a function of magnetic field for the two orientations. It is clear that the behaviour of Φ with field is very similar to that for the vanadium foils. It is also shown that for H parallel to the twin boundaries Φ is almost an order of magnitude larger than for H at an angle. This is in agreement with the critical-current anisotropy, as was described in sec. 3.2.3 (fig. 3.12). Pinning is a maximum if the vortex lines are parallel to the twin boundaries, so that the bundle size needed to overcome the pinning barriers is then also a maximum. This is consistent with the effect of structure on bundle size in the vanadium foils. In the case of the indium-thallium it is not quite clear whether the bundle size will be constant while crossing the specimen as the length of the vortex lines is not constant.

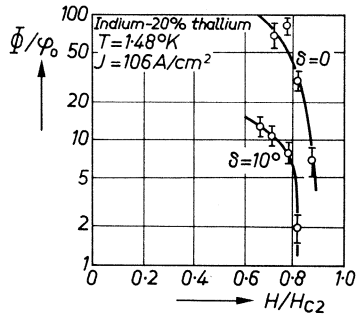

Fig. 5.21. Flux-bundle size versus reduced field for two orientations of In-20% Tl crystal with respect to field direction at $T = 1{\cdot}48$ °K. The uncertainty in bundle size is indicated by vertical bars.

5.4. Flicker noise

5.4.1. *Experiments in liquid helium* I

As was remarked earlier, the spectra were often found to exhibit a sharp rise towards low frequencies (below 100 Hz). This effect is absent or small at low transport currents and at low fields but increases rapidly with increasing current and field and, since the flux-flow noise decreases in this order, this is then sometimes entirely dominated by the low-frequency noise. The power spectra of this noise have been measured as a function of field, current and temperature on the vanadium foils and on the In-Tl crystal.

It was found that on cooling down through the helium λ point the flux-flow noise was not affected to a great extent, but the flicker noise was reduced by several orders of magnitude and became immeasurably small. This shows that the origin of the flicker noise is of a thermal character. At the λ point ($T =$

2·18 °K) the helium becomes a superfluid and the heat conductivity increases by many orders of magnitude [155]). Consequently the heat transfer from a heated surface to the liquid is increased considerably. The fact that the flicker noise virtually disappears below the λ point supports the hypothesis that this noise is caused by temperature fluctuations in the foil, as a result of fluctuations in the Joule-heat transfer from the foil to the helium bath, during nucleate boiling.

Flicker noise was found for heat fluxes ranging from about 0·5 mW/cm² to 40 mW/cm². In order to check that nucleate boiling takes place in this range, we observed the boiling process in helium with a microscope. A specimen was glued to a holder and mounted in the liquid helium, facing downwards. The helium and nitrogen dewars had a flat unsilvered bottom [156]). We watched the specimen and measured the power dissipation in it simultaneously. An In-Pb foil was used, so that the experiments could be done at 4·2 °K without applying

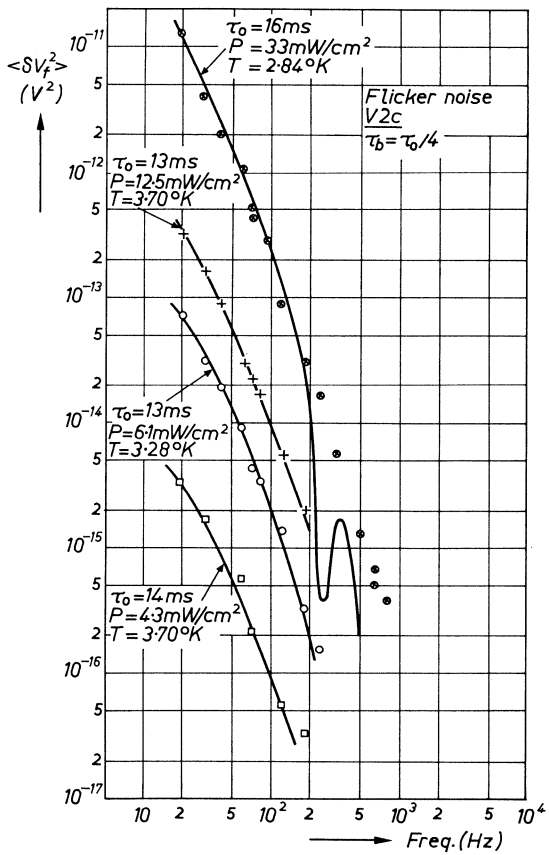

Fig. 5.22. Some flicker-noise spectra for various values of power dissipation P per unit surface area and temperature T. Specimen V2c. Drawn curves are calculated with eq. (4.44) for $\tau_b = \tau_0/4$. Best fit was obtained for value of τ_0 as indicated.

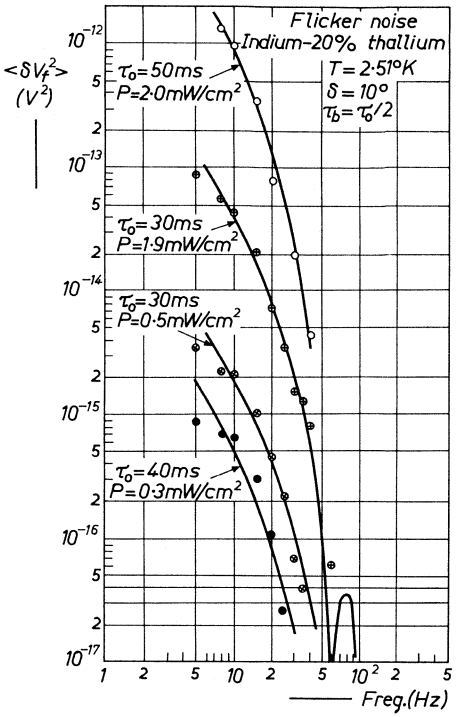

Fig. 5.23. The same as fig. 5.22 for indium-20% thallium crystal and $\tau_b = \tau_0/2$.

a magnetic field. Formation of bubbles on the specimen was observed to occur at heat-flux values above about 0·3 mW/cm^2. This value was calculated on the assumption that the heat was transferred only through the lower surface. These observations show that nucleate boiling indeed takes place for heat-flux values where flicker noise was found.

Some flicker-noise-power spectra are shown in figs 5.22 and 5.23 where the m.s. noise voltage is corrected for the flux-flow noise contribution.

The figures also show, as drawn curves, the power spectra, calculated with eq. (4.44). The best fit to the experimental points was found by choosing τ_b and τ_0 as indicated in the figures. The values of τ_b/τ_0 are $\frac{1}{2}$ to $\frac{1}{4}$ and τ_0 is about 12 to 16 ms in vanadium foils and 30 to 50 ms in the indium-thallium wire.

The agreement between experiment and the simple theory is reasonable. The theoretical maxima and minima in the power spectra are not found in practice, probably due to a distribution of bubble lifetimes over the surface, as was already indicated in sec. 4.4. The results show that the process of nucleate boiling in helium is very similar to this process in other liquids. It was found that the r.m.s. noise voltage was proportional to the product of transport cur-

rent I and power dissipation P per unit surface area irrespective of field and temperature. This is shown in fig. 5.24, where $\langle \delta V_f^2 \rangle$ at $f = 20$ Hz is plotted versus IP on a log-log scale for specimens V2c and V2a. The full line has a slope 2. Although there is some scatter, this overall dependence of $\langle \delta V_f^2 \rangle$ on $I^2 P^2$ is found over several orders of magnitude. This can be accounted for by considering the power spectrum at $f = 0$, as follows from eq. (4.44):

$$W(0) = \tfrac{1}{2} N \left[I \frac{D_b}{w} k_1 \, \Delta T_m \, \tau_0 \left(\frac{\tau_b}{\tau_0} + 2 \right) \right]^2 . \tag{5.15}$$

If heat transfer is only due to nucleate boiling, the bubble-generation rate can be written

$$N = \frac{6 \, q \, l \, w}{\pi \, D_b^{\,3} \, \varrho_v \, Q_v} , \tag{5.16}$$

where q is the heat flux through the helium-heater interface, ϱ_v is the vapour density and Q_v is the heat of vaporization.

The characteristic time τ_0 over which the temperatue rises after bubble de-

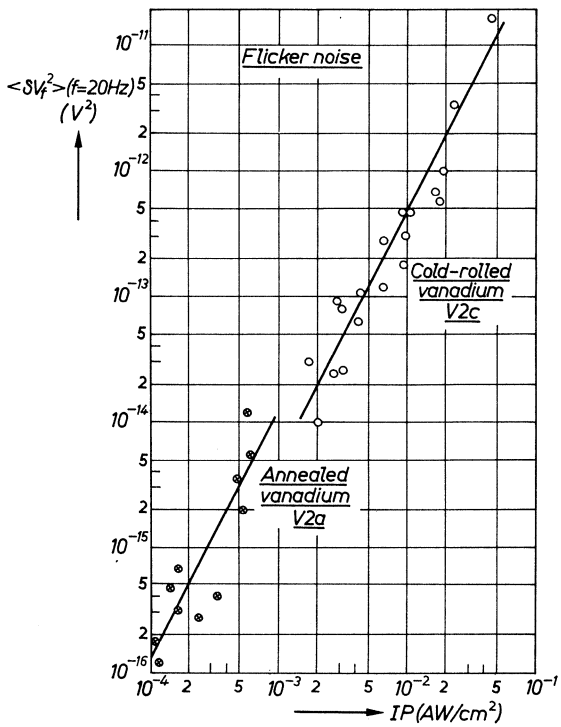

Fig. 5.24. M.s. flicker-noise voltage at $f = 20$ Hz versus product of transport current I and power dissipation P per unit surface area for specimens V2c and V2a. The drawn lines have a slope 2.

parture is determined by the thermal properties of specimen and liquid which we take approximately independent of temperature and power dissipation. We write $P = q$ and take $q \propto \Delta T_m^2$. If, furthermore, D_b is assumed to be constant (as it is for not too high values of q in water [157]), so that N is proportional to q, we then get from eq. (5.15):

$$W(0) \propto I^2 P^2. \tag{5.17}$$

In the derivation of eq. (4.44) we assumed that the resistance change ΔR was proportional to a temperature change ΔT. It was verified that in the field and temperature range where flicker noise was measured, this was indeed the case and that in this range the proportionality constant was roughly independent of field and temperature. The values were found to be 1 mΩ/°K for specimen V2c and 2 mΩ/°K for specimen V2a.

The value of the temperature minimum ΔT_m can now be estimated using eqs (5.15) and (5.16). The value of ΔT_m is of the order of 3 millidegrees for specimen V2c at a heat-transfer rate of about 40 mW/cm², whereby D_b is of the order of 0·5 mm. At lower values of the dissipated heat ΔT_m is smaller. There is too much scatter to check whether ΔT_m^2 is proportional to P, as was assumed in the derivation of eq. (5.17).

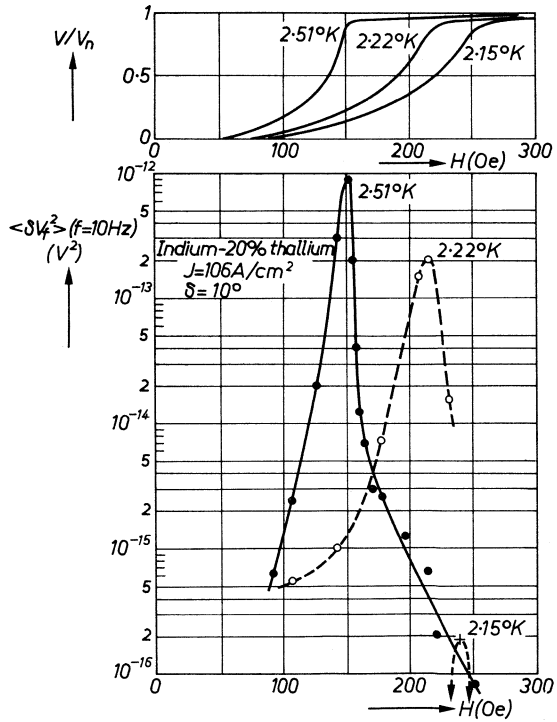

Fig. 5.25. M.s. flicker-noise voltage at $f = 10$ Hz and d.c. voltage at constant current density as a function of magnetic field at three temperatures for indium-20% thallium crystal.

The flicker-noise voltage, when measured at constant current and temperature as a function of magnetic field, goes through a maximum. This is reflected in the dependence of ΔR on ΔT, since both at low fields and at high fields $\Delta R/\Delta T = 0$. For the In-Tl crystal the noise was measured through the resistance transition. Figure 5.25 shows the m.s. noise voltage at $f = 10$ Hz at constant transport current as a function of field for the temperatures 2·51, 2·22 and 2·15 °K. Noise was found up to high fields, approaching H_{c3}. The curves for $T = 2{\cdot}22$ and 2·15 °K show that on going through the λ point the noise is decreased by a factor of 1000, because the boiling phenomenon disappears below 2·18 °K.

The results for flicker noise have shown that the surface temperature of the specimens fluctuates during nucleate boiling of helium in much the same way as this occurs in other liquids. The flicker noise was described in terms of a resistance change ΔR. In fact the resistance is caused by flux flow and it would be more appropriate to treat it as a flux-flow voltage. Variations of this voltage with temperature should be expressed as variations of the flow velocity, since in a thin foil the induction B can be considered to be constant in a constant field. The flicker noise can thus be described as due to velocity fluctuations, caused by temperature fluctuations.

5.4.2. *Experiments in liquid helium* II

It appeared that a noise voltage could still be found at temperatures below the λ point. Apparently there were still temperature fluctuations present. On increasing the field, the noise in the In-Tl crystal was found to go through a maximum, which was higher for steeper resistance transitions, presumably because $\Delta R/\Delta T$ is larger there. The spectrum of this noise was quite different from that above 2·18 °K and looked like a resonance curve, with the maximum at about 8 Hz, as shown in fig. 5.26 for $T = 1{\cdot}35$ °K.

The noise decreased considerably on increasing the temperature from 1·3 °K to about 2 °K and could therefore only be measured at low temperatures.

In order to check that temperature fluctuations indeed were present, a thin layer of aquadag was painted on rice paper and the noise voltage across this aquadag resistor in the liquid helium was measured with a small current flowing through it, with no current through the In-Tl wire. The spectrum is also shown in fig. 5.26 and it can be seen that it is practically the same as the noise spectrum on the superconductor. The noise level was increased by switching on a transport current through the superconductor.

The results can easily be explained as due to pressure variations in the pumping line. The speed of revolution of the rotary pump was 510 rpm, i.e. 8·5 Hz. This introduces a pressure oscillation above the liquid with the same frequency because the pump is closed half of every period. The width of the

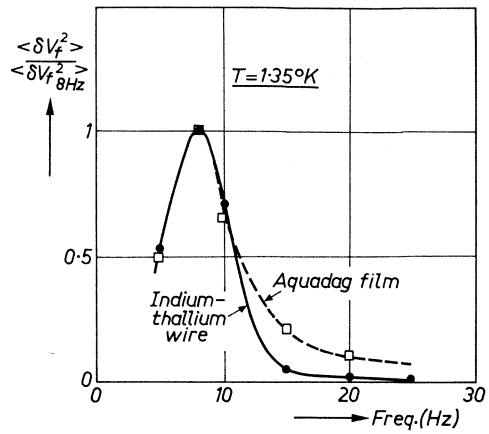

Fig. 5.26. Flicker-noise-power spectra relative to the value at $f = 8$ Hz for the indium-thallium wire and an aquadag film; $T = 1{\cdot}35$ °K.

resonance curve is determined by the damping of the system, which is governed by the flow resistance of the pumping line.

At temperatures below the helium λ point the liquid very quickly reaches the temperatures at which it is in equilibrium with the vapour pressure above the surface. The pressure variations are therefore converted to temperature variations with the same frequency.

Since the temperature of the helium varies with vapour pressure much more strongly at low temperatures than at higher temperatures, the effect of a given pressure variation is greater for lower temperatures. The temperature variations therefore decrease with increasing temperature.

The r.m.s. temperature fluctuations as calculated from the measured temperature coefficient of the aquadag resistor was about 0·4 millidegrees, with no current through the superconductor and about 15% higher with a current of 3 A switched on. If the temperature variation is a sine wave, then the peak-to-peak value is of the order of a millidegree. This corresponds to a pressure fluctuation of about 10^{-2} mm at $T = 1{\cdot}35$ °K. In the experiments the liquid-helium volume was of the order of 0·25 litre, i.e. about 30 grammes. From the specific heat of helium at 1·35 °K (0·15 cal g^{-1} deg^{-1}) the total heat inleak causing a temperature increase of the helium bath of 1 millidegree during half of each period (0·06 s) can be calculated as about 0·3 watt. This is the right order of magnitude, so that apparently the whole bath has a uniform fluctuating temperature.

It was also found that for high values of the power dissipation in the sample at temperatures below the λ point noise could be heard in the cryostat. This acoustic noise is due to film boiling of liquid helium, as was shown by Bussières and Leonard [158]).

5.5. Concluding remarks

The occurrence of flux-flow noise shows that the flux cannot be moving as a rigid vortex lattice, since the generation is random and also because of the velocity distribution for the flux bundles. The flux presumably moves by vortex–grain-boundary glide and by vortex–dislocation motion. Within the grains the vortex lattice may be conserved. The results suggest that at high fields and currents there is a liquid-like vortex structure. This seems to be in contradiction to calculations [159]) of the elastic constants of a vortex lattice, which show that the lattice becomes stiffer when the field is increased. These calculations were done for a vortex lattice at rest, where only mutual interaction forces exist. If the vortices are moving, additional effects come into play of which we mention:

(1) Interaction with pinning centres, causing fluctuations of the flow velocity.
(2) Distribution of threshold current-density values over the specimen, so that in different parts of the specimen the vortices move with different velocity. For a given distribution function this difference is greater for higher velocities. Since the velocity increases with increasing current or magnetic field, this should cause more disorder in the vortex lattice.
(3) A time-dependent flow velocity, so that for example sinusoidal or triangular pulses are generated. The vortex-lattice parameter is then not a constant, but varies in the flow direction. This variation is greater for higher flow velocities.

These effects show that some disordering effects increase with field, which may overrule the increase of the vortex-lattice stiffness.

The sensitivity of our noise measurements was too small to detect Johnson noise. From eq. (4.41) it can be derived that the Johnson noise in a bandwidth of 4 Hz in our specimens should be of the order of 10^{-24} V^2 which is well below the detection limit.

The noise caused by fluctuations of the flux content of the superconductor or by creation and annihilation voltage pulses, as described in sec. 4.2.4, is apparently too small to be detected.

Since the flux does not move as a rigid vortex lattice, a line spectrum, as discussed in sec. 4.2.4, if present, should exhibit a considerable line broadening. The frequencies of these lines are in the MHz range as can be found from the values of the velocity and the vortex-lattice parameter.

We have, in this chapter, discussed measurements of noise spectra. The total noise power can be found by integrating these spectra. It can be shown with Campbell's theorem, eq. (4.3), that for the flux-flow noise $\langle \delta V^2 \rangle$ is of the order of $\Phi V/c\,\tau$. Since at low fields V is zero and at high fields Φ goes to very low values, the flux-flow noise should go through a maximum when the field is varied. The flicker noise is a function of power dissipation and of the

resistance variation with temperature. This latter quantity is practically zero in the normal state, so that the flicker noise also goes through a maximum when the field is varied, as was shown in fig. 5.25. This explains that the total noise voltage should in general exhibit two maxima as a function of field as was found earlier [160]). At higher current densities the flicker noise increases much more rapidly than the flux-flow noise, so that then only one maximum is found.

We conclude that the agreement between the experimental and theoretical flux-flow-noise spectra provides strong evidence for the flux-flow model, for type-II superconductors. This agreement also shows that the generation of flux bundles is more or less random and that the rigid vortex lattice is not retained during flux flow. The measurements have also made possible the determination of transit time and bundle size and given information on the effect of pinning on flux flow.

The measurements of flicker noise have shown that at temperatures both above and below the helium λ point the temperature may fluctuate so that then no isothermal situation exists. They have yielded new information on the nucleate-boiling process in liquid helium.

6. MEASUREMENTS OF FLUX-MOTION NOISE IN TYPE-I SUPERCONDUCTORS

As we saw in chapter 2, there is evidence for flux motion in type-I superconductors from different experiments. This flux motion gives rise to a noise voltage as in type-II superconductors, as will now be shown.

Measured power spectra are in this chapter compared with the theory, as given in chapter 4. The measurements of the noise cut-off frequency are explained by assuming that the d.c. voltage is composed of components due to flux flow and to ohmic loss in immobile normal domains. The domain size, determined from the noise level, is given as a function of current and field. Power spectra were also measured at a temperature close to T_c.

6.1. Experimental

Measurements were done on indium-2 at.% lead. This material is a type-I superconductor with $\varkappa \approx 0{\cdot}35$ [161]). This alloy was chosen because of the high resistivity, so that the noise voltage, which is proportional to the d.c. voltage, would be higher than for a pure superconductor. The indium-lead was melted in a quartz crucible and cold-rolled. After rolling, specimens were cut in a shape as shown in fig. 6.1 and annealed for several days at about 120 °C. They were then glued to a polystyrene holder, and current and potential leads were connected. Specimen dimensions are given in table IV.

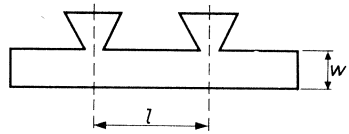

Fig. 6.1. Shape of In-2% Pb specimen.

TABLE IV

Thickness, length between potential contacts and width of In-2% Pb specimens

number	thickness d_0 (μ)	length l (mm)	width w (mm)
B	45	9·4	1·4
C	50	10·9	1·4
F	50	9·0	1·65

The critical temperature is 3·47 °K and the resistivity at 4·2 °K is 1·2 $\mu\Omega$ cm. The critical field was calculated with $H_c = H_0 (1 - T^2/T_c^2)$ and $H_0 = 310$ Oe [161]).

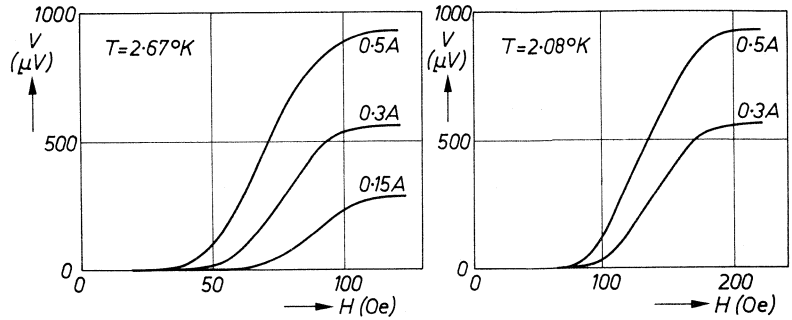

Fig. 6.2. D.c. voltage versus perpendicular field for specimen B at various values of the transport current; $T = 2{\cdot}67$ °K and 2·08 °K.

The d.c. voltage V as a function of external perpendicular field H is shown in fig. 6.2 for specimen B for different values of the transport current. At low fields no voltage is found although flux has penetrated the superconductor. Apparently no flux motion can take place at these fields due to pinning of the normal domains.

The magnetic field which was generated either by a copper-wound coil or by a pair of Helmholtz coils outside the helium dewar vessel, was always increased from zero.

The noise-power spectra were measured at different values of temperature, current and field with the same set-up as was described in sec. 5.1 with a bandwidth of 4·4 Hz.

6.2. Flux-flow noise-power spectra

Figure 6.3 shows some experimental power spectra of specimen B, measured at $T = 2{\cdot}67$ °K and with a transport current $I = 0{\cdot}3$ A. The spectra are com-

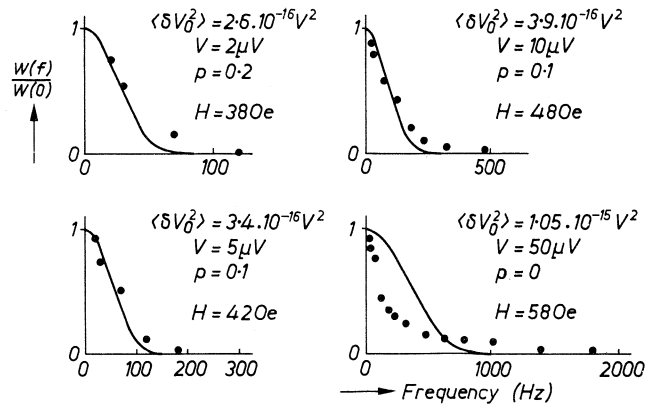

Fig. 6.3. Experimental noise-power spectra on a linear scale normalized at $W(0)$ for specimen B at different values of the magnetic field; $I = 0{\cdot}3$ A, $T = 2{\cdot}67$ °K. The drawn curve is the spectrum given by eq. (4.23) calculated with a value of p as indicated. The figures also give the values of the extrapolated m.s. noise voltage $\langle \delta V_0{}^2 \rangle$ and d.c. voltage V.

pared with the theoretical spectrum $W(f)$ for sinusoidal voltage pulses as given by eq. (4.23), where Φ is now the flux contained in a moving normal domain and τ is the transit time for these domains. At low fields the agreement between experiment and the theory for random generation and a constant transit time is reasonable and a value for the pinned fraction p is found from the expression for τ as was earlier given in eq. (5.7):

$$\tau = \frac{l\, w\, B\,(1-p)}{c\, V}. \tag{6.1}$$

At higher fields a negative value of p would be required to bring eq. (6.1) into agreement with the values of τ, derived from the spectra, which would have no physical meaning. This will be discussed in sec. 6.3.

As regards the shape of the power spectrum, this drops more rapidly than that of eq. (4.23) at low frequencies and exhibits a long tail at high frequencies. This is more evident on a log-log plot, as shown in fig. 6.4, where power spectra for specimen B at $T = 2{\cdot}67$ °K are given for various values of the magnetic field with $I = 0{\cdot}3$ A. The spectra for the lower three fields correspond to those of fig. 6.3. Figure 6.5 shows some spectra measured with $I = 0{\cdot}15$ A. The maximum noise level, which is found at about the same value of H/H_c, is the same for the two current values.

The experiments show that for intermediate fields the spectra exhibit a $1/f$ behaviour at high frequencies. At lower and at higher fields the power spectra are of the type as those generated by identical voltage pulses, such as e.g. those leading to eqs (4.21) or (4.23).

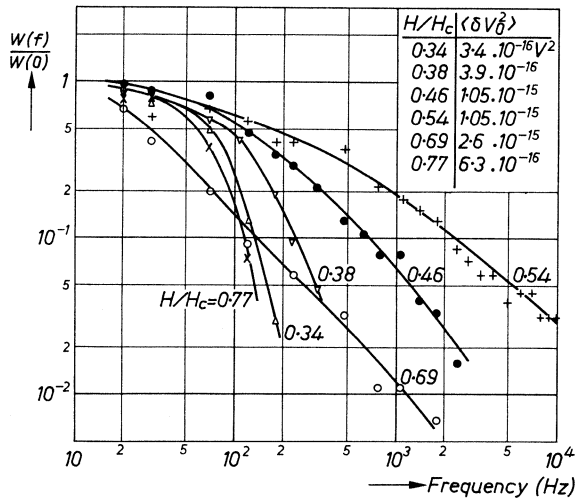

Fig. 6.4. Log-log plot of experimental noise-power spectra normalized at $W(0)$ for specimen B at different values of the reduced magnetic field H/H_c; $I = 0{\cdot}3$ A, $T = 2{\cdot}67$ °K. The figure also gives the value of the extrapolated m.s. noise voltage $\langle \delta V_0{}^2 \rangle$.

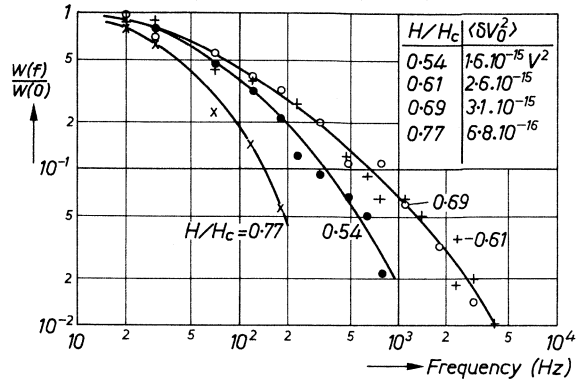

Fig. 6.5. As fig. 6.4, with $I = 0{\cdot}15$ A.

In order to find out whether thermal effects play a role in determining the noise spectra, the same measurements were carried out at a temperature below the helium λ point, at 2·08 °K, which gave very similar results. This was also checked on specimen C by making measurements at $T = 2{\cdot}21$ °K and 2·15 °K, just above and below the λ point (2·18 °K) at such values of the magnetic field that the d.c. voltage and the power dissipation (0·7 mW/cm²) was the same in both cases. This is shown in fig. 6.6. The spectra are practically identical.

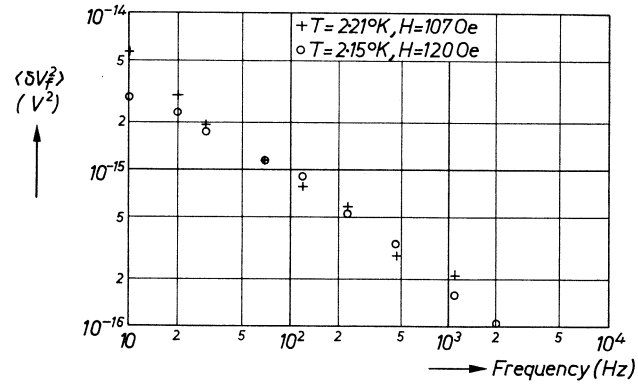

Fig. 6.6. Experimental noise-power spectra for specimen C at two temperatures $T = 2{\cdot}21$ °K and 2·15 °K with the same value of the power dissipation P. Magnetic field H as indicated, $I = 0{\cdot}3$ A.

There may be some slight indication of extra low-frequency noise at the lowest frequencies for $T = 2{\cdot}21$ °K, but this effect is insignificant. We therefore conclude that the spectra are not determined by thermal effects. Moreover, the power dissipation in the specimens during many of the measurements is well below the nucleate-boiling limit, so that no flicker noise should be expected.

The experimental spectra in intermediate fields agree qualitatively with the

theoretical spectra for the case of a jerky flux motion as were shown in fig. 4.3. It was discussed in sec. 4.2.2 that, if flux bundles on their way across the superconductor are halted a number of times, but only for such short periods that the total transit time is practically not affected, $1/f$ noise is generated. This was shown to be valid for various pulse-time distribution functions.

The power spectra can be explained as follows. At low fields only small flux domains are present, as was discussed in sec. 1.1.1. The situation is then similar to type-II superconductors. Apparently these small domains move across the superconductor in the same transit time and a spectrum for identical pulses is found like that of fig. 4.3, curve e, for $H/H_c < 0{\cdot}4$.

At intermediate fields the situation is more complicated. We saw in sec. 2.6 that in not too low fields the intermediate state consists of normal domains of different shapes and sizes. When there is flux flow, there is a tendency for the normal domains to become oriented perpendicular to the current. The bigger the domains the greater the probability that they become immobile during flux flow. The movement of smaller domains will now be interrupted when they strike a large immobile normal region. The flux motion may be continued on the other side of such a region because a small domain may be split off there. The motion of flux units will be jerky and the time between collisions may be randomly distributed.

The calculated spectra for various distribution functions for the pulse duration were shown in fig. 4.3. They are qualitatively in agreement with the experimental spectra for $0{\cdot}4 < H/H_c < 0{\cdot}7$.

The shape of the spectra is dependent on the magnetic field. In increasing field the contribution of the high-frequency components of the noise goes through a maximum. This means presumably that the average transit time goes through a minimum as a function of field.

At high fields ($H/H_c > 0{\cdot}7$), where the experimental spectra can again be described with one transit time, the immobile domains are now oriented perpendicular to the current. It is suggested that the noise is due to a few domains which move in between these normal laminae and cross the superconductor without interaction with immobile domains.

Some power spectra were measured on specimens C and F at a temperature close to T_c. The results for specimen F at $T = 3{\cdot}28$ °K are shown in fig. 6.7 together with the d.c.-voltage transition at a current of 0·3 A.

The power spectra exhibit one or more maxima at frequencies below 50 Hz. The origin of this structure is rather puzzling. At lower temperatures it is not found. The maxima are also found with a transport current of 0·5 A; the height of the maxima is not much dependent on the current. The measurements do not exclude other maxima, since in the experiments no measurements can be made close to the mains frequency (50 Hz) and its harmonics. The sharp rise of the noise voltage towards $f = 10$ Hz is steeper for the higher field values, where the dissipation in the foil may give rise to flicker noise. The maxima are also present when the dissipation in the specimen is below the nucleate-boiling limit and should therefore not be attributed to this mechanism.

A possible explanation should perhaps be sought in terms of shrinking of current-induced

vortex rings. At high temperatures the values of the magnetic field where the transition to the normal state occurs are very low, so that the magnetic field generated by the transport current can no longer be neglected. This field is of the order of a few oersteds at the surface of the foil. The motion of vortex rings may give rise to an unknown part of the measured d.c. voltage. If this motion is periodic [103]), the power spectrum should exhibit maxima.

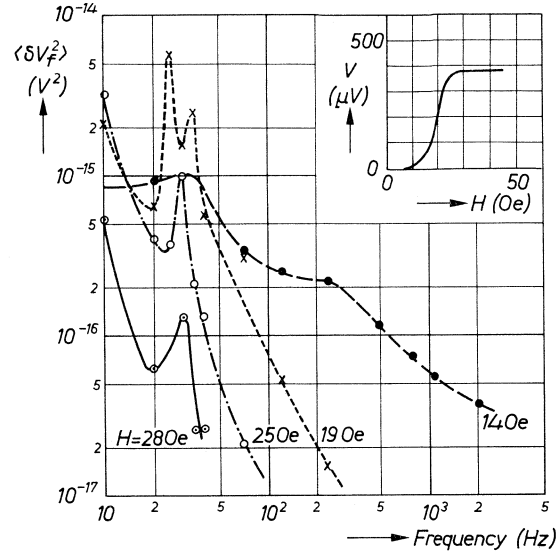

Fig. 6.7. Experimental noise-power spectra for specimen F at $T = 3{\cdot}28$ °K and various values of the magnetic field; $I = 0{\cdot}3$ A. In the inset the d.c.-voltage transition.

6.3. Determination of the flux-flow voltage

Except at low fields, there is a discrepancy between the value of τ as determined from the d.c. voltage with eq. (6.1) and the experimental value from the noise measurements. The experimental value of τ may be considerably smaller than the value calculated with eq. (6.1).

This difference is probably due to the mixed character of the d.c. voltage. We make the assumption that part of the voltage is caused by ohmic loss in immobile normal regions and does not have a measurable noise component associated with it. The Johnson noise can be shown to be several orders of magnitude less than the noise level that we measured.

We now write for the d.c. voltage component due to flux flow, by analogy to eq. (6.1),

$$V_{\mathrm{fl}} = \frac{l\, w\, B(1 - \nu)}{c\, \tau}, \tag{6.2}$$

where ν is the fraction of flux in domains that are at rest and contribute to the d.c. voltage by ohmic loss. It is assumed that $p = 0$, which means that there are no pinned normal domains through which the transport current does not flow.

The total voltage is

$$V = V_{fl} + V_l, \tag{6.3}$$

where V_l is the ohmic-loss voltage component. We assume that the fraction of flux that is not moving, and which causes the ohmic loss, is proportional to the ohmic-loss voltage

$$v = V_l/V_n, \tag{6.4}$$

when V_n is the normal-state voltage.

The value of V_{fl} cannot be derived from d.c. experiments only. It can be calculated if τ and v are known. If we write $f_c = 1/\tau$, it follows from eqs (6.2) to (6.4) that

$$V_{fl} = \frac{l\,w\,B f_c}{c} \frac{V_n - V}{V_n - l\,w\,B f_c/c}. \tag{6.5}$$

We have calculated V_{fl} from values of f_c determined from the measured noise-power spectra. This determination of f_c is uncertain, as the analytical expression of the spectrum is unknown. We have taken as a somewhat arbitrary criterion the frequency where the mean square noise voltage has dropped by a factor of 3 relative to the low-frequency level.

Because of these assumptions the calculation of V_{fl} is only of a semiquantitative character. The flux-flow voltage V_{fl} was calculated from the power spectra of specimen B for various values of the magnetic field and transport current at temperatures $T = 2{\cdot}67$ °K and $2{\cdot}08$ °K.

The results are shown in fig. 6.8, where V_{fl}/V is plotted as a function of field. It is clear that at low fields the d.c. voltage is caused by flux flow. If the field is increased, an increasing fraction of the d.c. voltage is caused by ohmic loss and at high fields no flux-flow voltage is left.

The effect of decreasing the current at a constant field is to increase the flux-flow fraction of the d.c. voltage V_{fl}/V. Since it follows from fig. 6.2 that the

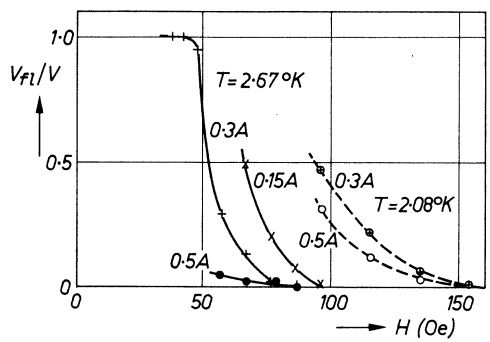

Fig. 6.8. Flux-flow fraction of the d.c. voltage V_{fl}/V versus magnetic field for specimen B at various values of the transport current; $T = 2{\cdot}67$ °K and $2{\cdot}08$ °K.

same is true for V/V_n, this suggests that it is the value of V/V_n that determines the flux-flow voltage fraction rather than the current. We therefore plotted V_{fl}/V as a function of V/V_n in fig. 6.9 for the same combinations of current, field and temperature as in fig. 6.8. It can be seen that the experimental points roughly fall on one curve so that V_{fl}/V is a function of V/V_n only.

The conclusion that flux flow takes place only at low fields, is supported by microscopic observations of superconducting Nb powder on a current-carrying superconducting Pb foil at $T = 4{\cdot}2$ °K in a perpendicular field *). The motion of the Nb particles was observed for different values of field and current and the d.c. voltage across the foil was recorded at the same time.

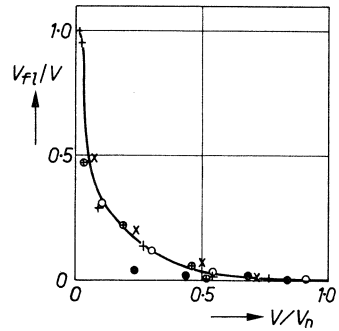

Fig. 6.9. Flux-flow fraction of the d.c. voltage V_{fl}/V versus voltage fraction of normal-state voltage V/V_n for specimen B. The symbols correspond to the values of current and temperature in fig. 6.8.

It was found, when the field was increased, that the Nb particles started to move in a direction perpendicular to current and field as soon as a d.c. voltage could be detected across the Pb foil. This was proof of the flux-flow character of the d.c. voltage at low fields. When the field was increased further the d.c. voltage was increasing continuously, but the number of the moving particles was seen to go through a maximum and the particles came to a standstill long before the critical field was reached. It may therefore be concluded that at high fields no flux motion took place.

These microscopic observations support the results of the noise measurements.

Our results for the field dependence of V_{fl}/V and the microscopic observations are in substantial agreement with the results obtained by Solomon [102]). He determined values of V_{fl}/V for small currents from experiments on flux coupling between a foil and an evaporated film and made measurements of the Ettingshausen effect. Solomon found that V_{fl}/V for small currents dropped to zero for $H/H_c \approx 0{\cdot}5$, which agrees with our results. His microscopic observations of diamagnetic powder on a current-carrying foil also showed motion of the powder grains in the direction of flux motion. At high fields an immobile laminar structure, perpendicular to the current direction, was found.

*) These experiments were done in cooperation with A. P. Severijns.

6.4. Domain size

The noise measurements also permit a determination of the size of the moving flux units. The value of the noise power, extrapolated to zero frequency, is given by

$$W(0) = 2\,\Phi\,V_{\mathrm{fl}}/c. \tag{6.6}$$

The value of Φ is determined from measurements of $W(0)$ and calculations of V_{fl} as described in the previous section.

Since the induction inside the normal domains is equal to H_c, we write for the cross-section area S of these domains

$$S = \Phi/H_c. \tag{6.7}$$

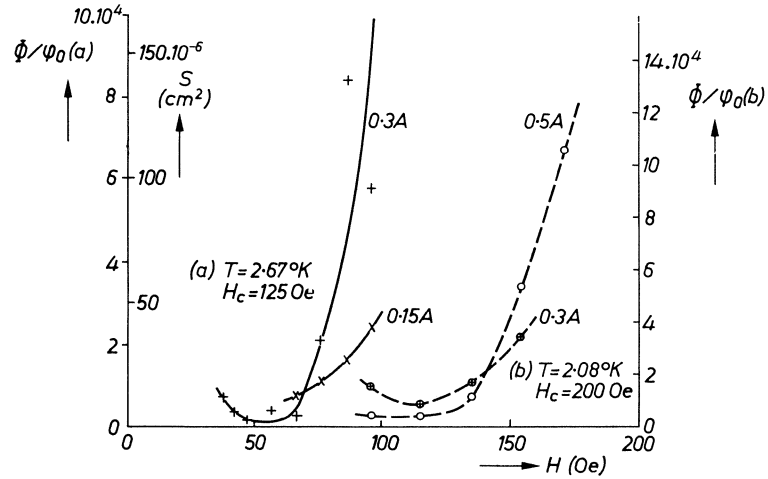

Fig. 6.10. Surface area S and number of flux quanta Φ/φ_0 of moving flux domains versus field for specimen B at various values of transport current; $T = 2{\cdot}67$ °K and 2·08 °K.

The values of S and Φ/φ_0 are given in fig. 6.10 as a function of magnetic field for specimen B at $T = 2{\cdot}67$ °K and 2·08 °K and at different values of the current. The value of S varies with field in the measurements at 2·67 °K from about 2.10^{-6} cm² to about 150.10^{-6} cm². These values correspond to approximately 1300 to 10^5 flux quanta.

The results for low fields are similar to those in type-II superconductors, as described in sec. 5.2.3. The flux domains decrease in size with increasing field, current and temperature. In type-II superconductors this behaviour was thought to be associated with pinning centres in the material. If the situation is similar in a type-I superconductor this could mean that at low fields the flux is flowing in bundles of flux tubes (see sec. 1.1). An increase of field, current or temperature would result in smaller bundles.

At higher fields the normal domains grow as was discussed in sec. 2.6, so that then the values of S and Φ/φ_0 increase with field.

6.5. Concluding remarks

The noise measurements suggest that at low fields ($H/H_c < 0{\cdot}4$) the intermediate state in a foil behaves as the mixed state of a type-II superconductor. Except at very low fields, where the domain boundaries are pinned, flux is flowing either in bundles or as single flux tubes which are presumably generated at random times. The d.c. voltage is caused by this flux flow. At intermediate fields ($0{\cdot}4 < H/H_c < 0{\cdot}7$) normal regions grow and some of them may extend across the superconductor, thereby becoming immobile. These immobile regions may have complicated shapes and may be oriented at some angle with the flux-flow direction. The still moving domains interact with these immobile regions, causing voltage pulses with a distribution of duration times. The d.c. voltage is caused partly by this flux flow and partly by ohmic loss in the immobile normal domains. At high fields ($H/H_c > 0{\cdot}7$) most of the flux is contained in immobile normal domains which have a laminar structure perpendicular to the current direction, and very few big domains move between the normal layers across the superconductor. The d.c. voltage is almost entirely due to ohmic loss in the normal layers.

A combination of noise measurements with simultaneous microscopic observations of the structure would presumably give more insight in the details of the mechanisms of voltage generation.

The flow velocity had in our experiments values of up to about 60 cm/s.

The generation of the big normal domains during flux flow was assumed to be random. The process by which these domains are generated is not clear. Perhaps small flux units are nucleated, combining to bigger domains after nucleation.

The measured power spectra do not exhibit noise reduction at low frequencies. Apparently the correlation effects, which lead to this reduction in type-II superconductors, are absent in type-I superconductors.

In the explanation of the experimental results we have disregarded for simplicity a few effects which may be present, but are probably not significant.

In our discussion of the power spectrum, it was assumed that there was a distribution of pulse durations due to interrupted motion of the normal domains. A distribution of pulse lengths may also be caused by a size distribution of moving domains. A normal domain that is elongated in the flow direction generates a longer pulse than a small domain. This effect gives rise to a somewhat lower cut-off frequency for the noise than flux flow by small domains.

Additional noise may be due to fluctuations of the size or the velocity of the moving flux domains (flux-modulation noise). There is some experimental evidence for variations of direction of flux motion and of the absolute value

of the velocity [9]). These effects presumably give some additional high-frequency noise.

Fluctuations of the size of immobile normal regions (irregular domain-wall motion) may also give rise to noise. The fluctuations were found in the past in unannealed inhomogeneous specimens, as was reviewed in sec. 1.3. These fluctuations could be associated with steps in the resistance transition. We have assumed that they are not significant in our experiments since no voltage steps were found in the transition and the material was well annealed. This was also demonstrated by the fact that the magnetization curve, in a field perpendicular to the foil, was reversible.

Flicker noise due to temperature fluctuations (as discussed in chapters 4 and 5) was found both above and below the helium λ point and had power spectra very similar to those measured on vanadium foils and the In-Tl wire. The characteristic time τ_0 for the temperature fluctuations due to nucleate boiling was about 10 ms for the In-Pb foils.

Acknowledgement

The work described in this thesis was carried out in the Philips Research Laboratories at Eindhoven. I wish to express my gratitude to the Directors of these laboratories for their permission to present the results of this work as a thesis.

The noise experiments were started in cooperation with Dr D. J. van Ooijen to whom I am much indebted for introducing me to the subject of noise and for many stimulating ideas and discussions.

I would also like to thank Mr A. K. Niessen, Prof. Dr J. Volger, Dr A. G. van Vijfeijken and Dr C. H. Weijsenfeld for numerous discussions.

Finally I want to thank all those, both in and outside the Philips laboratories, who have contributed in any way to this work.

REFERENCES

[1]) E. A. Lynton, Superconductivity, Methuen and Co, London, 1964.
[2]) P. G. de Gennes, Superconductivity of metals and alloys, Benjamin, New York, 1966.
[3]) D. Shoenberg, Superconductivity, Cambridge Univ. Press, 1965.
[4]) F. London, Superfluids I, Dover Publications, New York, 1961.
[5]) L. D. Landau, Phys. Z. Sowjet Union **11**, 129, 1937.
[6]) A. B. Pippard, Proc. Roy. Soc. **A203**, 210, 1950; **A216**, 547, 1953.
[7]) F. Haenssler and L. Rinderer, Helv. phys. Acta **40**, 659, 1967.
[8]) H. Träuble and U. Essmann, Phys. Stat. sol. **18**, 813, 1966.
[9]) H. Träuble and U. Essmann, Phys. Stat. sol. **25**, 395, 1968.
[10]) D. C. Baird, Can. J. Phys. **42**, 1682, 1964.
[11]) V. L. Ginzburg and L. D. Landau, Zh. eksp. teor. Fiz. **20**, 1064, 1950 (German transl. Phys. Abh. Sov. Union **1**, 7, 1958).
[12]) L. P. Gor'kov, Zh. eksp. teor. Fiz. **36**, 1918, 1959; **37**, 1407, 1959 (English transl. Sov. Phys. JETP **9**, 1364, 1959; **10**, 998, 1960).
[13]) C. Caroli, P. G. de Gennes and J. Matricon, Phys. kondens. Materie **1**, 176, 1963.
[14]) B. B. Goodman, I.B.M. J. Res. Dev. **6**, 63, 1962.
[15]) A. A. Abrikosov, Zh. eksp. teor. Fiz. **32**, 1442, 1957 (English transl. Sov. Phys. JETP **5**, 1174, 1957).
[16]) D. Cribier, B. Jacrot, L. Madhav Rao and B. Farnoux, Phys. Letters **9**, 106, 1964.
[17]) U. Essmann and H. Träuble, Phys. Letters **24A**, 526, 1967.
[18]) W. H. Kleiner, L. M. Roth and S. H. Autler, Phys. Rev. **133**, A1226, 1964.
[19]) H. Träuble and U. Essmann, Phys. Stat. sol. **25**, 373, 1968; J. appl. Phys. **39**, 4052, 1968.
[20]) A. G. van Vijfeijken, Thesis, Amsterdam 1967; Philips Res. Repts Suppl. **1968**, No. 8.
[21]) U. Essmann and H. Träuble, Phys. Letters **27A**, 156, 1968.
[22]) M. Tinkham, Phys. Rev. **129**, 2413, 1963; Rev. mod. Phys. **36**, 268, 1964.
[23]) G. Lasher, Phys. Rev. **154**, 345, 1967.
[24]) K. S. Knol and J. Volger, Physica **19**, 46, 1953.
[25]) H. J. Fink and A. Zacharias, Phys. Rev. **135**, A1, 1964.
[26]) Proceedings Conf. on fluctuations in superconductors (editors W. S. Goree and F. Chilton), Stanford Res. Inst., Menlo Park, 1968.
[27]) Proceedings 11th Conf. on low temperature physics (editors J. F. Allen, D. M. Finlayson and D. M. McCall), University of St. Andrews, 1968.
[28]) L. W. Schubnikov, W. I. Chotkewitsch, J. D. Shepelev and J. N. Rjabinin, Phys. Z. Sowjet Union **10**, 165, 1936.
[29]) E. Justi, Phys. Z. **43**, 130, 1942; Ann. Physik **5**, 84, 1942.
[30]) D. J. van Ooijen and W. F. Druyvesteyn, Phys. Letters **6**, 30, 1963.
[31]) D. J. van Ooijen, Phys. Letters **14**, 95, 1965; Philips Res. Repts **22**, 219, 1967.
[32]) G. Boato, G. Gallimaro and C. Rizzuto, Sol. St. Comm. **3**, 173, 1965.
[33]) S. L. Wipf, Phys. Rev. **161**, 404, 1967.
[34]) C. R. Wischmeyer, Phys. Letters **19**, 543, 1965.
[35]) C. Heiden and G. I. Rochlin, Phys. Rev. Letters **21**, 691, 1968.
[36]) C. Heiden, ref. 27, paper B 5.8.
[37]) Y. B. Kim, C. F. Hempstead and A. R. Strnad, Phys. Rev. **131**, 2486, 1963.
[38]) F. B. Silsbee, R. B. Scott and F. G. Brickwedde, J. Res. Nat. Bur. Stand. **18**, 295, 1937.
[39]) A. D. Misener, Proc. Cambr. phil. Soc. **34**, 465, 1938.
[40]) D. H. Andrews, R. M. Milton and W. de Sorbo, J. opt. Soc. Am. **36**, 518, 1946. D. H. Andrews, Annual Report Task Order IV, Contract N5-ori-166, Inst. for Coop. Research, John Hopkins Univ., Baltimore, 1948.
[41]) R. T. Webber, Phys. Rev. **72**, 1241, 1947.
[42]) A. A. Galkin, Ya. S. Kan and B. G. Lazarev, Zh. eksp. teor. Fiz. **20**, 865, 1950.
[43]) W. F. Love, Phys. Rev. **85**, 715, 1952.
[44]) B. Kaplan, Thesis Ohio State University, 1953.
[45]) D. C. Baird, Can. J. Phys. **37**, 129, 1959.
[46]) B. Lalevic, Phys. Rev. **128**, 1070, 1962; J. appl. Phys. **35**, 1785, 1964; Phys. Stat. sol. **9**, 63, 1965.
[47]) A. K. Johnson and P. M. Chirlian, I.E.E.E. Trans. Magn. **2**, 390, 1966.
[48]) R. J. Warburton and W. W. Webb, Bull. Am. phys. Soc. **13**, 379, 1968.
[49]) J. A. Cape and I. F. Silvera, Phys. Letters **27A**, 13, 1968.
[50]) G. I. Rochlin, ref. 27, paper B 1.11.
[51]) Ref. 3, edition 1952, p. 113.

[52]) C. J. Gorter, Phys. Letters **1**, 69, 1962.
[53]) J. Bardeen and M. J. Stephen, Phys. Rev. **140**, A1197, 1965.
[54]) A. G. van Vijfeijken and A. K. Niessen, Philips Res. Repts **20**, 505, 1965.
[55]) P. Nozières and W. F. Vinen, Phil. Mag. **14**, 667, 1966.
[56]) Y. B. Kim, C. F. Hempstead and A. R. Strnad, Phys. Rev. **139**, A1163, 1965.
[57]) P. R. Solomon and F. A. Otter Jr, Phys. Rev. **164**, 608, 1967.
[58]) I. Giaever, Phys. Rev. Letters **15**, 825, 1965.
[59]) I. O. Kulik, Zh. eksp. teor. Fiz. **50**, 1617, 1966 (English transl. Soviet Phys. JETP **23**, 1077, 1966).
[60]) A. Schmid, Phys. kondens. Materie **5**, 302, 1966.
[61]) C. Caroli and K. Maki, Phys. Rev. **164**, 591, 1967.
[62]) R. G. Jones, E. H. Rhoderick and A. C. Rose-Innes, Phys. Letters **15**, 214, 1965.
[63]) B. D. Josephson, Phys. Letters **16**, 242, 1965.
[64]) A. K. Niessen, F. A. Staas and C. H. Weijsenfeld, Phys. Letters **25A**, 33, 1967.
R. R. Hake, Phys. Rev. **168**, 442, 1968.
[65]) C. H. Weijsenfeld, ref. 27, paper B8.3; Phys. Letters **28A**, 362, 1968.
[66]) M. Tinkham, Phys. Rev. Letters **13**, 804, 1964.
[67]) W. F. Vinen and A. C. Warren, Proc. phys. Soc. **91**, 409, 1967.
[68]) J. Volger, F. A. Staas and A. G. van Vijfeijken, Phys. Letters **9**, 303, 1964.
[69]) C. C. Chang and A. C. Rose-Innes, Phys. Letters **26A**, 634, 1968.
[70]) R. G. Jones, E. H. Rhoderick and A. C. Rose-Innes, Phys. Letters **24A**, 318, 1967.
[71]) J. Baixeras and G. Fournet, J. Phys. Chem. Solids **28**, 1541, 1967.
[72]) K. Yamafuji and F. Irie, Phys. Letters **25A**, 387, 1967.
[73]) A. T. Fiory and B. Serin, Phys. Letters **25A**, 557, 1967.
[74]) J. A. Cape and I. F. Silvera, Phys. Rev. Letters **20**, 326, 1968.
[75]) A. K. Niessen, J. van Suchtelen, F. A. Staas and W. F. Druyvesteyn, Philips Res. Repts **20**, 226, 1965.
A. K. Niessen and C. H. Weijsenfeld, J. appl. Phys. **40**, 384, 1969.
[76]) P. W. Anderson, Phys. Rev. Letters **9**, 309, 1962.
P. W. Anderson and Y. B. Kim, Rev. mod. Phys. **36**, 39, 1964.
[77]) J. D. Livingston and H. W. Schadler, Progr. Mat. Science **12**, 183, 1965.
[78]) D. Dew-Hughes, Mat. Sci. Eng. **1**, 2, 1966.
[79]) G. J. van Gurp and D. J. van Ooijen, J. de Phys. **27**, C3-51, 1966.
[80]) E. J. Kramer and C. L. Bauer, Phil. Mag. **15**, 1189, 1967.
[81]) A. M. Campbell, J. E. Evetts and D. Dew-Hughes, Phil. Mag. **18**, 313, 1968.
[82]) V. P. Galaĭko, Zh. eksp. teor. Fiz. Pisma **7**, 294, 1968 (English transl. JETP Letters **7**, 230, 1968).
[83]) R. Labusch, Phys. Rev. **170**, 470, 1968.
[84]) W. W. Webb, Phys. Rev. Letters **11**, 191, 1963.
[85]) A. V. Narlikar and D. Dew-Hughes, Phys. Stat. sol. **6**, 383, 1964.
[86]) A. V. Narlikar and D. Dew-Hughes, J. Mat. Science **1**, 317, 1966.
[87]) C. P. Bean and J. D. Livingston, Phys. Rev. Letters **12**, 14, 1964.
[88]) V. P. Galaĭko, Zh. eksp. teor. Fiz. **50**, 1322, 1966 (English transl. Soviet Phys. JETP **23**, 878, 1966).
[89]) B. B. Goodman and J. Matricon, J. de Phys. **27**, C3-39, 1966.
[90]) H. R. Hart Jr and P. S. Swartz, Phys. Rev. **156**, 403, 1967.
[91]) Ref. 4, p. 110.
[92]) C. J. Gorter, Physica **23**, 45, 1957.
[93]) See e.g. W. K. H. Panofsky and M. Phillips, Classical electricity and magnetism, Addison-Wesley Publ. Co., Reading, 1956.
[94]) A. F. Andreev, Zh. eksp. teor. Fiz. **51**, 1510, 1966 (English transl. Soviet Phys. JETP **24**, 1019, 1967).
A. F. Andreev and Yu. V. Sharvin, Zh. eksp. teor. Fiz. **53**, 1499, 1967 (English transl. Soviet Phys. JETP **26**, 865, 1968).
[95]) F. Haenssler and L. Rinderer, Helv. phys. Acta **33**, 505, 1960.
[96]) P. R. Solomon, Phys. Rev. Letters **16**, 50, 1966.
[97]) Yu. V. Sharvin, Zh. eksp. teor. Fiz. Pisma **2**, 287, 1965 (English transl. JETP Letters **2**, 183, 1965).
[98]) B. S. Chandrasekhar, D. E. Farrell and S. Huang, Phys. Rev. Letters **18**, 43, 1967.
[99]) B. L. Brandt and R. D. Parks, Phys. Rev. Letters **19**, 163, 1216, 1967.
[100]) G. J. van Gurp, Phys. Letters **24A**, 528, 1967.
[101]) A. P. Severijns, quoted in ref. 100. A cine film was made of these observations.

[102]) P. R. Solomon, ref. 27, paper B4.2; Phys. Rev., to be published.
[103]) C. J. Gorter and M. L. Potters, Physica **24**, 169, 1958.
[104]) R. Radebaugh and P. H. Keesom, Phys. Rev. **149**, 217, 1966.
[105]) J. W. Stout and L. Guttman, Phys. Rev. **88**, 703, 1952.
[106]) E. Fromm, Z. Metallk. **56**, 493, 1965.
G. Hörz, Z. Metallk. **59**, 832, 1968.
[107]) G. J. van Gurp, Philips Res. Repts **22**, 10, 1967.
[108]) J. O. Stiegler, C. K. H. Dubose, R. E. Reed and C. J. McHargue, Acta met. **11**, 851, 1963.
[109]) C. Baker and M. T. Taylor, Phil. Mag. **16**, 1129, 1967.
[110]) L. L. Campbell, Galvanomagnetic and thermomagnetic effects, Longmans Green and Co, London, 1923, p. 125.
A. C. Beer in Solid state physics (editors F. Seitz and D. Turnbull), Academic Press Inc., New York, 1963, Suppl. **4**, p. 71.
[111]) G. J. van Gurp, Phys. Stat. sol. **19**, 173, 1967.
[112]) M. P. Shaw and P. R. Solomon, Phys. Rev. **164**, 535, 1967.
[113]) J. B. McKinnon and A. C. Rose-Innes, Phys. Letters **26A**, 92, 1967.
[114]) F. A. Staas, A. K. Niessen and W. F. Druyvesteyn, Philips Res. Repts **22**, 445, 1967.
[115]) N. Usui, J. Ogasawara and K. Yasukochi, Phys. Letters **27A**, 139, 1968.
[116]) H. van Beelen, J. P. van Braam Houckgeest, H. M. Thomas, C. Stolk and R. de Bruyn Ouboter, Physica **36**, 241, 1967.
[117]) N. V. Sarma and J. R. Moon, Phil. Mag. **16**, 433, 1967.
[118]) See e.g. H. G. van Bueren, Imperfections in crystals, North Holland Publ. Co., Amsterdam, 1960, p. 451.
[119]) R. W. Meyerhoff and J. F. Smith, Acta met. **11**, 529, 1963.
[120]) H. L. Luo, J. Hagen and M. F. Merriam, Acta met. **13**, 1012, 1965.
M. F. Merriam, J. Hagen and H. L. Luo, Phys. Rev. **154**, 424, 1967.
[121]) J. T. A. Pollock and H. W. King, J. Mat. Science **3**, 372, 1968.
[122]) L. Guttman, Trans. AIME **188**, 1472, 1950.
J. S. Bowles, C. S. Barrett and L. Guttman, Trans. AIME **188**, 1478, 1950.
[123]) Z. S. Basinski and J. W. Christian, Acta met. **2**, 148, 1954.
[124]) R. G. Boyd, Phys. Rev. **153**, 444, 1967.
[125]) D. K. C. MacDonald, Noise and fluctuations, John Wiley & Sons, Inc., New York, 1962.
[126]) P. Grivet and A. Blaquière, Le bruit de fond, Masson & Cie, Paris, 1958.
[127]) A. van der Ziel, Noise, Prentice Hall Inc., Englewood Cliffs, N.J., 1956.
[128]) A. van der Ziel, Fluctuation phenomena in semiconductors, Butterworths Sci. Publ., London, 1959.
[129]) R. D. Stuart, An introduction to Fourier analysis, Science Paperbacks, Methuen and Co., London, 1966.
[130]) J. R. Clem, ref. 27, discussion paper IB5, and private communication.
[131]) G. Fournet and J. Baixeras, Phys. Letters **25A**, 552, 1967.
[132]) S. Machlup, J. appl. Phys. **25**, 341, 1954.
[133]) C. Heiden, ref. 26, p. 231; J. appl. Phys., to be published.
[134]) A. van der Ziel, Phys. Letters **25A**, 672, 1967.
[135]) F. A. Otter and G. B. Yntema, Bull. Am. phys. Soc. **11**, 107, 1966.
[136]) G. B. Yntema, Phys. Rev. Letters **18**, 642, 1967.
[137]) J. R. Clem, Phys. Rev. Letters **20**, 735, 1968.
[138]) D. N. Lyon, Advan. cryog. Eng. **10**, 371, 1965.
[139]) R. D. Cummings and J. L. Smith, Bull. Inst. intern. Froid, Annexe 5-1966, p. 85.
[140]) R. R. Sharp, The nature of liquid film evaporation during nucleate boiling, NASA Techn. Note TN D-1997, October 1964.
[141]) F. B. Moore and R. B. Mesler, Am. Inst. chem. Engrs J. **7**, 620, 1961.
[142]) T. F. Rogers and R. B. Mesler, Am. Inst. chem. Engrs J. **10**, 656, 1964.
[143]) M. G. Cooper and A. J. P. Lloyd in Proc. 3rd intern. heat transfer conference (Chicago, Illinois), Am. Inst. chem. Engrs, New York, 1966, III, p. 193.
[144]) S. J. D. van Stralen and W. M. Sluyter, Ned. T. Natuurk. **34**, 292, 1968.
[145]) Ref. 127, p. 338.
[146]) U. Essmann, private communication.
[147]) J. L. Harden and V. Arp, Cryogenics **3**, 105, 1963.
[148]) H. Kirchner, Phys. Letters **26A**, 651, 1968 and ref. 27, paper B4.1.

[149]) H. Träuble and U. Essmann, Phys. Stat. sol. **20**, 95, 1967.
[150]) L. Brägg and J. F. Nye, Proc. Roy. Soc. **190**, 474, 1947.
[151]) F. Chilton, ref. 26, p. 193.
[152]) W. F. Druyvesteyn, private communication.
[153]) U. Essmann and H. Träuble, Phys. Stat. sol., to be published.
[154]) Ref. 125, p. 85.
[155]) See e.g. K. R. Atkins, Liquid helium, Cambridge Univ. Press, Cambridge, 1959.
[156]) This set-up was designed by J. van Suchtelen.
[157]) R. F. Gaertner and J. W. Westwater, Chem. Eng. Progr. Symp. Ser. nr. 30, **56**, 39, 1960.
[158]) F. Bussières and A. C. Leonard, Bull. Inst. intern. Froid, Annexe 5-1966, p. 61.
[159]) R. Labusch, Phys. Stat. sol. **19**, 715, 1967.
[160]) D. J. van Ooijen and G. J. van Gurp, Philips Res. Repts **21**, 343, 1966.
[161]) S. Gygax, J. L. Olsen and R. H. Kropschot, Phys. Letters **8**, 228, 1967.
[162]) G. J. van Gurp, Phys. Stat. sol. **17**, K 135, 1966.
[163]) G. J. van Gurp, Phys. Rev. **166**, 436, 1968; **178**, (10 Feb), 1969.

List of symbols

a	radius of vortex core
$\mathbf{a}$	local vector potential
$\mathbf{a}_i$	local vector potential due to transport current
$\mathbf{a}_v$	local vector potential due to vortex
$A(t)$	output of thermocouple detector
$\mathbf{b}$	local magnetic induction
$\mathbf{b}_c, b_c$	magnetic induction in vortex core
$\mathbf{b}_n$	magnetic induction in normal domain
$\mathbf{B}, B$	averaged magnetic induction
c	light velocity
C_1, C_2	normalization constants
d	nearest-neighbour distance between vortex lines
d_i	periodicity of laminar intermediate state
d_0	thickness
D	wire diameter
D_b	bubble diameter
e	electron charge
$\mathbf{e}$	local electric field
$\mathbf{e}_c$	electric field in vortex core
$\mathbf{e}_n$	electric field in normal domain
$\mathbf{E}, E$	averaged electric field
$E_{\parallel}, E_{\perp}$	electric-field components parallel and perpendicular to transport current
f	frequency
f_c	noise cut-off frequency
f_n	volume fraction of normal material
f_0	tuning frequency of wave analyzer
Δf	bandwidth
$F(f), F_i(f), F_2(f)$	Fourier transforms
$\mathbf{F}_p, F_p$	pinning force per unit length of vortex line
$F(t)$	fluctuating force
$g(J_t), g(\tau_i)$	distribution functions
$G(f)$	power-transfer function of measuring circuit
h	Planck's constant
$h(\omega)$	frequency-dependent part of flicker-noise-power spectrum
$\mathbf{h}_n$	magnetic field in normal domain
H	external magnetic field
H_c	thermodynamic critical field
$\mathbf{H}_c$	magnetic field with magnitude H_c
H_{c1}, H_{c2}, H_{c3}	lower, upper and surface critical fields

$\mathbf{H}_{c2}$	magnetic field with magnitude H_{c2}
H_i	internal magnetic field
H_0	thermodynamic critical field at $T = 0$
I	current
$I(f)$	interference term in power spectrum
$\mathbf{J}, J$	current density
J_c	critical current density
$\mathbf{J}_t, J_t$	threshold current density
k	integer
k_B	Boltzmann's constant
k_1, k_2, k_3	constants
l	length between potential probes
l_e	electron mean free path
$L, L(r)$	length of a vortex line
m	electron mass
M	magnetic moment per unit volume
M_v	mass of vortex line per unit length
n	normal-electron concentration
n_s	superconducting-electron concentration
N, N_i	average generation rate
N_d	demagnetizing coefficient
p	pinned flux fraction
$\mathbf{p}_v$	canonical momentum due to vortex
P	power dissipation per unit surface area
P_J	Joule-power dissipation in vortex core per unit length
P_t	total power dissipation in vortex core per unit length
q	heat flux
Q_v	heat of vaporization
$\mathbf{r}$	space vector
R	electrical resistance
R_c	critical hopping rate
R_{fl}	flux-flow resistance
R_h	hopping rate
R_0	constant
ΔR	resistance variation
s	correlation time
S	cross-section area of normal domains
t, t_i	time
δt	time element
t_r	transmissivity of tunnelling barrire
T	temperature
T_c	critical temperature

T_h	temperature of heater
T_l	temperature of liquid
$\Delta T(t)$	temperature variation
ΔT_m	maximum temperature drop
$u(t)$, $u_1(t)$, $u_2(t)$	elementary event
$\mathbf{v}$, v	velocity of vortex lines or normal domains
δv	velocity fluctuation
$\mathbf{v}_c$	electron drift velocity in vortex core
$\mathbf{v}_i$, v_i	electron drift velocity
$\mathbf{v}_s$	superconducting-electron velocity
$\mathbf{v}_v$	superconducting-electron velocity around vortex
$v_{\|\|}$, $v_\perp$	vortex velocity components parallel and perpendicular to v_i
V, $V(t)$	voltage
V_{fl}	flux-flow component of voltage
V_l	ohmic-loss component of voltage
V_n	normal-state voltage
$\langle \delta V^2 \rangle$	m.s. noise voltage
$\langle \delta V_f{}^2 \rangle$	m.s. noise voltage between f and $f + \mathrm{d}f$
w	width
$W(f)$	power spectrum
$W_0(f)$	power spectrum without interference terms
x	variable
$y(t)$	fluctuating variable
δy	fluctuation of $y(t)$
z	distance from surface
α	b_c/H_{c2}
α_r	relative error of single noise measurement
β	$(\alpha + 1)/2$
γ	shear strain
γ_e	electronic specific-heat coefficient
Γ	$e\, H_{c2}\, \tau_n/m\, c$
δ	angle of rotation
ε, $\varepsilon(z)$	vortex-line energy
ζ	variable
η	viscosity coefficient for flux flow in mixed state
η'	viscosity coefficient for flux flow in intermediate state.
ϑ	angle between preferred flux-flow direction and transport current
θ	Hall angle
$\varkappa$	Ginzburg-Landau parameter
$\varkappa_0$	Ginzburg-Landau parameter for pure material
$\varkappa_1$	$H_{c2}/2^{1/2}\, H_c$
λ	penetration depth

$\lambda_L(0)$	London penetration depth
Λ	surface-energy parameter
μ, μ_c	generalized electrochemical potential per particle (μ_c in vortex core)
μ_0, μ_{c0}	chemical potential per particle (μ_{c0} in vortex core)
ν	flux fraction in immobile domains giving ohmic loss
ξ	coherence length
ξ_0	coherence length of pure material
ϱ_n	normal-state resistivity
$\varrho(J)$	flux-flow resistivity dE/dJ
ϱ_{fl}	flux-flow resistivity in linear part of E-J curve
ϱ_i	dE/dJ in intermediate state
ϱ_v	vapour density
σ_{ns}	surface energy of normal–superconducting-domain boundary
τ	transit time
τ_b	bubble-departure time
τ_d	time constant of detector circuit
τ_g	pairing-depairing relaxation time
τ_i	duration time of voltage pulses
τ_j	time between starting of two subsequent pulses
τ_m	effective time constant for process with two time constants
τ_n	normal-state-electron relaxation time
τ', τ''	upper and lower limit of duration-time distribution
τ_0	surface-heating time constant
τ_1	time constant of distribution function of τ_i
τ_2	time constant of flux-modulation noise
τ_3	time constant of Johnson noise
τ_4	time constant of distribution function of τ_j
φ_0	flux quantum $(h\,c/2\,e)$
$\boldsymbol{\varphi}_0$	magnetic flux with magnitude φ_0
ϕ	electrostatic potential
ϕ_c	electrostatic potential in vortex core
Φ	magnetic flux in moving flux bundles or normal domains
$\delta\Phi$	bundle-size fluctuation
$\psi(s)$	autocorrelation function
Ψ	Ginzburg-Landau order parameter
ω	$2\pi f$

Summary

This thesis deals with the d.c. and noise voltage across a superconductor due to the motion of regions with magnetic flux. This magnetic flux is present in type-I superconductors in the intermediate state in the form of domains containing many flux quanta and in type-II superconductors in the mixed state in the form of vortex lines, each containing one flux quantum. These states are briefly described in chapter 1, which also contains a historical review of noise measurements on superconductors.

Chapter 2 gives a summary of some existing theories concerning the motion of vortex lines in type-II superconductors at zero temperature and at low fields. If a transport current flows through a superconductor in the mixed state, a Lorentz force sets the vortex lines into a viscous motion (flux flow). By this motion an electric field is generated which drives the electrons through the normal vortex core. Power dissipation in this core provides a frictional force proportional to and in the opposite direction of the velocity. Interaction of the vortex lines with inhomogeneities, such as e.g. dislocations, grain boundaries and the surface, gives rise to pinning forces counteracting the driving force. Flux motion only occurs when the driving force is greater than the pinning force, i.e. when the transport current is greater than a critical value. The theories show that the d.c. voltage across the superconductor at constant magnetic field is a linear function of the current. The slope is called the flow resistance. A brief review of various pinning mechanisms is included in this chapter. In type-I superconductors at low magnetic fields flux motion also takes place under the influence of a transport current. At higher fields, when the normal domains grow and become immobile, the current goes through these domains and power dissipation is then caused by ohmic loss as well as by the flux-flow mechanism.

Chapter 3 describes measurements of the d.c. voltage across superconducting vanadium foils and a single-crystal indium-20% thallium wire. The voltage is a linear function of the current, except at low values of the current. There is then a fraction of the flux that is pinned and does not take part in the motion. In cold-rolled vanadium foils the critical current density J_c for flux motion is higher for flux flowing perpendicularly to the rolling direction than for flux flowing in this direction due to the anisotropic structure of the material. In annealed foils J_c is smaller than in unannealed foils. Vortex-line pinning is presumably caused in the unannealed vanadium mainly by dislocations and fibre boundaries and in the annealed vanadium by grain boundaries and surface valleys. From measurements on a Corbino disc, where the flux-flow velocity is a function of the distance from the centre, it is concluded that flux is not flowing as a rigid lattice of vortex lines. Such a lattice exists when the vortex lines are at rest. In the In-Tl crystal a set of parallel twin boundaries, due to a

martensitic transition from the cubic to the tetragonal structure, gives rise to anisotropy in J_c and in the d.c. voltage. With the field parallel to the twin boundaries J_c is much higher and the d.c. voltage is much lower than with the field at a small angle. This is explained qualitatively by the interaction of a vortex line with its image at a boundary. The measurements show that J_c decreases with increasing temperature.

Chapters 4 and 5 deal with the theory and the measurement, respectively, of the noise voltage caused by the random generation and subsequent flow of bundles of vortex lines across the superconductor, thus generating series of voltage pulses. Power spectra of this flux-flow noise are calculated for identical pulses of various shapes. The spectra are little dependent on the shape of the pulses. For voltage pulses with a distribution of transit times the theoretical power spectra exhibit a tail at the high-frequency side of the spectrum. The experiments on the vanadium foils at the higher temperatures show noise spectra closely resembling the theoretical spectra for pulses with one transit time. From these spectra the transit time and thus the flow velocity can be determined. The determination of the transit time allows the calculation of the fraction p of the vortices that is at rest. These values agree with independent calculations of p from d.c. measurements, which supports the simple model. At lower temperatures the experimental spectra cannot be described with one transit time but with a distribution of transit times. This distribution is presumably caused by a velocity distribution for the flux bundles due to small inhomogeneities in the sample or by a jerky motion due to interaction of flux bundles with pinning centres. A certain amount of correlation between successively generated bundles causes the low-frequency components of the noise to be reduced. Existing models for noise reduction can be applied to this case and describe the results in a qualitative way. The size of the flux bundles, as determined from the noise measurements, decreases strongly with diminished pinning and with increasing magnetic field. The bundle size is assumed to be determined by pinning effects. If these effects are weak, small bundles are found. In increasing fields the increased interaction between the vortices is believed to cause the bundles to become smaller. It is not completely clear whether the bundle size is determined by bulk properties only or also by properties of the edge where the bundles are generated. At high fields a bundle size of only one flux quantum is found in annealed vanadium. Noise measurements on the In-Tl crystal yield values for the bundle size which are dependent on the field direction. With the field parallel to the twin boundaries the bundle size is an order of magnitude greater than with the field at some angle.

In a Corbino disc hardly any noise could be detected in agreement with the fact that the flux flows in circles and does not generate a series of voltage pulses.

A Nyquist expression is derived for Johnson noise due to thermodynamic

fluctuations of the vortex lines. The noise resistance is equal to the flow resistance. This noise could not be detected due to its smallness.

In liquid helium, during nucleate boiling, a low-frequency noise voltage is found which disappears on cooling the liquid through the λ point. It is called flicker noise and ascribed to temperature fluctuations in the specimen surface. The experimental spectra are compared to calculated spectra, based on temperature pulses with shapes similar to those found in other boiling liquids. The agreement is reasonable. At temperatures below the λ point, the helium bath showed temperature oscillations due to pressure variations above the liquid, originating in the rotary pump. These fluctuations also gave rise to voltage fluctuations.

In chapter 6 noise measurements on type-I superconductors (In-2% Pb foils) in the intermediate state are discussed. At low and at high fields the spectra can be described with one transit time. At intermediate fields there is a distribution of pulse duration times due to a jerky flux motion, giving rise to spectra with an approximate $1/f$ frequency dependence. From the noise cut-off frequency the flux-flow fraction of the d.c. voltage is determined. This is found to be a decreasing function of the total d.c. voltage relative to the normal-state voltage. At low fields the intermediate state is similar to the mixed state: flux moves probably as bundles of flux tubes. At higher fields the noise is due to moving normal domains which increase in size with increasing field. Due to the complexity of the intermediate-state structure the information obtained from the flux-flow noise is less quantitative than for type-II superconductors.

Some results of this investigation have already been published. This concerns parts of chapters 3 [107, 162]) and 4, 5 and 6[160, 163]).